ARTIFICIAL INTELLIGENCE BASED SOLAR/DIESEL HYBRID WATER PUMPING SYSTEM

by

RANGANAI T MOYO

Student Number: 21855926

Submitted in fulfilment of the requirements of the degree of

MASTER OF ENGINEERING

in

Mechanical Engineering

in the

Department of Mechanical Engineering

Durban University of Technology

Durban

September 2021

Declaration

This dissertation presents my work except where stated in the text and it has not been submitted in any form to any other University.

This research work was conducted under the Department of Mechanical Engineering, Durban University of Technology, under the supervision of Professor Pavel. Y Tabakov and Professor Sibusiso Moyo.

Student: *Ranganai Tawanda Moyo*

Signature: ……... Date: …….

Approved for Final Submission by:

Supervisor: *Prof. P, Y Tabakov*

Signature: …… Date: …….

Co-supervisor: *Prof S. Moyo*

Signature: ……. Date: …….

Acknowledgement

I would like to thank my supervisors, Professor Pavel Y Tabakov and Professor Sibusiso Moyo, for their support and guidance throughout my studies.

I sincerely thank the Durban University of Technology and the National Research Foundation of South Africa for their financial and moral support over these years.

I also would like to thank my family members and friends, who supported and encouraged me to achieve my ultimate goal. Finally, I would like to thank my dear God for leading and protecting me throughout my studies.

Publications and research outputs

1. R. T. Moyo, P. Y. Tabakov, and S. Moyo, "The Efficacy of the Maximum Power Transfer Theorem in improving the efficiency of Photovoltaic Modules: A REVIEW," presented at the *South African Solar Energy Conference (SASEC)*, East London, 2019
2. R. T. Moyo, P. Y. Tabakov, and S. Moyo, "Design and Modelling of the ANFIS based MPPT controller for a Solar Photovoltaic (SPV) System," *Journal of Solar Energy Engineering*, pp. 1-9, 2020, doi:10.1115/1.4048882 **(Impact factor: 1.641).**

Abstract

Solar energy powered systems are increasingly being implemented in different areas due to the advances in solar energy technologies. Some of the major areas for solar energy applications include solar water heating, solar electric power generation, and solar water pumping. Solar water pumping has become the most adopted solar energy technology in the last decade. It has been considered as an attractive way to provide water in remote areas. A major advantage of using solar water pumps is that they are naturally matched with solar irradiation since usually water demand is high in summer when solar irradiation has its maximum values. However, solar energy powered systems are weather dependent. In most cases, a solar energy source has to be combined with another energy source to form a hybrid system to overcome the demerits of using solar alone.

This thesis provides the detailed design, modelling and analysis of an Artificial Intelligence (AI) based solar/diesel hybrid water pumping system. This research aims to develop an optimization model that uses AI techniques to maximize the solar energy output and manage the energy flow within the solar/diesel hybrid water pumping. Thus, the proposed system is composed of solar photovoltaic modules, battery bank, Variable Speed Diesel Generator (VSDG), Adaptive Neuro-Fuzzy Inference System (ANFIS) based Maximum Power Point Tracking (MPPT) controllers and an Energy Management Controller (EMC). The EMC, which is based on Fuzzy Logic (FL), is responsible for managing the flow of energy throughout the hybrid system to ensure an undisturbed power supply to the water pump. The PV array, battery bank, VSDG are all sized to power a 5Hp DC water pump and the ANFIS based MPPT controllers are proposed for improving the efficiency of PV modules.

The modelling of the system components is performed in the MATLAB/Simulink environment. For evaluation of the proposed system, several case scenarios were considered and simulated in the MATLAB/Simulink environment. The simulation results revealed the effectiveness of the proposed ANFIS based MPPT controllers since the controllers were able to extract maximum available power from PV modules for both steady-state and varying weather conditions. The proposed EMC demonstrated the successful management and control of the energy flow within the hybrid system with less dependency on the VSDG. The EMC was also able to regulate the charging and discharging of the battery bank.

Contents

List of Figures

1.0 INTRODUCTION.

Renewable energy systems have attracted wide attention globally due to the growing concern for environmental conservation [1]. In 2019, the International Energy Agency (IEA) forecasted the global renewable energy capacity to expand by 50% between 2019 and 2024 [2]. This increase of 1200 GW is equivalent to the total installed power capacity of the United States today [2]. In the same context, South Africa, according to the Integrated Resource Plan (IRP 2010), set a target of 17800 MW of renewable energy sources to be reached by 2030 [3]. From these statistics, it can be argued that the future is characterized by a mix of energy technologies with renewable energy sources such as solar and wind having a greater contribution to the new global energy economy.

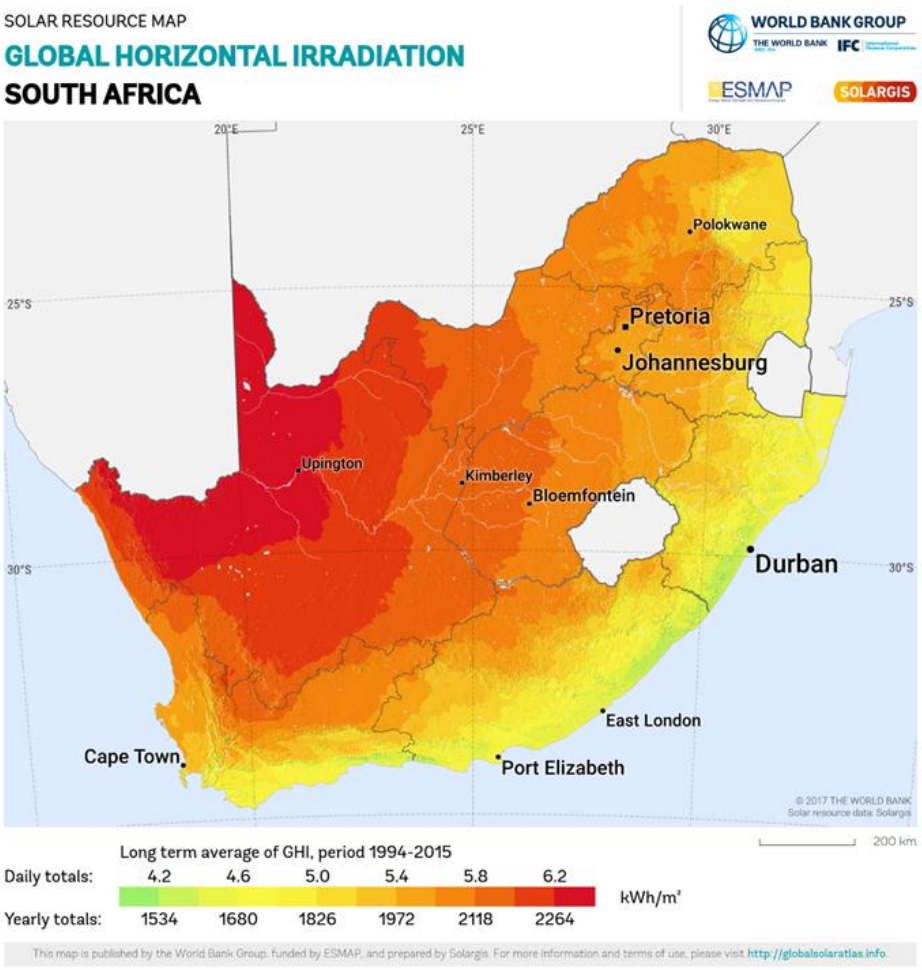

Figure 1: South Africa global horizontal irradiation map [4].

Among the above stated renewable energy sources, solar is considered as one of the most attractive energy sources for electricity generation [5]. The interest in solar energy is growing worldwide due to the continuous price drop of both the Photovoltaic (PV) modules & solar

batteries and the advances in power electronic systems [6]. According to Gottsche and Hove [7], Zimbabwe has an annual average of 2100 peak sunshine hours, an equivalent of 3100kW/m^2 per annum. At the same time, most places in South Africa have an average of 2500 peak sunshine hours per year giving an average solar irradiation level between 4.5 and 6.5kWh/m2 in a single day as shown in **Fig. 1** [8]. This high amount of horizontal radiation makes it suitable to harness solar energy cost-effectively in the Southern African region.

Solar energy powered systems are increasingly being implemented in different areas due to the advances in solar energy technologies. Some of the major areas for solar energy applications include solar water heating, solar electric power generation, and solar water pumping. Solar water pumping has become a widely adopted solar energy technology in the last decade [9]. It has been considered as an attractive means of providing water in remote areas. However, solar energy powered systems are weather dependent. In most cases, a solar energy source has to be combined with another energy source to form a hybrid system to overcome the demerits of using solar alone [10]. This dissertation proposes the development of a solar/diesel hybrid water pumping system that uses Artificial Intelligence (AI) techniques to maximize solar energy output as well as managing the energy flow within the hybrid system.

1.1 OVERVIEW OF HYBRID RENEWABLE ENERGY SYSTEMS

With the fast growth of the renewable energy market, the idea of combining different power sources to form Hybrid Renewable Energy Systems (HRES) has received more attraction worldwide [11]. HRES can be defined as a combination of two or more renewable energy sources or a combination of renewable energy sources and conventional energy sources [12]. HRES offer attractive configurations in remote areas for applications such as water pumping, electrification, lighting, and powering telecommunication systems [13]. An important feature of HRES is that they combine different power technologies to get efficiencies higher than what could be attained using a single power source [14-16]. It has been demonstrated that HRES significantly reduce the total life cycle costs as compared to stand-alone power supplies, and they provide a more reliable energy supply through the involvement of different energy sources [17].

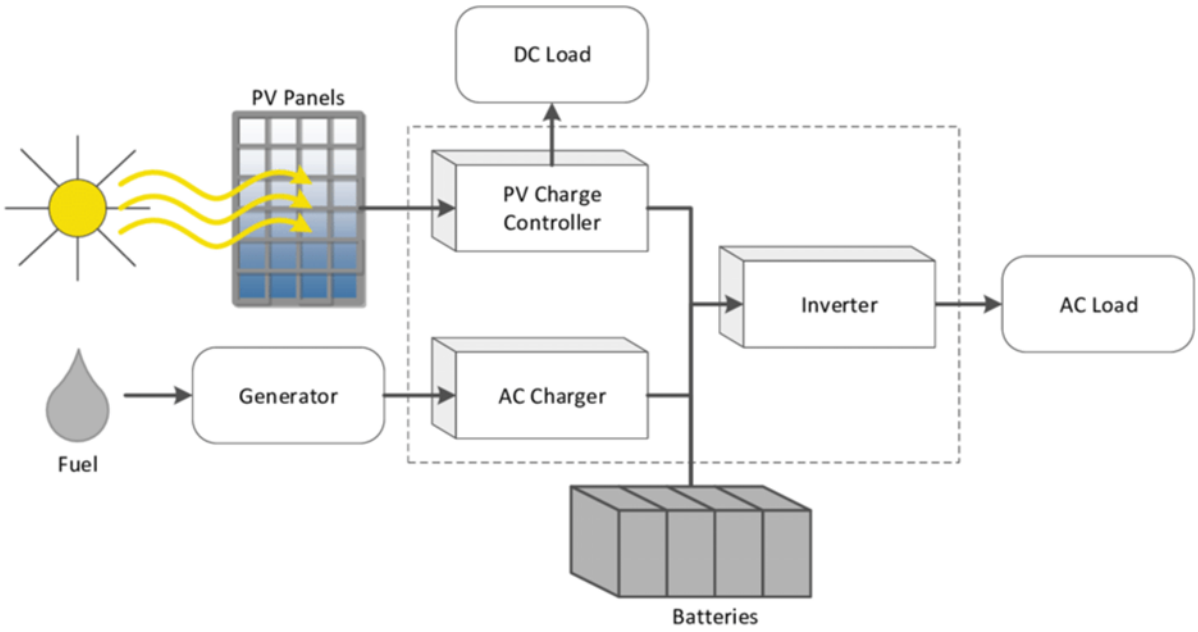

Figure 2: PV/diesel hybrid system [18].

One of the common hybrid renewable energy systems is a solar/diesel hybrid system shown in **Fig. 2**. A solar/diesel hybrid system combines the energy from the PV modules with that from the diesel generator to power the load. The PV system may or not include the battery bank but the use of a battery bank is advisable to enhance power stability in the system [19]. In a solar/diesel hybrid system, a diesel generator is used to regularly fill up the gap between the power generated by the PV system and the system load [20]. According to the studies, solar/diesel hybrid systems have been developed and successfully implemented in islands such as in Thailand [21-23] and Maldives [24-27]. Another common example of HRES is a wind/solar hybrid system. A wind/solar hybrid system is mainly comprised of wind turbines, solar panels, controllers, batteries and a backup generator for some instances. In [28-32] wind/solar hybrid systems were proposed and studied for different applications like rural electrification and water pumping. Currently, in South Africa, there are two pilot wind/solar hybrid systems in the Eastern Cape [33]. One of them is the Hluleka hybrid mini-grid which consists of three shells solar PV module arrays (56 × 100W), two 2.5 kW wind generators, and a diesel generator for backup supply to give a total power of 10.6 kW. The second one is the Lucingweni hybrid system that consists of 36 kW wind generators, 50 kW PV panels, and a backup diesel generator serving 220 houses in the Eastern Cape. The data is being collected from these pilot hybrid systems to investigate their feasibility.

Figure 3:Hluleka hybrid mini-grid system [33].

The main concern when dealing with HRES is the stochastic nature of wind and solar energy resources. The power output variation from these renewable energy sources leads to system instability and poor power quality which is not common in conventional power systems. Thus, the optimum design and sizing of the components of HRES are of prime importance for their economic and technical feasibility. Because of the complexity of the HRES, several optimization tools have been developed and applied in the design of these hybrid systems [34]. These optimization methods include classical, soft computing as well as hybrid techniques. Classical optimization techniques find optimum solutions by differentiating the continuous objective function of a problem being solved. Examples of widely used classical techniques for optimizing HRES are the Linear Programming Model (LPM), the Dynamic Programming (DP), and the Non-Linear Programming model (NLP). These classical optimization models have been incorporated in some HRES modelling packages such as the Hybrid Optimization Model for Electric Renewables (HOMER), the Linear, Interactive and Discrete Optimizer (LINDO), and the General Algebraic Modelling System (GAMS). In [35] the linear programming model in the GAMS software was proposed to find the optimum configuration of power supply from a mix of several renewable energy sources. The NLP and the DP have also been utilized for HRES optimization in the studies found in [36, 37] respectively. However, for applications where the objective functions are not differentiable or continuous, classical methods have limited capabilities. With the rise of Artificial Intelligence (AI), several soft computing optimization techniques have emerged for solving complex and non-linear

objective functions [38]. These AI techniques include Fuzzy Logic (FL), Artificial Neural Networks (ANN), Genetic Algorithms (GA), and Particle Swarm Optimization (PSO). The literature reports voluminous research where AI techniques offer better results over classical methods in the design, sizing, control, and optimization of HRES. Fuzzy logic was utilized for the optimum power management of HRES in [39-41], ANNs were used in [42, 43] for forecasting solar and wind energy for optimum sizing of HRES and GAs were adopted for the design of an optimized hybrid renewable energy system in [44, 45].

1.2 PROBLEM STATEMENT AND JUSTIFICATION.

Many remote areas in developing countries lack the supply of electricity due to the poor distribution of grid electricity and the unavailability of financial resources to support grid extension [19]. For irrigation, people from these areas mainly use diesel or petrol powered water pumps. The use of diesel water pumps has many negative environmental impacts like the emission of carbon dioxide which leads to global warming and noise pollution [46]. Remarkably some of these areas are rich in solar radiation energy which is enough to power water pumps. Solar energy has many benefits such as being environmentally friendly and abundant in nature [47]. However, solar energy is weather dependent, for example, if it goes for some days without sunlight farmers can have a challenge when they need to water their crops. For the smooth running of the water pumps at the farm, it is therefore difficult to throw away diesel-powered water pumps, hence, the need to integrate solar and diesel energy sources to form a hybrid system is an excellent option. Because of the unpredictable nature of solar energy, the only challenge when dealing with solar HRES is the management and control of energy distribution. It is therefore essential to manage the flow of energy throughout the hybrid system to ensure an undisturbed power supply to the water pump. This research project proposes a solar/diesel hybrid water pumping system for a 10-hectare irrigation scheme located in Chiredzi, Zimbabwe. The hybrid system consists of a Variable Speed Diesel Generator (VSDG), PV modules, a battery bank, MPPT charge controllers, energy management controller and a water pump. The VSDG is proposed in this research work to ensure maximum solar energy penetration in a hybrid system since the VSDG has a wider operating range as compared to constant speed generators.

This research project aims to address the following problems:

- *High emission of greenhouse gases* – stand-alone diesel water pumps cause high emissions of greenhouse gases. An increase in greenhouse gases results in the greenhouse effect which ultimately leads to global warming.
- *High maintenance costs* – stand-alone diesel water pumps have many moving parts and they have to be serviced regularly to reduce failures and downtimes. These costs include servicing costs and costs for new parts.
- *High operational costs* – these are the costs of running the pump. These include costs for fuel, oil, and others.
- *Power stability issues* – power instability issues are very common in HRES. They are caused by the variation of the energy generated from PV modules due to changes in weather during the day.

1.3 AIMS OF THE STUDY.

This research aims to develop an optimization model that uses AI techniques to maximize solar energy output as well as managing the energy flow within the solar/diesel hybrid water pumping system.

1.3.3 Objectives

The main objectives of this project are:

- To develop an optimization model that uses FL to manage the energy flow in a solar/diesel hybrid water pumping system.
- To design and model Adaptive Neuro-Fuzzy Inference System (ANFIS) based Maximum Power Point Tracking (MPPT) controllers for maximizing the solar energy output of PV modules.
- To size up the PV array, the battery bank and the VSDG to power a 5Hp water pumping system.
- To come up with a digital model of the whole system focusing on the control system.

1.4 PROJECT METHODOLOGY

To fulfil the objectives of this research, the following methodology was used:

- **Literature review:** The literature related to solar photovoltaic systems, AI techniques, diesel generators, solar water pumping systems, maximum power point tracking

techniques and different control strategies used in HRES was reviewed. The review helps one to understand the previous studies by other researchers on the same topic.

- **System modelling:** The models of the components of the solar/diesel hybrid water pumping system were developed after reviewing previous studies. The models were developed and implemented in MATLAB/Simulink environment.
- **Simulation of models:** The developed models were simulated using MATLAB tools to study the dynamic behaviour of the proposed system.
- **Assessment and results analysis:** After simulations, several case studies were considered to analyze the performance of the proposed hybrid system. The conclusion was drawn from this analysis.

2.0 LITERATURE REVIEW

2.1 HISTORY OF ARTIFICIAL INTELLIGENCE

Research in the field of artificial intelligence (AI) has a long tradition and it is very difficult to pinpoint its roots. [48]. However, in 1950, Alan Turing published a paper titled "Computing Machinery and Intelligence" which was coined as a major turning point in the history of AI [49]. The paper explained machine intelligence using the imitation game which involved a teletype conversation between a human being, a machine, and an interrogator. Afterwards, in 1956, John McCarthy and others held the first workshop on Artificial Intelligence (AI) named the Dartmouth workshop and they declared the first use of the phrase "Artificial Intelligence" [50]. After the Dartmouth workshop, the field of AI received so much attention and several governments and institutes were interested in funding AI-related research. In the 1970s, the AI industry entered a phase described as "AI winter" when all AI activities declined dramatically [51]. The AI winter was caused by little progress in AI research than expected leading to funding cuts by governments and companies [52]. In the 1980s, AI research resumed with the introduction of "Expert Systems", which were developed and quickly implemented by several corporates all around the World [53]. Expert systems are computer programs that aim to model human expertise to solve complex problems in one or more specific knowledge areas [54]. The field of AI experienced another major winter from 1987 to 1993 [55]. This was because expert systems computers were proven to be clumsy and slow as compared to desktop computers built by Apple and IBM [53]. After difficult times in the early 1990s, the AI industry finally recovered in the 2000s and this was all possible through the development of big data faster computers and advancements in AI techniques [56]. The AI research field is now big such that tracking the proliferation of the studies becomes a difficult task [57].

2.2 A REVIEW OF ARTIFICIAL INTELLIGENCE TECHNIQUES

Human activities such as doing mathematics, driving a car, understanding human language, and decision making are said to require "intelligence" [58]. Over the past years, several computer programs have been developed to perform such tasks. For example, there are computer programs that can diagnose diseases, solve complex mathematical equations, recognize natural language, and analyze electrical circuits. Because of their capabilities, these computer systems might be said to have some degree of artificial intelligence. In general, the term artificial intelligence implies the ability of a machine or an artefact to perform tasks that characterize human thought [59]. AI has already changed our daily lives by improving safety,

human health, and industrial productivity. Real-life artificial intelligence-based systems examples include industrial robots, medical diagnostics machines, navigation systems, self-driving cars, chat-box & digital assistants, video games, data mining systems. The literature reports a lot of AI techniques that can be used for solving complex problems. These techniques include genetic algorithms, fuzzy logic, heuristics and artificial neural networks to mention a few. This study will focus on two main AI techniques of interest that are going to be explained in the next section.

2.2.1 Fuzzy logic

Fuzzy logic (FL) was invented by Lotfi Zadeh in 1964 to address uncertainty and imprecision which widely exist in many real-life engineering problems [60]. FL mimics decision making in humans because it takes all possible intermediate values between "yes" and "no". The inventor of FL, Lotfi Zadeh, discovered that decision making in human beings includes all the possibilities between digital "yes" and "no" which is unlike in computers [61].

A fuzzy logic system has four main parts:

- ***Fuzzification Module*** – this module transforms crisp system inputs into fuzzy values using membership functions.
- ***Knowledge-base*** – this stores the IF-THEN rules and acts as a database for information that describe the membership functions of the fuzzy set.
- ***Inference Engine*** – it mimics human reasoning by making an inference on the system inputs and the fuzzy rules in the knowledge base.
- ***Defuzzification Module*** – it converts a linguist variable from the inference engine into a crisp output number.

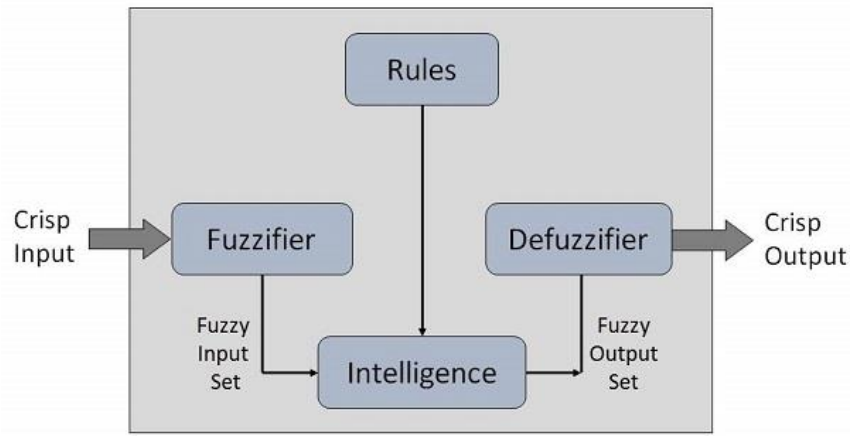

Figure 4: A diagram showing the components of a fuzzy logic system [62].

2.2.1.1 Fuzzy sets theory

Fuzzy logic can be described as an extended multivalued logic but in a broader sense, it is centred on the fuzzy sets theory [63]. The theory of fuzzy sets explains the classes of objects with ambiguous boundaries where the membership is a matter of degree [64]. The basic concept underlying fuzzy logic is the use of linguistic variables to represent quantitative values [65]. **Fig. 5 (a)** shows a classical set A in the universe of discourse, X. Classical sets are characterized by crispy boundaries and this means there is no doubt about the position of the boundaries of the set [66]. For fuzzy sets, because of their ambiguous properties, they have vague boundaries as shown in **Fig. 5(b).**

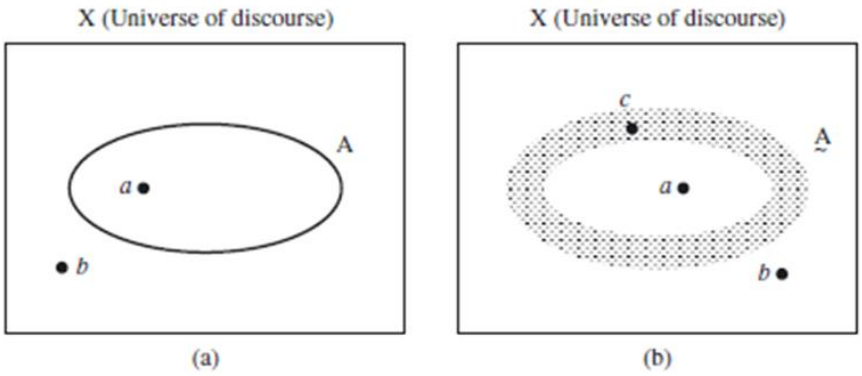

Figure 5: A diagram describing crisp sets and fuzzy sets [67].

Point a in **Fig. 5 (a)** is with no doubts a member of a crisp set A and point b is not a member of set A. **Fig. 5 (b)** shows the vagueness and ambiguous properties of the fuzzy set $\underline{A}$ on the same universe of discourse. The shaded region in **Fig. 5 (b)** symbolizes the boundary of the fuzzy set $\underline{A}$ where point a is a full member of the fuzzy set. However, point c which is located on the shaded boundary has an ambiguous membership. The point c has some intermediate degree of membership thus it is partially the member of fuzzy set $\underline{A}$ and this shows the ambiguity of fuzzy sets.

The transition of elements from membership to non-membership in classical sets is well defined [68]. In fuzzy sets, this transition is gradual and characterized by various degrees of membership. Therefore, the membership of an element from the universe in a fuzzy set is dignified by a function that tries to explain vagueness and ambiguity. From these explanations, a fuzzy set can be then described as a set having elements with varying degrees of membership. Elements of a fuzzy set are mapped from linguistic variables to real numbered values using theoretic membership functions [69].

2.2.1.2 Fuzzy logic membership functions

Fuzzy sets consist of membership functions that map elements to a membership value between 0 and 1. Suppose X is the universe of discourse and $x \in X$, then the mapping of the fuzzy set $\underline{A}$ by the membership functions is represented as:

$$\mu_{\underline{A}}(x): X \rightarrow [0,1] \quad \textbf{(1)}$$

Thus, for all $x \in X$, $\mu_{\underline{A}}(x)$ shows the extent the element x belongs to a fuzzy set $\underline{A}$. Membership functions are graphical representations that show the magnitude of participation of each input in a fuzzy set [70]. The following are the constraints that guide membership functions [71]:

- The lower and upper boundaries of a membership function must be 0 and 1 respectively.
- $\mu_{\underline{A}}(x)$ must be unique for every $x \in X$. That is, one element cannot be mapped to different degrees of memberships in the same fuzzy set.

Several membership functions can be used in fuzzy sets and these include:

- Triangular functions, defined by:

$$\mu_{\underline{A}}(x) = \begin{cases} 0 & x < \alpha_{min} \\ \dfrac{x - \alpha_{min}}{\beta - \alpha_{min}} & x \in (\alpha_{min}, \beta) \\ \dfrac{\alpha_{max} - x}{\alpha_{max} - \beta} & x \in (\beta, \alpha_{max}) \\ 0 & x > \alpha_{max} \end{cases} \quad \textbf{(2)}$$

- Trapezoidal functions, defined by:

$$\mu_{\underline{A}}(x) = \begin{cases} 0 & x \leq \alpha_{min} \\ \dfrac{x - \alpha_{min}}{\beta_1 - \alpha_{min}} & x \in (\alpha_{min}, \beta_1) \\ \dfrac{\alpha_{max} - x}{\alpha_{max} - \beta_2} & x \in (\beta_2, \alpha_{max}) \\ 0 & x \geq \alpha_{max} \end{cases} \quad \textbf{(3)}$$

- **Γ**- membership function, defined as:

$$\mu_{\underline{A}}(x) = \begin{cases} 0 & x < \alpha \\ 1 - e^{\gamma(x-\alpha)^2} & x > \alpha \end{cases} \quad \textbf{(4)}$$

- **S** – membership function, defined as:

$$\mu_{\underline{A}}(x) = \begin{cases} 0 & x \leq \alpha_{min} \\ 2\left(\frac{x-\alpha_{min}}{\alpha_{max}-\alpha_{min}}\right)^2 & x \in (\alpha_{min}, \beta) \\ 1-2\left(\frac{x-\alpha_{min}}{\alpha_{max}-\alpha_{min}}\right)^2 & x \in (\beta, \alpha_{max}) \\ 0 & x \geq \alpha_{max} \end{cases} \quad \textbf{(5)}$$

- Gaussian function, defined as:

$$\mu_{\underline{A}}(x) = e^{-\alpha(x-\beta)^2} \quad \textbf{(6)}$$

- Exponential-like membership function, defined as:

$$\mu_{\underline{A}}(x) = \frac{1}{\{1+\ \gamma(x-\beta)^2\}} \qquad \gamma > 1 \quad \textbf{(7)}$$

2.2.1.3 Fuzzy sets operations

In classical set theory, binary logic operators are used to describe the behaviour of the set. Binary logic operators work properly for bivalent logic where there is a finite set of probabilities for each input but not in fuzzy logic. In fuzzy logic, the operators should be expressed as functions for all probable fuzzy values. Let X be the universe of discourse, and let $\underline{A}$ and $\underline{B}$ be defined in the universe of discourse. For a given element x over the domain X, the fuzzy logic operators defined for sets $\underline{A}$ and $\underline{B}$ are as follows:

Union: $$\mu_{\underline{AUB}}(x) = \mu_{\underline{A}}(x) \vee \mu_{\underline{B}}(x) \quad \textbf{(8)}$$

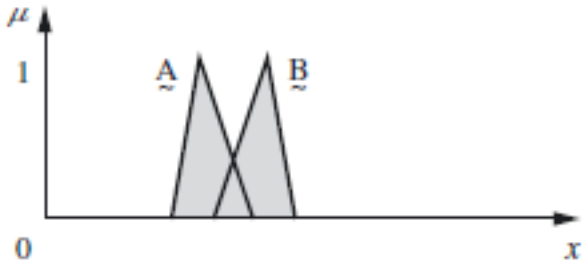

Figure 6: A diagram showing the union of two fuzzy sets [67].

Intersection: $$\mu_{\underline{AUB}}(x) = \mu_{\underline{A}}(x) \wedge \mu_{\underline{B}}(x) \quad \textbf{(9)}$$

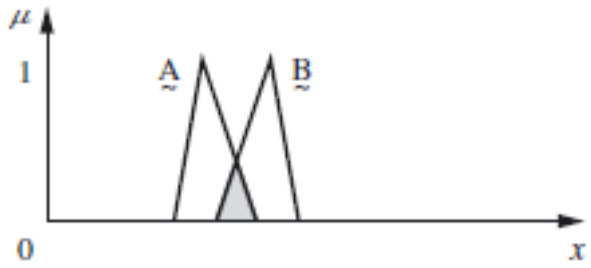

Figure 7: A diagram showing the intersection of two fuzzy sets [67].

Compliment: $$\mu_{\overline{\underline{A}}}(x) = 1 - \mu_{\underline{A}}(x) \quad \textbf{(10)}$$

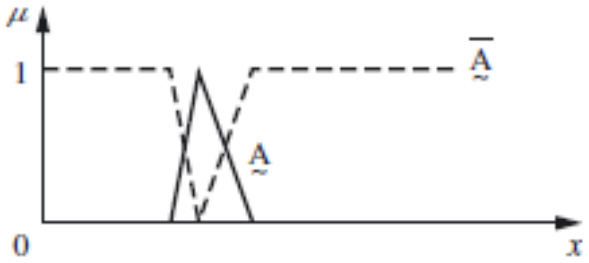

Figure 8: A diagram showing the complement of a fuzzy set [67].

2.2.2 Artificial neural networks

An artificial neural network(ANN) is a mathematical method that tries to simulate how biological neural networks work [72]. Artificial neurons learn from previous or given examples so that if they encounter such a situation again in the future, they will be able to solve it. Depending on the problem to be solved, ANNs are good in some applications and lack in some others [73]. ANNs are good in tasks with incomplete data and for complex problems where humans usually give solutions on an intuition basis [74]. ANNs lack in applications that require high accuracy and precision for example problems involving arithmetic and logic.

ANNs have been useful in various areas including the field of medicine, neurology, mathematics, engineering, economics, and meteorology [75]. They can be trained to forecast weather, navigate robotics movements, perform financial forecasts and for pattern and facial recognition [58].

2.2.2.1 Biological and artificial neurons

ANNs are inspired by biological neurons and they are designed to simulate how the human brain operates [76]. The biological neural system is made up of three elements which are

receptors, a neural network, and effectors [77]. The receptors receive the information in the form of electrical impulses and pass it to the neural network. The neural network receives the stimuli and then processes the inputs to make a proper decision on the outputs [78]. The final stage consists of effectors that convert electrical impulses given by the neural network to give responses in the outside environment. The neural network is made up of four main elements which are the soma, axon, dendrite, and synapse. These elements are shown in the figure below.

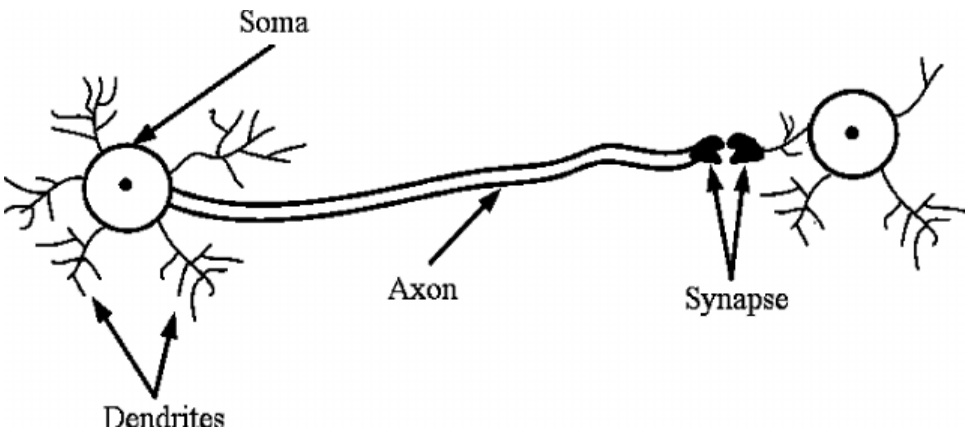

Figure 9: A diagram showing a biological neural network system [79].

- ***Soma/Cell body*** – it has a nucleus that controls all the activities. The soma is connected to the dendrites and the axon. Dendrites are responsible for bringing the information to the neuron and the axon directs the information to other neurons.
- ***Axon*** – it is a longer part of the neuron and it transmits nerve impulses away from the neuron's cell body. Therefore, the main task of the axon is to transmit information to other neurons.
- ***Dendrites*** – these are structures on the neuron that receive electrical impulses for the neuron to become active. The electrical impulses come in two forms: excitatory & inhibitory.
- ***Synapse*** – it is the part that allows a neuron to pass an electrical or chemical signal to other neurons. The transfer can be neuron to neuron or neuron to body cells.

The first computational model of a neural network was developed by Warren McCulloch and Walter Pitts in 1943 [80]. The model was based on mathematics and algorithms to simulate the behaviour of a biological neuron. Their model calculated the weighted sum of the inputs to give the outputs as 0 or 1 depending on whether the sum is above or below a certain threshold.

$$n_i(t+1) = \emptyset\left(\sum_j w_{ij} n_j(t) - \mu_i\right) \quad \textbf{(11)}$$

The equation above shows a McCulloch-Pitts neuron where n_i is either 1 or 0 and it represents the state of the neuron as firing or not firing respectively. The step function or Heaviside function, $\emptyset$, is given by:

$$\emptyset(x) = \begin{cases} 1 & if\ x \geq 0 \\ 0 & otherwise \end{cases} \quad \textbf{(12)}$$

The strengths of the synapses connecting neurons j and i is represented by w_{ij} and μ_i represents the threshold value for unit i. For the neuron to fire, the weighted sum of the inputs must be equal to or have exceeded this threshold value [81]. The McCulloch and Pitts neuron was capable of performing any computation an ordinary digital computer could perform for suitably chosen weights w_{ij}. In 1949, Donald Hebb took the idea of the mathematical neural network proposed by Warren McCulloch and Walter Pitts further when he published a book named "The Organization of Behavior". Thereafter, Frank Rosenblatt developed a "perceptron" model in 1958 [82]. This model was recognized as the first mathematical neural network for pattern recognition but was later disapproved by Marvin Minsky and Seymour Papert after they had found some irregularities with the proposed perceptron [83]. In 1975, Paul Werbos finally solved these problems by introducing the back-propagation learning technique. The back-propagation and gradient descent techniques form the backbone of today's ANNs [84].

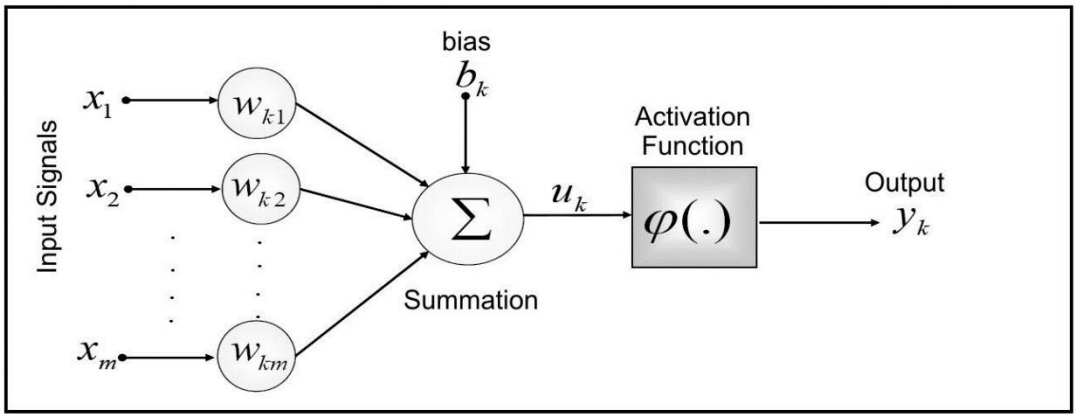

Figure 10: A diagram showing an artificial neuron model [85].

Generally, an artificial neuron (AN) receives input signals from either the environment or other ANs, gathers the information and when fired, transmits the signal to other connected ANs as shown in **Fig. 10** [71]. Each neuron is connected to the next neuron through adaptive synaptic

weights. The strength and firing of each AN are controlled by the activation function. The activation function also calculates the output signal of each AN before passing it to the next neuron. The commonly used activation functions include linear, sigmoid, step, hyperbolic tangent, and rectified linear unit (ReLU) functions [86]. A collection of several connected ANs creates an artificial neural network. The artificial neural network has three layers namely, the input, hidden, and output layers as shown in **Fig. 11** [87]. The input layer receives information from the external environment but does not do any computations. The hidden layers receive the information from the input layer, perform computations and then pass the output layer. Finally, the output layer communicates with the user or external environment about the results. ANNs can store experiential data and make it available when needed [88]. ANNs resemble the human brain in two different aspects which are [87]:

(a) They acquire knowledge through the learning process.

(b) Synaptic weights, which are interneuron connections are used to store the knowledge.

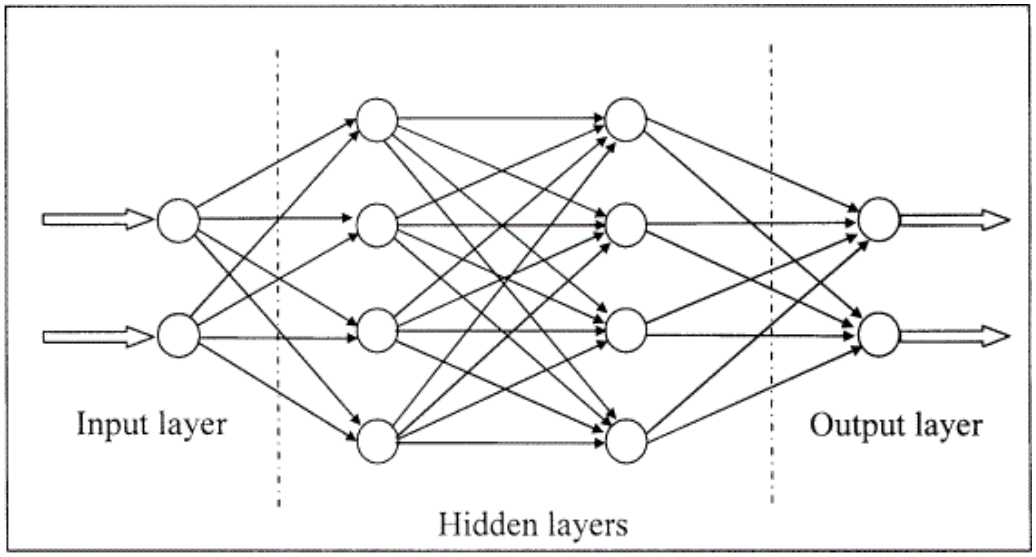

Figure 11: A diagram representing an artificial neural network [89].

Artificial neural networks operate like a " black box" in the sense that they don't need detailed information to perform their tasks [59]. The only important information to supply the neural network is the learning data sets. When training ANNs, the network is given an input to give an output. The network output is then compared to the desired or correct output and if there is a difference, the synaptic weights are adjusted in such a way that decreases the error [90]. The process of adjusting the weights and running through the inputs is repeated until the errors are within the desired tolerance. After the training has reached the desired level, the weights are then held constant and the network will be ready to be used

to make decisions and solving problems. Various algorithms can be used for achieving minimum errors in the shortest time possible. The suitability of these algorithms depends on the type of the problem to be solved. The most common learning algorithm is the back-propagation technique which was introduced by Paul Werbos in 1974 [91]. The back-propagation method is a gradient descent algorithm that improves the performance of the neural network by adjusting the weights along its gradient [92]. Using this method, the error E, is calculated by the root-mean-square (RMS) value as [93]:

$$E = \sqrt{\frac{\sum_{i=1}^{N} (t_i - o_i)^2}{N}}, \quad \textbf{(13)}$$

where t is the neural network output, o is the desired output, N represents a number of samples and subscript i . If the error is zero it means that all the network outputs perfectly match the desired outputs and the network is said to be well trained. In the RMS method, the term epoch refers to the number of iterations through the training data set the machine learning has completed [94].

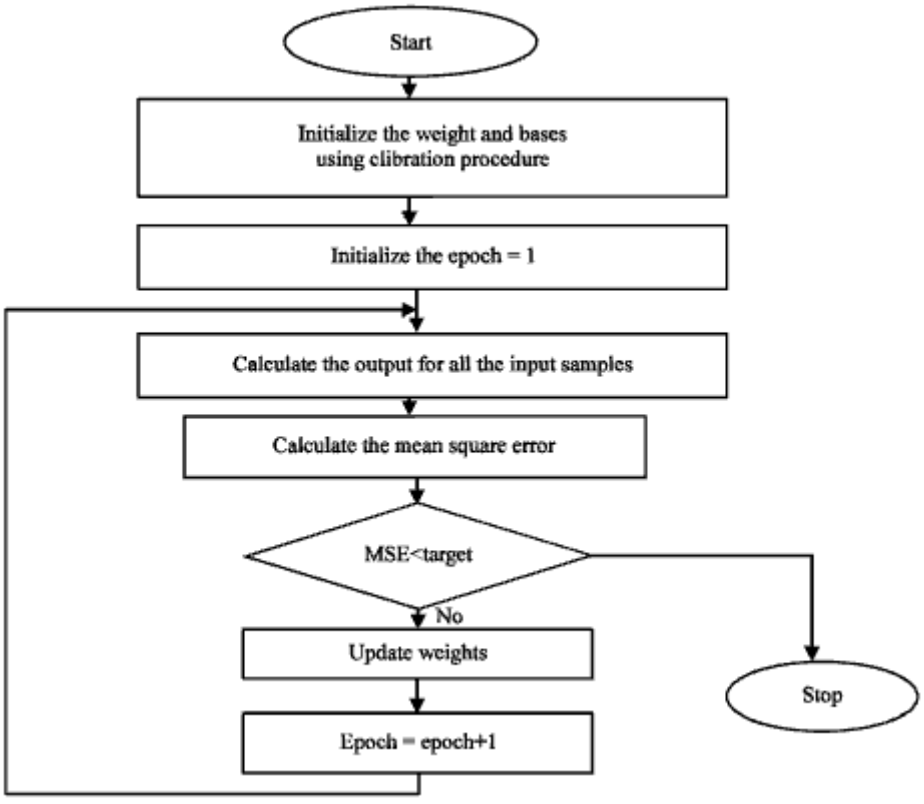

Figure 12: Flowchart of the back-propagation learning algorithm [95].

2.2.2.2 Artificial neural network training

Once the neural network has been structured for a certain application, it should be trained first and the initial weights of the network system are selected randomly [96]. There are two techniques employed when training ANNs namely supervised and unsupervised training. For supervised training, the network is provided with data sets of inputs and desired outputs whilst in unsupervised training the network has to give an output without any outside help [97].

(a) Supervised training

In this method, data sets of the inputs and desired outputs are provided to the network. The inputs to the network are firstly processed and then the network outputs are compared to the desired outputs. If there is a deviation between the two outputs, the error is propagated back to the system, making the system adjust weights in a way that reduces the error [92]. This process continues until the desired output is attained. To adjust network weights, there are many algorithms used and the backward propagation technique is the most common in many applications [91]. However, in some cases, the neural networks never learn. The reason might be that the input data might not have the specific information from which the desired output was derived. If the trained network does not solve given problems, the designer should review the inputs, desired outputs, number of layers, summation transfer functions, activation functions, and the initial weights. Two common supervised learning models are linear regression and the classification technique.

(b) Unsupervised training

In this type of training, the network is provided with inputs but without desired outputs. The ANN itself must decide the features it will use to organize the input data. The network must classify cases based on relationships in the data or naturally occurring patterns. This process is called self-adaption or self-organization [98]. The popular unsupervised learning technique is the clustering method. At present, the use of unsupervised training methods is not very common but some researchers are working on how best to implement this technique.

2.2.2.3 Types of artificial neural networks

There are different types of ANNs and their applications depend on the nature of the problem to be solved. The subsequent section provides a brief description of the commonly known artificial neural networks.

(a) Feedforward neural network.

There is no feedback connection in this type of neural network. The signals travel in one direction only from the inputs to the outputs. The network may or may not include hidden layers and based on that, the network can be further classified as a Single-Layered Perceptron (SLP) or Multiple-Layered Perceptron (MLP) [99]. The number of layers is derived from the complexity of the function and the network has a unidirectional forward propagation. The feedforward network is mainly used for approximations [100]. The diagram below shows an example of a simple feedforward neural network.

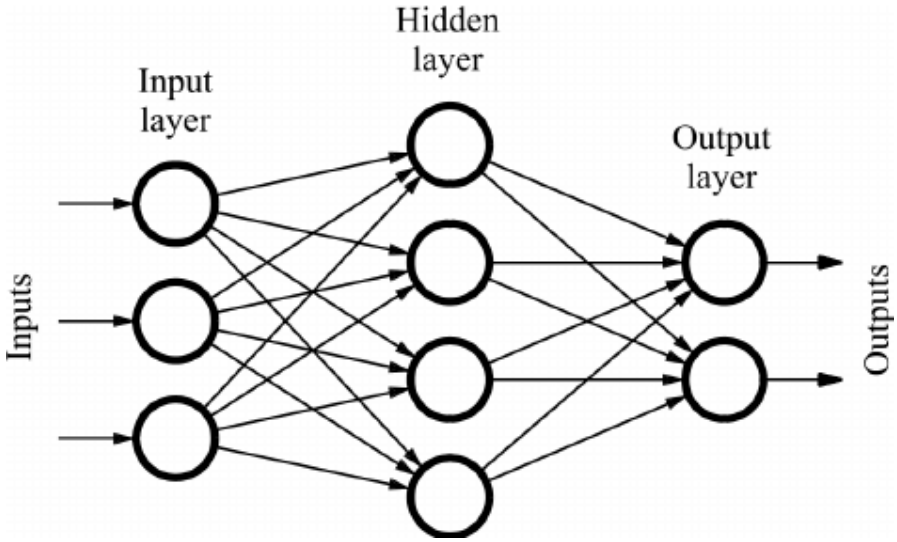

Figure 13: A feedforward artificial neural network [89].

(b) Recurrent neural network

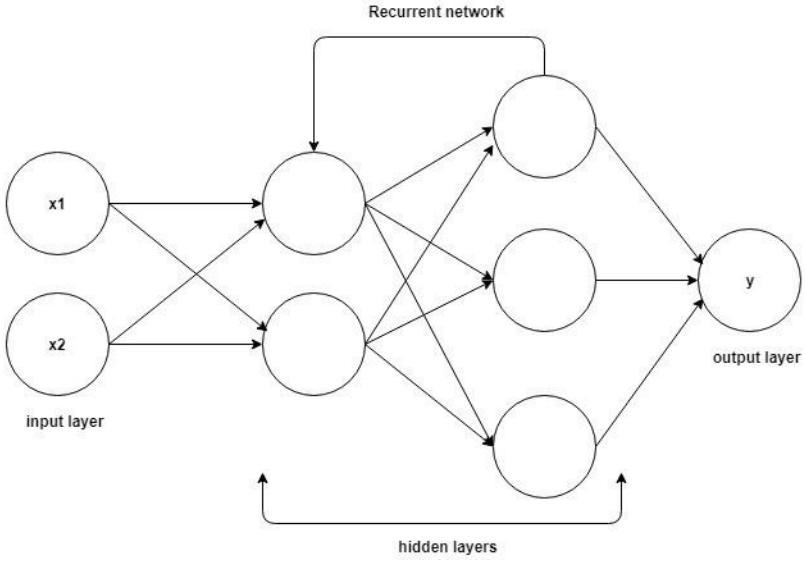

Figure 14: A diagram showing a recurrent network [101].

A Recurrent Neural Network (RNN) is known as the feedback neural network and the connections between neurons form directed cycles [102]. The signals in an RNN travel both in the forward direction and backward direction by the use of loops. RNNs are capable of learning sequences and performing temporary signal processing within the network. Common examples of RNNs are the Hopfield network and the Elman network. **Fig. 14** shows a diagram of an RNN.

2. 3 APPLICATIONS OF AI TECHNIQUES IN RENEWABLE ENERGY TECHNOLOGIES.

The rapid growth of installed renewable energy sources has shown a significant change in the energy industry with a move to replace traditional power generation sources like coal and diesel with renewable energy sources like wind and solar [1]. According to the International Renewable Energy Agency (IRENA), the world installed 176 GW of renewable energy capacity in 2019 with solar and wind having a bigger contribution [2].

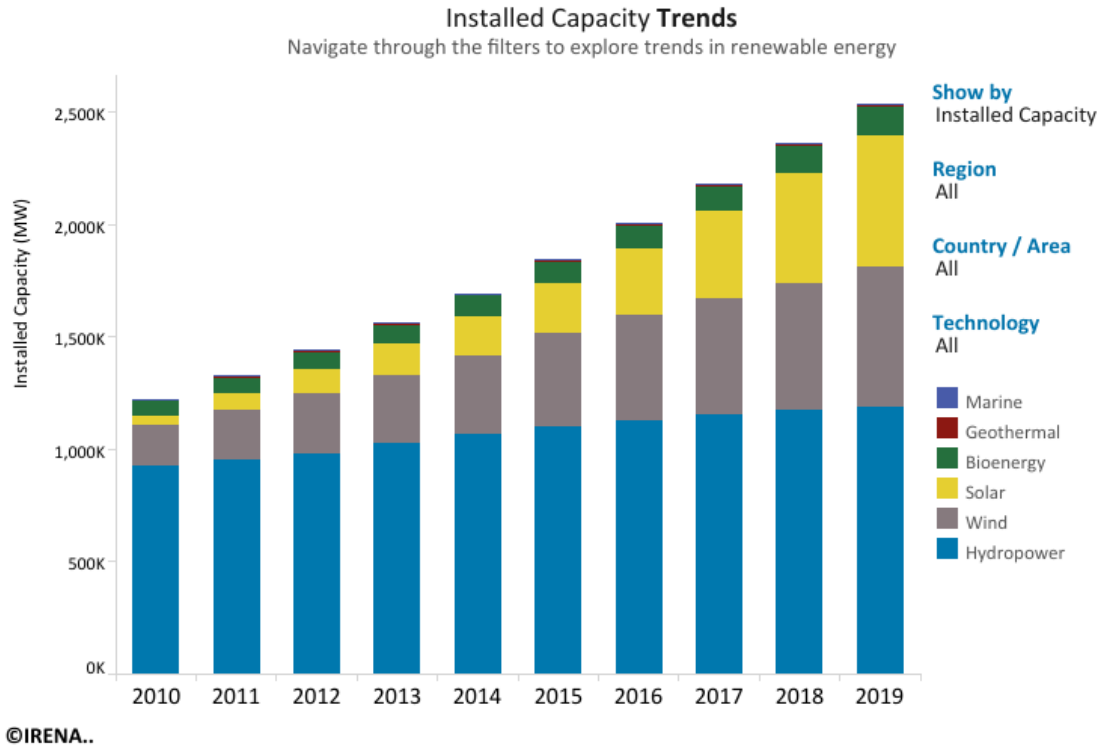

Figure 15: The installed capacity trend of renewable energy sources [103].

The non-linear behaviour of renewable energy sources is a big challenge when designing and implementing renewable energy systems. As the energy sector continues to utilize more renewable energy sources, it is, therefore, crucial to use advanced techniques to maintain

system reliability and efficiency whilst maximizing renewable energy resources. AI techniques (e.g. neural networks, fuzzy logic, genetic algorithms) have emerged as an alternative approach to conventional techniques in solving problems such as modelling and parameter estimation, system optimization, forecasting, energy efficiency, and power flow management of renewable energy systems [104]. The section below gives an overview of where AI techniques were successfully utilized in the field of renewable energy.

2.3.1 Applications of fuzzy logic in the field of renewable energy.

Fathia Checkired [105] published a paper that focused on a fuzzy logic based energy management strategy which was to be used for a home with a grid-tied PV system in 2017. The efficiency of the energy management strategy was tested using a favourable week in summer and an unfavourable week in winter. Their proposed system was able to manage home energy and it was able to save up to 26 % of energy.

In 2011, Onur Ozdal MENGI [106] presented a paper on the designing of a fuzzy logic controller that will give a constant voltage and frequency output amplitude of 380V and 50Hz respectively from the wind/battery hybrid system. The controller was responsible for improving the energy quality coming from a wind/battery hybrid system by stabilizing the voltage and frequency amplitudes at the load terminals. The proposed fuzzy logic-based controller was then compared to the PI controller for results validation. The whole system was modelled and simulated in MATLAB/Simulink.

Yingshu Liu [107] published a paper on the design of a router-based smart home energy management system in 2017. The energy router served as an intelligent interlink between renewable home energy and the power grid. In their paper, the interactions between the power grid, home energy source, and the energy router were analyzed. A control system composed of a reference voltage and a fuzzy logic power management was developed. The model was developed in MATLAB/Simulink and the results revealed that the proposed system was capable of stabilizing the system at the same time having full utilization of the renewable energy generated.

2.3.2 Applications of Artificial Neural Networks(ANNs) in the field of renewable energy

Fermin Rodriguez [108] published a paper on the use of ANNs for predicting the energy produced by PV generators in 2018. They developed a tool that was able to predict parameters involved in solar energy production and thus allowing the estimation of future power

generation. The developed tool used ANNs and it was developed using MATLAB software. The root mean square error method was used to validate the results of their proposed system. The difference between the actual solar energy produced and the estimated was between 0.5-9.0% which was within the desired tolerance.

Karoly Ronay [109] published a paper on the forecasting and system control of a renewable energy micro-grid using ANNs in 2017. In their research work, they used the network function rate to estimate the short time series power output. The predicted power output value was to be used for controlling a renewable energy system as a function of the load demand. Their system consisted of a solar photovoltaic unit and a micro-hydro unit. The main subsystem was the solar unit and the micro-hydro unit served as a reserve.

Masond Vakili [110] published a paper on the prediction of global solar radiation using ANNs. In their paper, they considered the effects of particulate matter air pollution to predict a value very close to the actual global solar radiation. Their ANN modelling strategy was used for estimating the amount of daily absorption of the global solar radiation on the land surface of Tehran. Their results showed a satisfying performance of the proposed strategy.

2.4 RENEWABLE ENERGY RESOURCES AND THE ENVIRONMENT.

Renewable energy can be defined as an inexhaustible energy source that is naturally replenished such as solar, wind, and biomass [111]. Sustainable application of renewable energy technologies must certainly include the analysis of environmental impacts associated with these energy sources. Substituting harmful fossil fuel-powered systems with renewable energy sources helps to mitigate issues like air and water pollution, excessive water and land use, global warming, and damage to public health [112]. On the other hand, we must also understand the impacts of those alternatives when assessing their use at a specific locale. In the next section, the environmental impacts of different types of renewable energy sources are explained.

2.4.1 Environmental Impacts of Solar Power

Solar power generation is now a proven technology with minimum negative environmental impacts as compared to other dangerous electricity-generating technologies [113]. Solar power generation can be grouped into two technologies namely photovoltaic solar cells and concentrating solar thermal plants (CSP) and the possible environmental impacts associated with these technologies include water use, land use, and use of harmful chemicals [114].

Depending on the site of installation, large solar farms may raise concerns about habitat loss and land degradation [115]. The total land use for solar systems varies depending on the intensity of the solar irradiation, the technology to be used and the topography of the location. PV cells do not need water to generate electricity. However, water is used in the manufacturing process of PV components. When it comes to concentrating solar thermal plants, a vast amount of water is needed for cooling the system. There are various chemicals used when manufacturing PV solar cells. These chemicals include 1,1,1-trichloroethane, hydrochloric acid, sulfuric acid, nitric acid, acetone and are used to clean and purify the semiconductor surfaces [116].

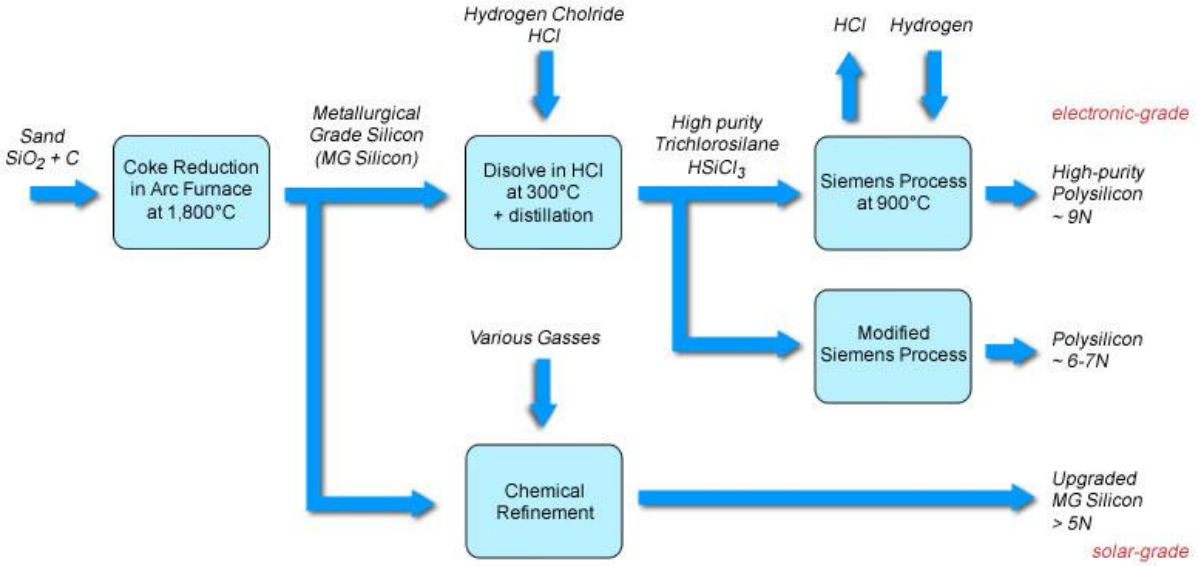

Figure 16: Manufacturing process of PV solar cells [117].

The chemicals could be released in the air, land, and water bodies and the types and amounts of chemicals used depend upon the type and quantity of solar cells being manufactured [118]. **Fig. 16** shows the manufacturing process of PV solar cells.

2.4.2 Environmental Impacts of Wind Power

Generating power from wind is one of the cleanest and sustainable methods that gives minimum environmental impacts [119]. Harnessing energy from wind turbines does not produce any greenhouse gases and substance pollution. Another advantage of wind power is that wind turbines occupy less land per unit kilowatt-hour (kWh) of power generated than other power generating sources [120]. Even though wind power has a lot of advantages, there are some environmental impacts associated with wind power generation that must be addressed. Noise pollution is the main concern when generating power from wind turbines [121]. The

sound produced is mostly created by the aerodynamic nature of the wind turbines when they move through the air and the mechanical movement of the parts that make up the turbines. Generally, the noise levels depend on the design and speed of the wind turbine. Another issue is that wind turbines may cause shadow flickers at locations where the turbine obstructs the sun's rays [122]. However, this problem may be resolved by an appropriate locating of wind farms or switching off the turbine for a few minutes when the sun's position is at an angle that produces a flicker. Another impact is related to wildlife, particularly bats and birds [123]. Several studies show how wind turbines can present hazards to avian species. Birds or bats can directly crash into stationary or moving wind turbines or crash into towers which may result in the deaths of these species.

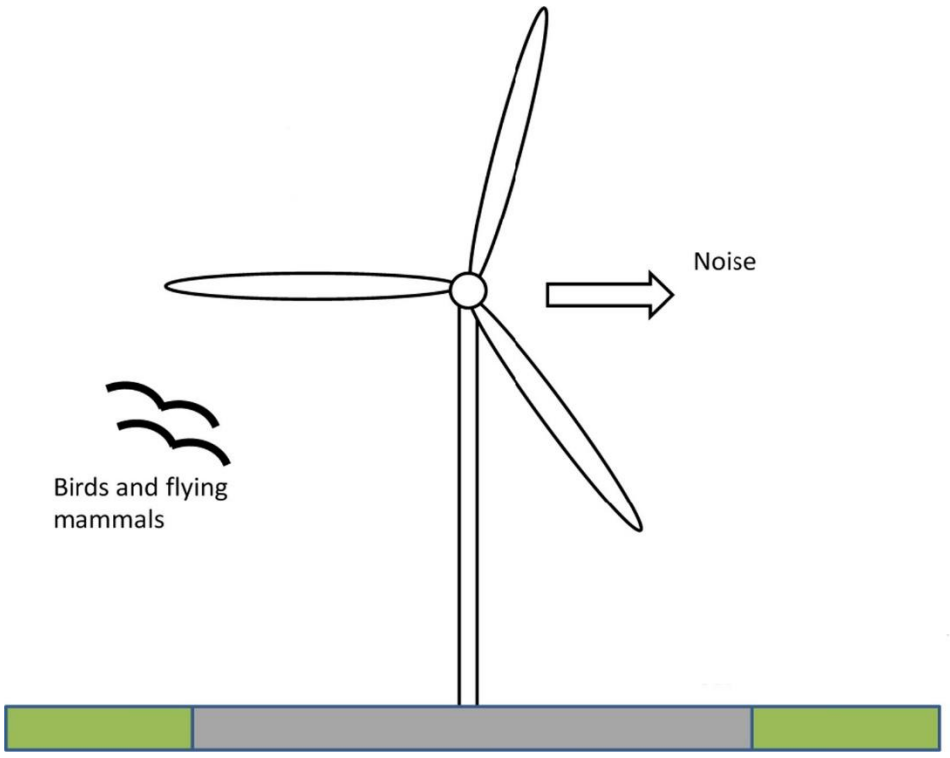

Figure 17: Environmental impacts of wind power generation [119].

However, through research and advances in wind turbine technology, the deaths of avian species were notably reduced [122].

2.5 SOLAR PHOTOVOLTAIC ENERGY

Photovoltaic (PV) is a process of converting solar irradiance into electricity by using semiconductors materials that exhibit a property known as the photovoltaic effect [124]. The photovoltaic effect is defined as the emission of electrons from a material that has absorbed light with a frequency above the material threshold frequency. PV power generation is

comprised of solar panels made of solar cells that contain photovoltaic materials. There are three main types of PV modules for both residential and commercial applications namely monocrystalline, polycrystalline, and thin film. Each type has its disadvantages and advantages depending on the application of that particular solar module.

1) Monocrystalline modules

Monocrystalline modules (also known as single crystalline silicon modules) are made up of solar cells that are made out of cylindrical silicon ingots. These PV modules offer higher efficiencies because they are made out of high silicon grade. However, the disadvantage of monocrystalline panels is that if the PV module is partially shaded, the entire circuit may break down. Another disadvantage is that they are expensive hence not quite suitable for large scale solar power plants. The diagram below shows an example of a monocrystalline solar module.

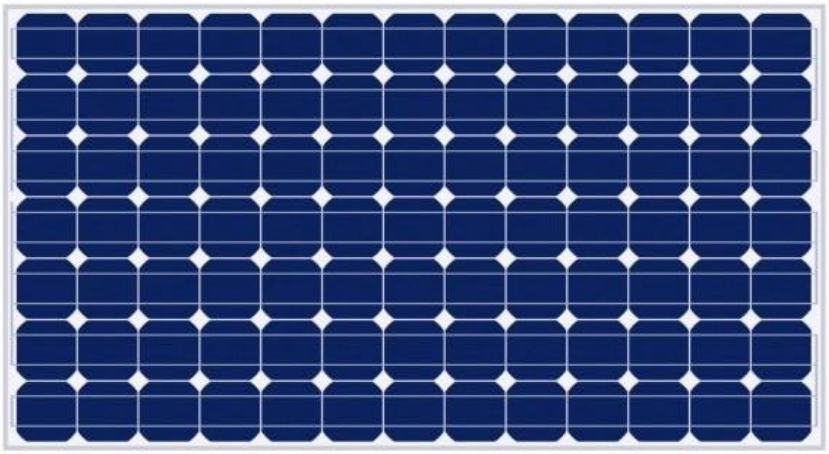

Figure 18: Monocrystalline solar cell [125].

2) Polycrystalline modules

Polycrystalline silicon solar cells are made by melting and pouring raw silicon into moulds, which are cooled and cut into square wafers. The amount of waste silicon used in these panels is less as compared to those in monocrystalline modules. The manufacturing of polycrystalline silicon is simpler and this is why polycrystalline silicon solar panels cost less, which makes them suitable for large scale solar PV plants and rural electrification. A typical polycrystalline module is shown in the diagram below.

Figure 19: Polycrystalline solar module [126].

3) Thin-film modules

Thin-film panels are made by mixing photovoltaic materials with a substrate. The type of substrate used determines the final product of the thin-film panel. There are different types of thin-film modules including amorphous silicon, organic photovoltaic cells and cadmium telluride cells. These have the lowest efficiency range (7- 13%) because of the lower level of purity of the silicon used in their production. Higher temperatures have less impact on the performance of the cell and they cost less compared to the monocrystalline and polycrystalline modules. However, thin-film modules tend to degrade at a faster rate as compared to the other two technologies. The diagram below shows a thin-film solar module.

Figure 20: A diagram of a thin-film solar module [127].

2.5.1 Solar photovoltaic systems

1) Grid-tied solar system

A grid-tied solar system is when the solar system is connected to the utility grid. Grid-tied solar systems can be either battery-less or battery-based. Grid-tied PV systems are only applicable in areas where there is access to grid electricity. The power from PV modules is converted from DC to AC to supply the load. If the solar system's power is not enough to supply the load, the power is drawn from the utility. Grid-tied systems range from small residential rooftop systems to large solar power plants. The main objective of this setup is to reduce daytime electrical bills by utilizing solar energy during the day [128]. Also, users of this system can sell their extra electricity to the utility and make profits.

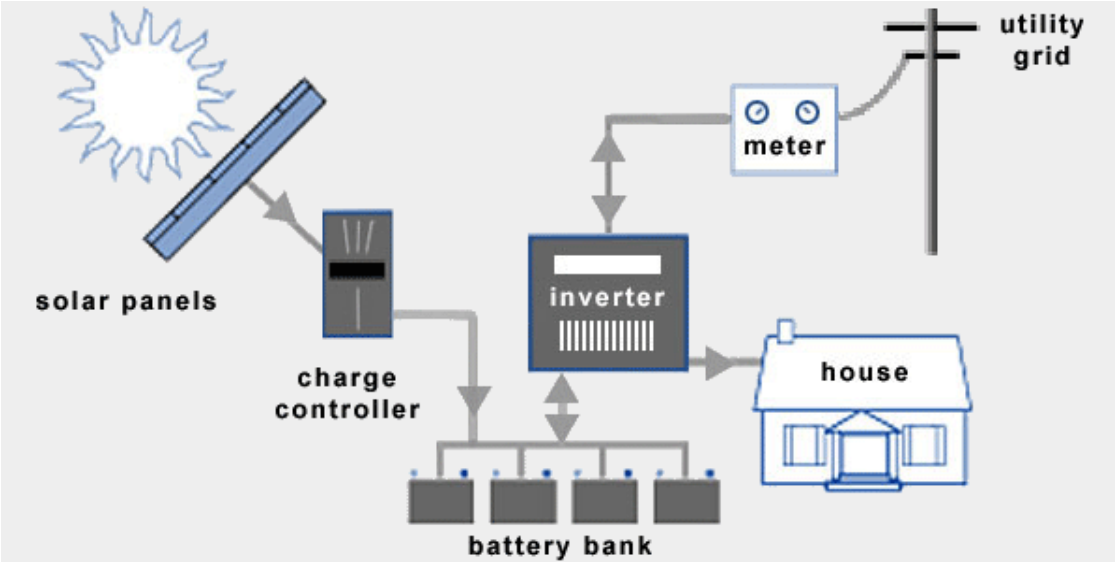

Figure 21: Typical grid-tied PV system [129]

2) Off-grid PV system

Off-grid PV systems, also known as stand-alone PV systems, are solar systems that are not connected to the utility grid [130]. They are usually backed up with batteries, diesel generators or both. The power generated from PV modules as DC power can directly supply DC loads or be converted to AC power using inverters to supply AC loads. They are most suitable for remote and off-grid applications like powering communication satellites, remote homes & villages, and water pumping systems [131].

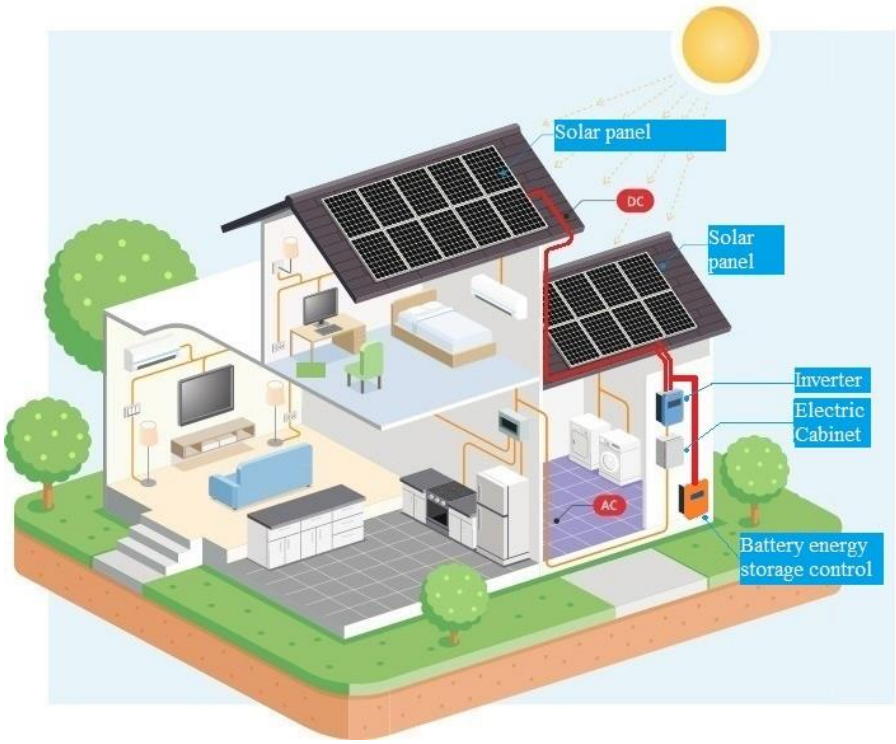

Figure 22: Typical stand-alone PV system [132]

3) Building-integrated PV system

Photovoltaic cells can be incorporated in building materials in the building's parts such as roofs, facades, and wall glasses [133].

Figure 23: Building-integrated PV system [134]

In Building-Integrated Photovoltaic (BIPV) systems, PV solar collectors are integrated into the building's structure as part of the design. Thus, the system serves a dual purpose; replacing conventional building materials and generating electricity. When conventional materials are

substituted with PV materials, there are some savings involved [135]. This advantage makes BIPV one of the promising technologies in the PV industry. BIPV systems can power up the whole building where peak electricity demand is during the daytime and uses the existing grid as backup. These systems are usually used in commercial buildings.

2.5.2 Solar geometry

When designing PV systems, it is essential to comprehend the relationship between the Earth and the Sun [136]. Such information is essential in assisting when selecting the most effective tilt angles, solar cells orientation as well as impacts of overshadowing obstructions. The following section will cover the terms that are used to explain the Earth-Sun relationship.

- **Solar radiation**

Solar radiation is defined as the radiated energy from the sun which comes in a form of electromagnetic waves including visible, ultraviolet and infrared light [137]. Solar radiation reaches the earth as direct/beam radiation, diffuse radiation and reflected radiation. Direct radiation travels down the earth's surface in a straight line without any atmospheric losses due to scattering or absorption. Diffuse radiation reaches the earth's surface after it has been scattered or absorbed by particles in the atmosphere. Lastly, reflected radiation is the one that reaches the earth's surface after being reflected with non-atmospheric substances like the ground. The total radiation which is the summation of these three types of radiation is called the Global Horizontal Irradiance (GHI).

- **The angle of declination, δ**

The solar declination angle is defined as the angle between the line drawn from the sun to the centre of the earth and the equator [138]. Solar declination is zero at equinoxes and ± 23.45° at solstices. The solar declination angle is given by Cooper's equation [139],

$$\delta = 23.45 sin\left[\frac{360(284+n)}{365}\right] \quad \textbf{(14)}$$

where n is the day number of the year i.e. $n = 1$ for January 1.

- **Solar hour angle, ω**

The solar hour angle is defined as the angular displacement of the sun which can be east or west of the local meridian due to the rotation of the earth on its axis. It is negative in the morning and positive in the afternoon [138]. It describes the difference between the local solar time of

the day when the rays of the sun are perpendicularly directed to a given line of longitude. The solar hour angle is given by the equation,

$$\omega = 15\{t - 12\} \quad \textbf{(15)}$$

where t is solar time.

- **Sunset and sunrise angle**

The sunset hour angle corresponds to the time of the evening when the sun disappears and it is useful in the solar energy yield analysis. It can be derived from the equation,

$$cos\ \omega_s = -tan\phi tan\delta, \quad \textbf{(16)}$$

where ϕ is the latitude of the site and δ represents the angle of declination. The sunrise hour angle is the angle that corresponds to the time when the sun rises. Assuming there is symmetry between the time of sunrise and sunset, the sunrise hour angle is given by:

$$\omega_r = -\omega_s \quad \textbf{(17)}$$

- **Tilt angle, β**

The tilt angle is defined as the angle between the horizontal and the plane of the PV module. Solar PV collectors can either be fixed optimum tilt or manually adjustable tilt depending on the system design. According to [7], the optimum tilt in Zimbabwe is given by:

$$\beta = |\phi| + 5^o \quad \textbf{(18)}$$

- **Surface azimuth angle**

The surface azimuth angle is defined as the deviation of projection that is on a horizontal plane, normal to the surface from the local meridian. It is positive in the east and negative in the west.

$$-180 \leq \gamma \leq 180 \quad \textbf{(19)}$$

- **The angle of Incidence, θ_i**

The angle of incidence can be defined as is the angle between the normal to the surface and the sun's beam radiation. The diagram below shows the orientation of the tilt angle, altitude angle, and the angle of incidence.

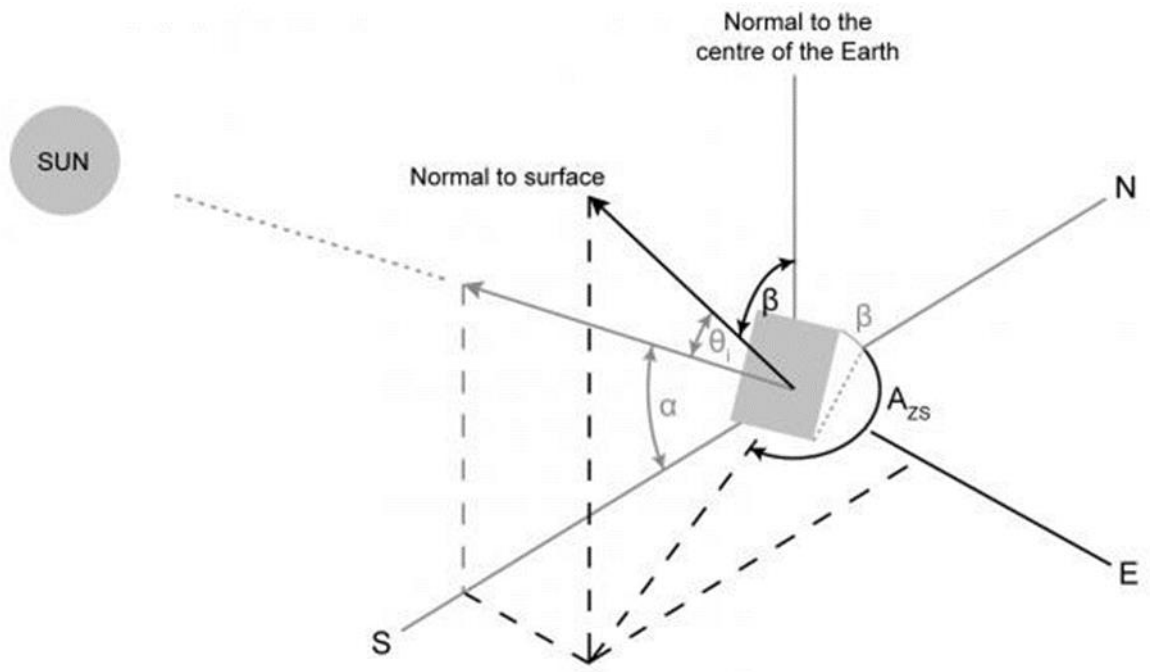

Figure 24: Visualization of the varying solar angles [140].

$$cos\theta i = sin\delta sin\varphi cos\beta - sin\delta cos\varphi cos\gamma + cos\delta cos\varphi cos\omega + cos\delta sin\varphi sin\beta cos\gamma cos\omega + cos\delta sin\beta sin\gamma sin\omega \quad \textbf{(20)}$$

- **Solar azimuth angle**

This describes the sun's position in the sky relative to the observer on earth. The range for this angle is $-180 \leq \boldsymbol{\gamma_s} \leq 180^{\circ}$ and it is calculated from the equation below,

$$\gamma_s = -\left(C_1 C_2 C_3 \gamma'_s + C_3 \left(\frac{1 - C_1 C_2}{2}\right) 180\right) \quad \textbf{(21)}$$

Where, $\gamma_s = \frac{sin\omega cos\delta}{sin\theta_z}$

$C_1 = 1\ if\ |\omega| < \omega_{EW},$

$= -1\ otherwise$

$C_2 = 1\ if\ \varphi(\varphi - \delta) \geq 0$

$= -1\ otherwise$

$C_3 = 1\ if\ \omega < 0$

$= -1\ otherwise$

$cos\omega_{EW} = \frac{tan\delta}{tan\varphi}$

And the rest of the symbols have their usual meanings.

2.5.3 Solar radiation data

PV system design depends on the accessibility of solar radiation data as well as parameters related to the site. The term solar radiation refers to the radiant energy emitted by the sun whereas the amount of the solar radiation received by a surface per unit area (W/m^2) is called solar irradiance [141]. The solar radiation data is very useful in predicting the long term performance of photovoltaic systems. The site-related parameters which must be considered when designing PV systems include latitude, longitude and ambient temperatures. Ambient temperatures are used to estimate the PV cell temperatures whilst the latitude and longitude values are utilized in solar angle calculations. Two main instruments that are used to measure solar radiation are the pyranometer (measures the total hemispherical radiation) and pyrheliometer (measures normal incidence direct beam radiation) [142]. Since the solar radiation measuring instruments are not always readily available, several isotropic and anisotropic hourly tilted surface radiation models have been developed and suggested by different researchers. These models include the Hays model, Muneer model and Perez model. The solar radiation data used in this research work was obtained from the PVGIS website database (*Appendix B*). The model used in PVGIS is the Muneer model which is classified as the anisotropic of two components. According to [143] the Muneer model offers better results since it can distinguish clear and overcast conditions, then sunlit and shaded surfaces.

2.5.3.1 The site and solar radiation data

The proposed water pumping system is to be used at the Makarepo irrigation scheme. Makarepo irrigation scheme is situated in Tshovani village, in Chiredzi, Zimbabwe. This village is in the low-veld area of the country where temperatures are relatively high. The village receives low rainfall and most of the farming activities are under irrigation schemes. Farmers at Makarepo rely on diesel or petrol-powered water pumps and the introduction of solar-powered water pumps will largely benefit them. The irrigation scheme is a 10 ha area divided into several plots where each farmer owns approximately 1 ha. They grow crops such as tomatoes, beans, onions, maize and several vegetables to supply the small town of Chiredzi. For the successful design and implementation of the proposed solar/diesel hybrid water pumping system, the solar radiation and temperature data is required for training the ANFIS based MPPT controller as well as sizing the PV array. To extract the solar radiation and temperature data from the PVGIS website, the geographical coordinates of the site are needed. The exact geographical location of Tshovani village is given below:

Latitude: - 20.983°

Longitude: 32.104°

Altitude: 508m

2.5.3.2 PVGIS data collection

The hourly irradiation data was collected at an optimum tilt angle of 35 °. The PVGIS application gives average solar irradiation data for every hour of each month, with the average taken over all days of each month and recorded over a multi-year period. Also, the daily radiation application calculates the variation of the daily clear-sky radiation for both fixed and solar-tracked surfaces. This solar daily radiation data consists of 24 hourly values of the average solar irradiance at each hour for every month of the year. The corresponding hourly temperature data was also given. The diagrams below show the extracted data for June.

Irradiance on a fixed plane

Time	00:45	01:45	02:45	03:45	04:45	05:45	06:45	07:45	08:45	09:45	10:45	11:45	12:45	13:45	14:45	15:45	16:45	17:45	18:45	19:45	20:45	21:45	22:45	23:45
G	0	0	0	0	22	58	88	168	223	247	232	179	100	65	26	0	0	0	0	0	0	0	0	0
Gb	0	0	0	0	0	0	21	82	124	139	126	86	28	0	0	0	0	0	0	0	0	0	0	0
Gd	0	0	0	0	21	56	60	77	87	95	94	83	64	63	25	0	0	0	0	0	0	0	0	0

G: Global irradiance on a fixed plane [W/m2].
Gb: Direct irradiance on a fixed plane [W/m2].
Gd: Diffuse irradiance on a fixed plane [W/m2].

Figure 25: Hourly solar irradiance data for June [144].

Average daily temperature profile

Time	00:45	01:45	02:45	03:45	04:45	05:45	06:45	07:45	08:45	09:45	10:45	11:45	12:45	13:45	14:45	15:45	16:45	17:45	18:45	19:45	20:45	21:45	22:45	23:45
Td	14.5	14.1	13.7	13.2	14.2	15.1	16	18	20.1	22.1	22.7	23.4	24	23.2	22.3	21.4	20.1	18.8	17.5	16.9	16.3	15.7	15.3	14.8

T: Average daily temperature profile [°C].

Figure 26: Average hourly temperature data for June [144].

2.5.4 Maximum power point tracking

Maximum power point tracking (MPPT) controllers are algorithms that are included in PV battery charge controllers or inverters to extract the maximum available power from a PV module for any given temperature and irradiance [145]. For any set of temperature and irradiance, the operating point of a PV module corresponds to a unique point on the current-voltage (I-V) curve. The operating point on the I-V curve also corresponds to some point on

the power-voltage (P-V). For the PV module to produce the highest power output, its operating point must correspond to the maximum point on the P-V curve known as the Maximum Power Point (MPP) as shown in **Fig. 27**. And if the irradiance or temperature changes, the position of the MPP also shifts. Therefore, it is the responsibility of the MPPT controller to continuously track the position of the MPPT for any given environmental condition. Generally, an MPPT is comprised of a DC-DC converter which is controlled by an algorithm to force the solar module's operating point to be at MPP at all times.

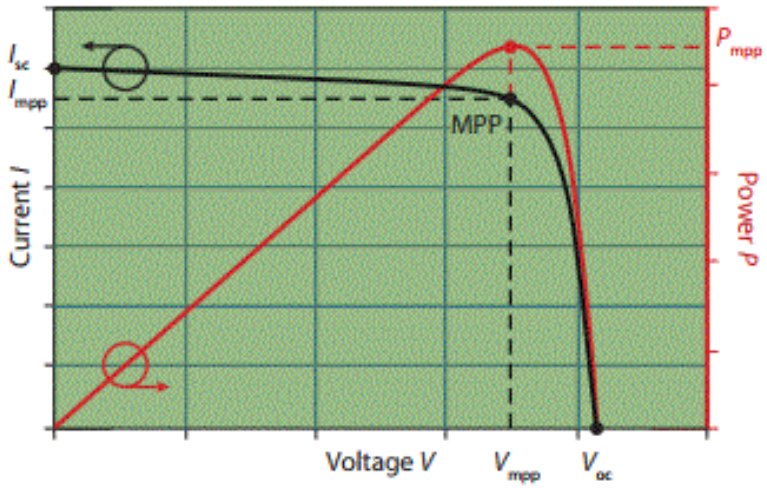

Figure 27: A diagram showing I-V and P-V curves for MPPT [146].

Connecting the PV module directly to the load makes the module's operating point to be dictated by the load. Thus, the PV module only operates at MPP if the load impedance matches the input impedance to the DC-DC converter as seen by the PV module otherwise it can operate at any point on the P-V curve which might not be the MPP. The concept of matching the impedances for maximum power extraction is well explained by the Maximum Power Transfer Theorem (MPTT).

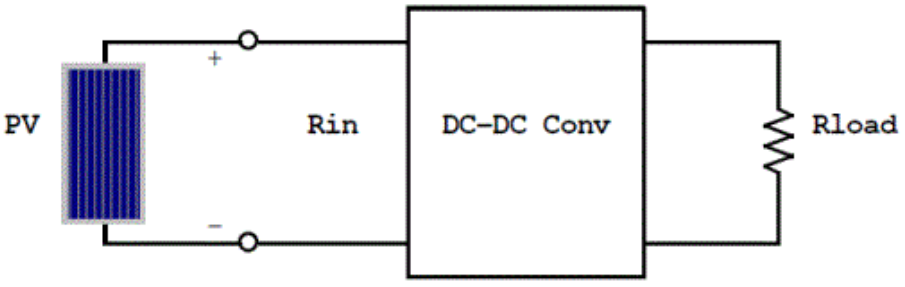

Figure 28: Impedance matching using DC-DC converters [147].

The load impedance R_{load} and the input impedance to the converter R_{in} rarely match and an appropriate algorithm must be employed to match these impedances by adjusting the duty cycle of the DC-DC converter. Various MPPT algorithms have been proposed for tracking the maximum power point of solar modules. MPPT techniques differ in many aspects such as complexity, tracking speed, efficiency, cost, and hardware implementation. The section below will give a brief description of commonly known MPPT techniques.

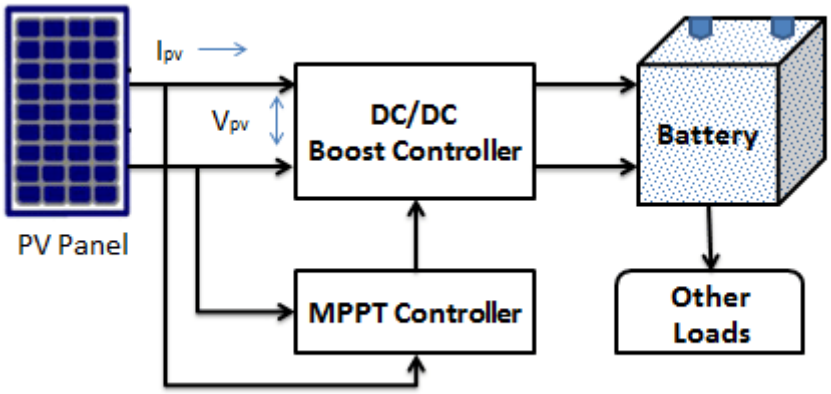

Figure 29: Typical setup of an MPPT controller and DC-DC converter [148]

Types of MPPT techniques

1) Incremental Conductance

Incremental conductance is one of the simplest and oldest techniques for tracking the maximum power point of solar modules. This technique is based on the fact that the gradient of the power-voltage curve of the PV module is zero at the MPP, negative on the right and positive on the left of the MPP [149]:

$$\begin{cases} \frac{dP}{dV} = 0, at\ MPP \\ \frac{dP}{dV} > 0, on\ the\ left\ of\ the\ MPP \\ \frac{dP}{dV} < 0, on\ the\ right\ of\ the\ MPP \end{cases} \quad \textbf{(22)}$$

And knowing that $P = IV$, the equation of the power curve at MPP is given as,

$$\frac{dP}{dV} = \frac{d(IV)}{dV} = I + \frac{V\Delta I}{\Delta V} \quad \textbf{(23)}$$

And equating **Equation 23** to zero, which is a condition for MPP, we get,

$$I + \frac{V\Delta I}{\Delta V} = 0 \tag{24}$$

Therefore, the equations for incremental conductance can be written as,

$$\begin{cases} \frac{\Delta I}{\Delta V} = -\frac{I}{V}, at\ MPP \\ \frac{\Delta I}{\Delta V} > 0, left\ of\ the\ MPP \\ \frac{\Delta I}{\Delta V} < 0, right\ of\ the\ MPP \end{cases} \tag{25}$$

Therefore, it can be seen from the above equations that this method depends on incremental conductance and instantaneous conductance. The diagram below shows the graphical explanation of the incremental conductance method.

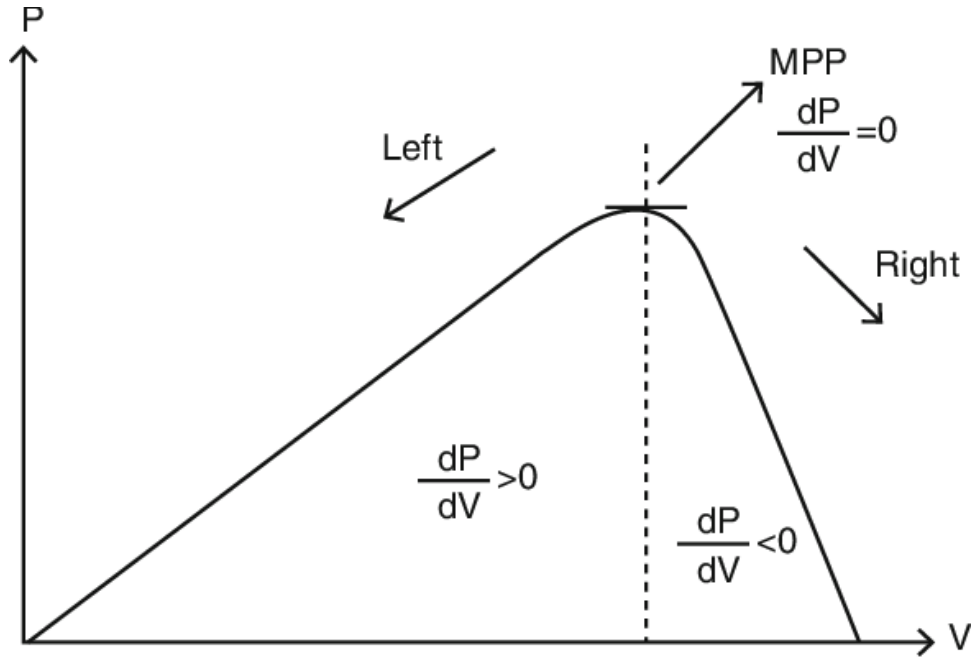

Figure 30: Incremental conductance method for MPPT [150].

This method can also be illustrated using a flowchart as shown in **Fig. 31**. The first step of this method is to calculate the change in voltage and current. If the voltage change is not equal to zero, then the instantaneous conductance is compared to the incremental conductance. If the incremental conductance is equal to instantaneous conductance, the algorithm gets terminated because the MPP will be reached. When the incremental conductance is not equal to the instantaneous conductance, the PV module's voltage is adjusted using a DC-DC converter in

such a way that meets the condition of the MPP. This technique uses fixed step sizes for updating the operating voltage of the system,

which is one of the drawbacks of using this method [38]. Thus, the selection of the step size is crucial for the efficiency of the algorithm.

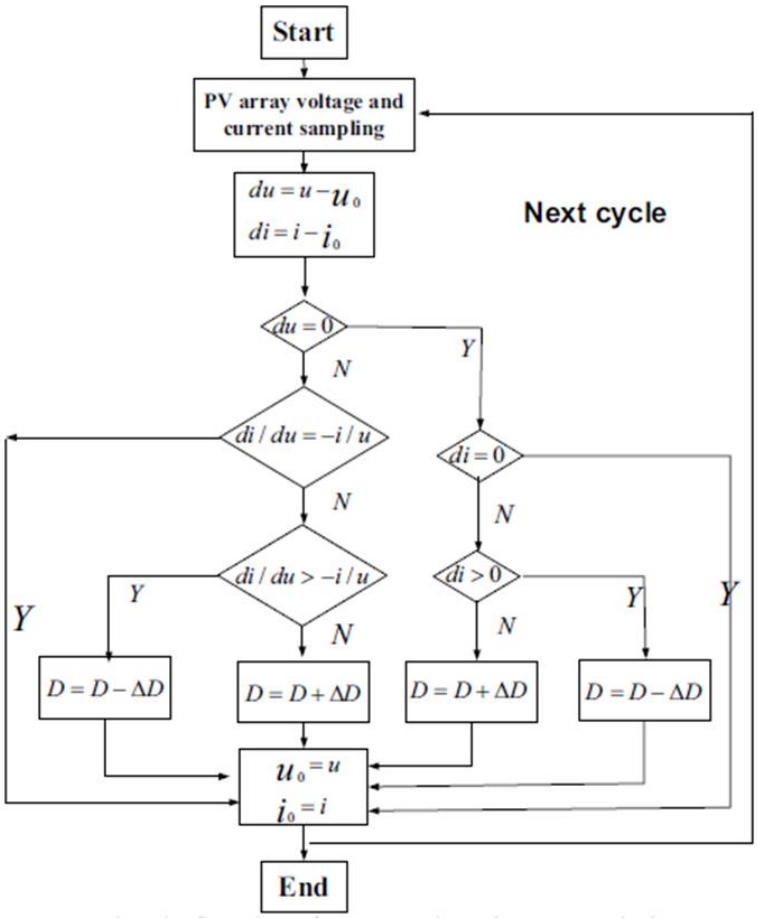

Figure 31: Incremental conductance method flow chart [151].

1) Perturbation and Observe technique

This method is also well-known as hill climbing and is one of the oldest algorithms for MPPT. The Perturbation and Observe (P&O) method is considered as the cheapest MPPT technique due to easy implementation and the requirement of fewer parameters [152]. The first step in this method is to introduce a perturbation/disturbance in the PV module's operating voltage. The modification of the module's voltage is achieved by varying the duty cycle of the DC-DC converter. After introducing a disturbance, the present value of the power output is calculated and compared to the previous value to give a difference in power, ΔP. If ΔP is greater than zero, the perturbation is kept in the same direction and when it becomes negative the perturbation is reversed. This process is repeated several times until the MPP is reached. The

main disadvantage of the P&O method is that it uses fixed step sizes to decrease or increase the voltage.

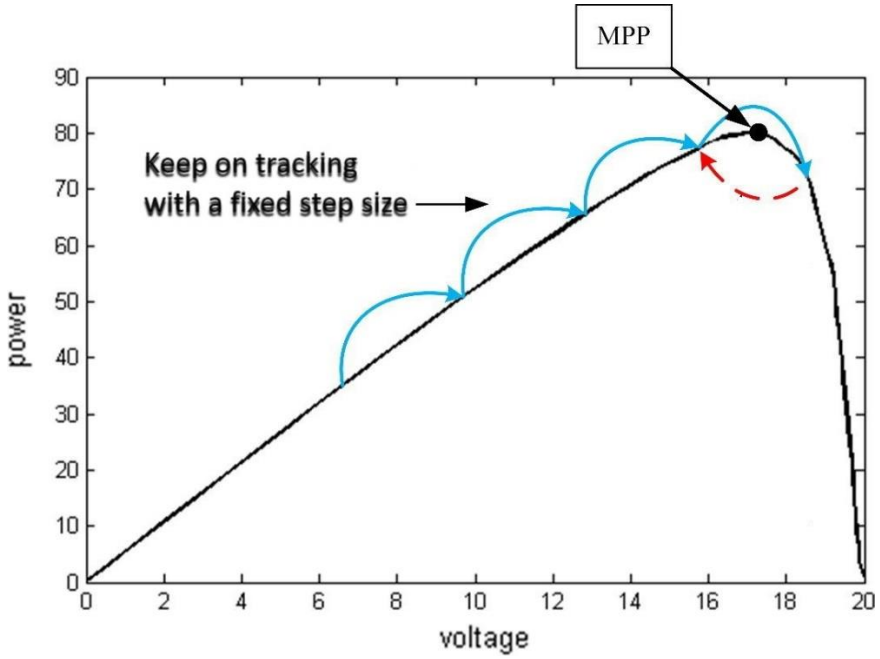

Figure 32: Illustration of the P&O method [153].

The selection of the step size determines the size of the deviation when oscillating about the MPP. A smaller step size gives reduced oscillations but having a slower tracking speed whilst bigger step sizes help to reach the MPP faster but much power is lost when oscillating about the MPP. The flowchart of the P&O technique is shown in the diagram below.

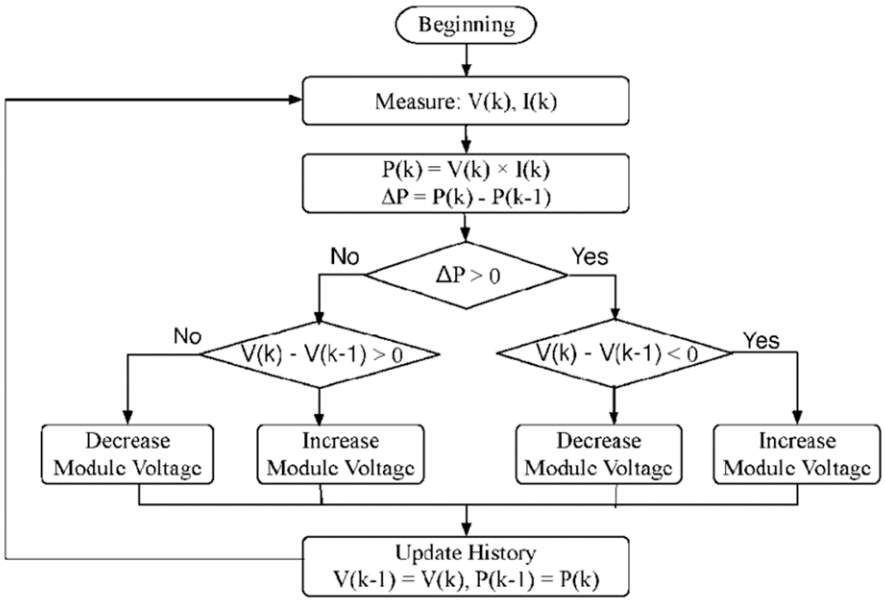

Figure 33: A flow chart for a P&O technique [154].

2) Fuzzy logic based MPPT controller

With the increase in the adoption of soft computing techniques, Fuzzy Logic (FL) has also been proposed for tracking the MPP of solar modules. FL is based on the theory of fuzzy sets and offers good results for complex and non-linear applications. Fuzzy logic control is implemented through three stages which are (a) fuzzification, (b) decision-making and (c) defuzzification. At the fuzzification stage, a crisp input variable is converted into a linguistic variable using membership functions. And the decision-making stage consists of IF-THEN rules to define the behaviour of the controller.

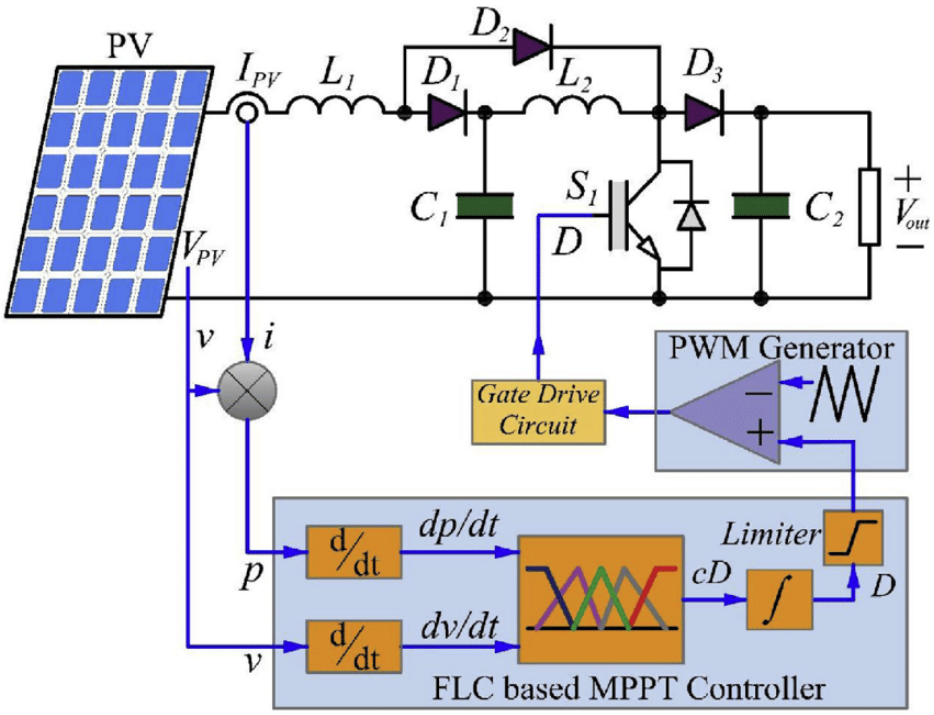

Figure 34: A typical fuzzy logic based MPPT controller [155].

Lastly, in the defuzzification stage, linguistic variables from the decision-making stage are converted to a crisp output value. This output value gives a control signal to the DC-DC converter to drive the PV module's operating point to be at the MPP. The FL algorithm tracks the MPP based on the rule that: if the change in the operating voltage has caused the power to increase, keep the changing in the same direction; else if it has caused the power to decrease, move it the opposite direction [156]. The inputs to the FL controller are usually the error, E and change in error with respect to change in voltage, ΔE and the output can be the duty cycle, V_{mp} or I_{mp} [155, 156]. The controller calculates the error and change in error using values from the PV module. The error and change in error are given by the following equations:

$$\begin{cases} E(k) = \dfrac{P(k) - P(k-1)}{V(k) - V(k-1)} \\ \Delta E = E(k) - E(K-1) \end{cases} \quad \textbf{(26)}$$

Where $P(k)$ and $V(k)$ are instantaneous power and voltage respectively.

3) Artificial neural network-based MPPT controller

Artificial neural networks have been proposed for different applications such as weather forecasting, industrial processes optimization as well as tracking the maximum power point of PV modules. ANNs imitate the behaviour of biological neural networks which makes them a perfect option for solving real-life non-linear problems. Artificial neural networks learn from given examples so that when they encounter the same situation in the future they will be able to give a solution. A typical ANN architecture is shown in **Fig. 35**. For MPPT, the inputs to the ANN controller vary depending on the design and application. The usual inputs are environmental variables like the solar irradiance and temperature as well as PV module's variables such as short-circuit current and open-circuit voltage. The outputs might be the duty cycle, current at the MPP, the voltage at the MPP or the desired maximum power value. The output of the ANN controller gives a signal to the DC-DC converter to force the panel to operate at MPP by varying the duty cycle.

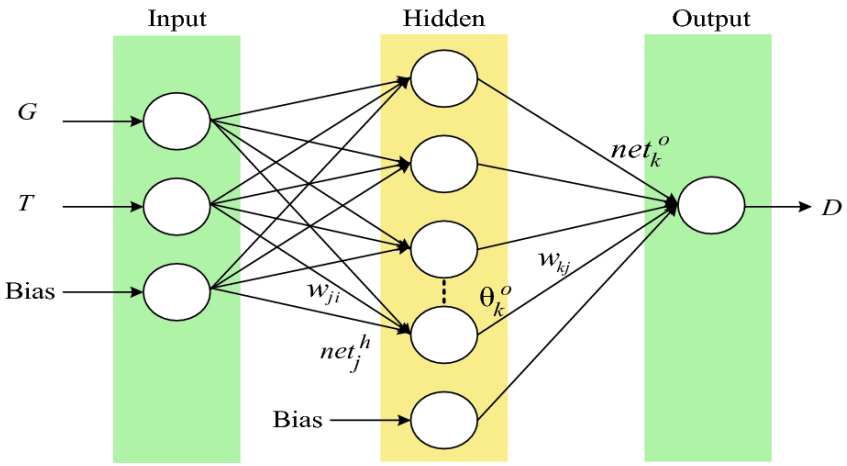

Figure 35: The structure of an ANN-based MPPT controller [157]

2.6 DIESEL GENERATORS

Diesel Generators (DG) are electrical machines that convert fuel/chemical energy (diesel) into electrical energy. The chemical energy is first converted to mechanical energy using combustion engines and then from mechanical energy to electrical energy using alternators

[158]. The key components in a diesel generator are an internal combustion engine, mechanical coupling, alternator, cooling & exhaust system, fuel system, voltage regulator, battery charger, lubrication mechanism, control panel and frame. The description of the main components of diesel generators is given below:

2.6.1 Main components of diesel generators

- **Internal combustion engine**

A diesel generator's principle of operation is based on the law of conservation of energy which states that energy can neither be created nor be destroyed but can only be converted from one form to another [159]. During the combustion process in the engine, the chemical energy in diesel is converted to heat energy and mechanical energy. The combustion process is done through a spontaneous ignition of the diesel when injected into a highly compressed hot charge of the air.

- **The alternator**

The alternator converts the mechanical energy from the internal combustion engine to electrical energy. The alternator is made up of stationary and moving parts enclosed in the housing. The relative motion which is created between the magnetic and electric fields is responsible for generating electricity in the alternator. The main components of the alternator are given below:

(a) *Stator* – it is the fixed part of the alternator and it doesn't rotate. The stator contains electrical wires coiled around an iron core.

(b) *Rotor* – this is the part that rotates in an alternator. The rotor creates a rotating magnetic field around the stator, which induces a potential difference between the stator windings thereby generating AC. The rotating magnetic field is produced by (a) induction (b) permanent magnets (c) using an exciter.

- **Fuel system**

The fuel system is comprised of a fuel tank, fuel pump, pipe connections, fuel injector and filter. For small generators, the fuel tank is assembled as part of the generator and large generators normally have external fuel tanks for safety reasons. A fuel tank stores the fuel for use and a fuel pump which is commonly found in large generators is used to transfer the fuel from the main storage to the day storage. The pipe connections include fuel pipes (to transfer the fuel from the tank to engine), ventilation pipes (to prevent build-up pressure which arises when draining or refilling the fuel tank), overflow pipes (to avoid any overflow during refilling of the fuel tank and to ensure that there are no spillages of fuel on generator surfaces. The fuel

injector is used to atomize the liquid fuel before transferring it to the combustion chamber of the engine and the fuel filter is used to separate water and other unwanted matter from liquid fuel to avoid contamination.

- **Voltage regulator**

The generator's output voltage is controlled by a voltage controller. The mechanism that plays an important role in the cyclical process of the voltage regulator is given below:

(a) *Voltage regulator* – firstly a small amount of AC voltage produced by the generator is converted to DC. This DC is fed back to the exciter windings which are the secondary windings of the stator.

(b) *Exciter windings* – after receiving the DC, the exciter windings will then behave as stator windings and produce a small AC. These exciter windings will be connected to the rotating rectifiers.

(c) *Rotating rectifiers* – the small AC produced by exciter windings is converted to DC and then fed to the rotor to create an electromagnetic field that adds up to the already rotating magnetic field of the rotor.

(d) *Rotor* – because of the increased magnetic field, the rotor then induces a larger AC voltage across the stator windings which in turn gives the generator a larger output voltage.

This cycle is repeated until the generator produces an output equal to its full capacity. The voltage regulator is said to have reached equilibrium once the generator reaches its full operating capacity. If there is an additional loading to the generator, the output voltage drops a bit and this gives a signal to the voltage regulator to start the cycle described above.

- **Cooling and exhaust system**

(a) *Cooling system* – because of the combustion process in the engine, continuous usage of the generator raises the temperatures of the parts of the generator. It is important to include a cooling and ventilation system for withdrawing the heat produced by the engine. Different coolants like water, hydrogen can be used to extract heat from the generator depending on the design of the manufacturer.

(b) *Exhaust system* – exhaust gases that come from the internal combustion of the generator contains toxic chemicals and should be handled properly. The exhaust pipes are normally made from cast iron or steel and the pipes must connect from the engine and then terminates outdoors.

- **Lubricating system**

The generator is made of several moving parts in its engine and it requires regular lubrication for it to last longer. The engine is normally lubricated using oil. The level of the oil and oil leakages must be checked regularly to prevent engine failure.

- **Battery charger**

Most generator sets include batteries for starting. The battery charger is responsible for charging the generator's battery. If the charging voltage is lower than the float voltage, the battery won't be charged and higher voltages can shorten the battery life.

- **Control panel**

Depending on the manufacturer, the control panel has different features and some of them are going to be explained below:

(a) *Start and shutdown control* – this can be done manually or automatically. For automatic control, the control panel automatically starts the generator at times of power outage and then shuts down the generator when it's no longer needed.

(b) *Engine gauges* – the control panel also indicate important parameters like the temperature of the coolant, oil pressure, engine rotational speed, and duration of operation of the engine. The generator constantly measures and monitor these parameters to automatically shut down the generator whenever these parameters exceed maximum allowed levels.

(c) *Generator gauges* – the information about the operating voltage, current and frequency of the generator is also provided on the control panel.

- **Frame**

All generators, small or big, have housings that give structural support to the generator. The frame also acts as a medium to earth the generator for safety.

2.6.2 Variable speed diesel generators

Diesel generators are made up of an engine that is connected directly to an alternator to produce electricity. Engines in conventional diesel generators run at an almost constant speed to produce a 50 Hz or 60 Hz power output regardless of the load demand of the system [160]. Thus, the sizing of these constant speed generators is done by selecting a DG basing on the peak load. For low or partial load applications, constant speed diesel generators give poor efficiency [161]. Running a constant speed generator under light load or partial loading

conditions for several hours can damage the engine due to the unburnt fuel in the combustion chamber. [160]. To prevent these problems, manufacturers advise that constant speed generators must be operated with a load above 50 % of the rated power output of the generator [162]. Although partial loading conditions are not recommended, the advent of HRES technologies has created an increased interest in this practice. And in HRES, the constant speed diesel generator face increased partial loading since the load has to be shared within different energy sources. Recently, the concept of variable speed in DG has been proposed as a solution to problems faced by fixed speed diesel generators. Variable speed operation of DG makes a engine to be efficiently operated over its entire functional range. Operating diesel engines at variable speed gives reduced fuel consumption and the generator has the capability of producing more power from the engine without exceeding the rated torque. According to the studies [163, 164], using VSDG can reduce the fuel consumption by up to 40% as compared to constant speed diesel generators especially when operated at lower electrical loads.

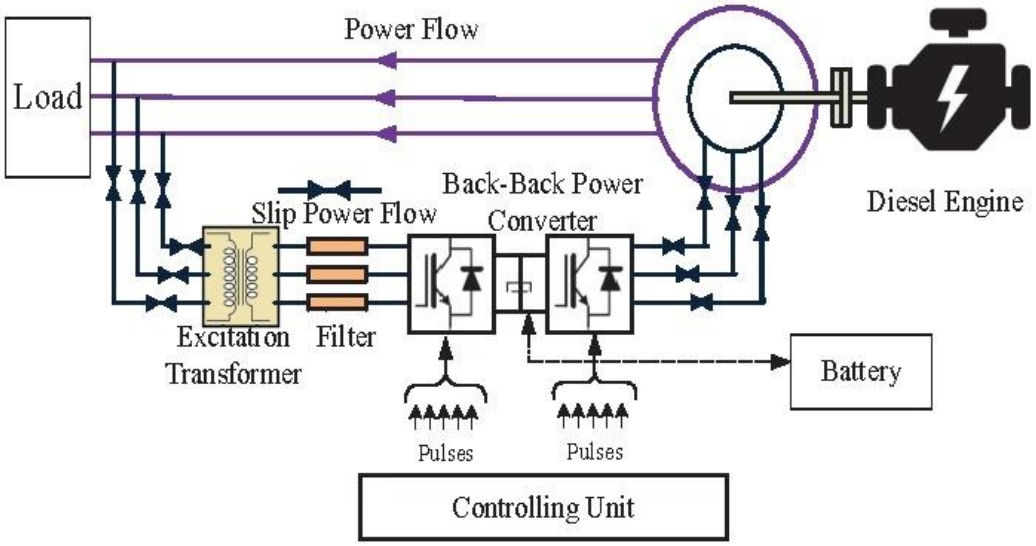

Figure 36:Typical VSDG based on DFIG [165].

There are two mechanisms used to achieve variable speed operation in diesel generators. The first mechanism uses a permanent magnetic generator to convert mechanical energy to electrical energy and it achieves variable speed constant frequency operation by utilizing full power electronic converter. This mechanism is simple but the use of a power electronic converter is expensive since the converter has to be sized to at least the same rating as the generator [160]. The second mechanism achieves variable speed constant frequency operation by using a Doubly-Fed Induction Generator (DFIG) and a smaller power converter (back-to-

back power converter). The power converter in this mechanism is only sized to around 30% of the generator's rated power. A mechanism using a DFIG has been considered as a good choice to achieve variable speed power generation for both wind and diesel power systems [161]. The following are some of the advantages for variable speed diesel generators based on the DFIG:

(a) The generator's torque is easily controlled using rotor current control.
(b) The power electronic converter used is smaller but capable of controlling the whole generator's output power by only controlling the current in the rotor windings.
(c) There are fewer harmonics since the control will be only on the rotor side and the stator will be connected to the grid.

3.0 SOLAR WATER PUMPING

Solar Photovoltaic Water Pumping (SPVWP) system is a technology that utilizes solar energy for water pumping [166]. It is similar to traditional water pumping systems but the only difference is that the pumps are powered by solar energy instead of fossil fuel or grid electricity. From crop irrigation to domestic use, solar pumps meet a wide range of water needs. Also considering the unavailability of grid electricity in rural areas, SPVWP becomes one of the promising technology in remote areas [167]. The design of solar water pumps is of prime importance for achieving a reliable and economical operation. Below are the benefits of using solar water pumping systems:

1) *Low operating cost* – a solar water pump uses solar energy at no cost at all. It does not depend on fuel or grid electricity so there are no recurring costs for electricity or fuel once the water pump is installed.
2) *Low maintenance costs* – solar water pumps are easy to maintain compared to other pumps. They have relatively fewer moving parts and the chances for pump failure are fewer. Solar water pumps can run for years without any maintenance needed.
3) *Eco-friendly* – common fuel-powered water pumps produce noise and air pollution whereas solar water pumps are environmentally friendly. They do not produce greenhouse gases that can cause global warming.

3.1 Types of solar pumps

Solar water pumps can be grouped into three categories according to their operations namely submersible, surface, and floating water pumps.

- *A submersible water pump* is designed to be submerged in water and its driving motor is hermetically sealed. Usually, this type of pump is used to draw water from deep wells. The power to the motor of the pump is fed down using water-resistant cables. **Fig. 37** shows a typical configuration of a submersible water pumping system.
- *A surface water pump* is placed on the ground, out of the water source and the inlet side of the pump is immersed into the water. The water is sucked up from the well into the pumping system then pushed to the farm.
- *Floating water pump or semi-submersible water pump* is designed to be semi-submerged into the water and held in place using a floating device. This water pump is commonly used where inline water pumps are not suitable. Floating water pumps are mainly used to draw water from lagoons, ponds, shallow wells and dams.

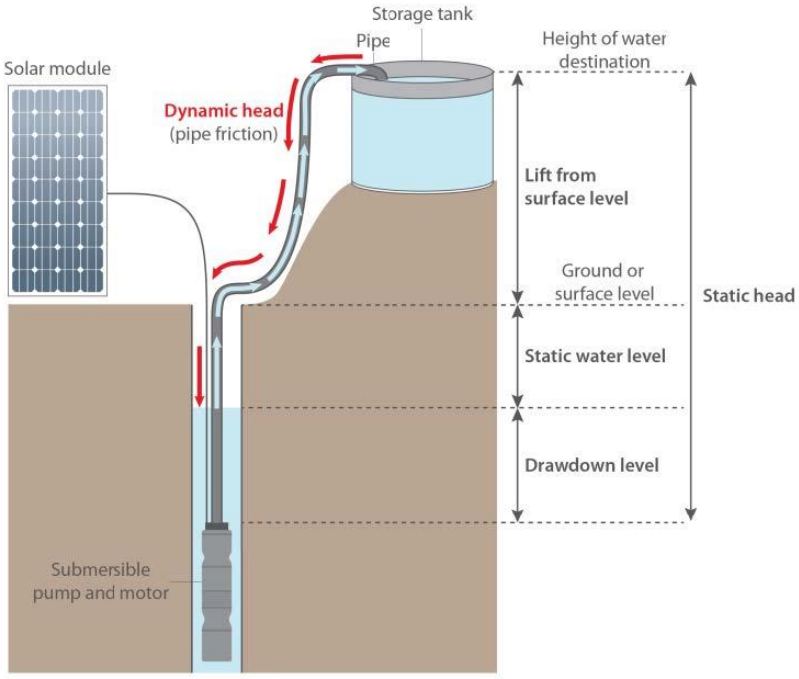

Figure 37: A diagram showing a typical submersible water pumping system.

Solar water pumps may also be grouped using their operating principles as either dynamic pumps or positive displacement pumps

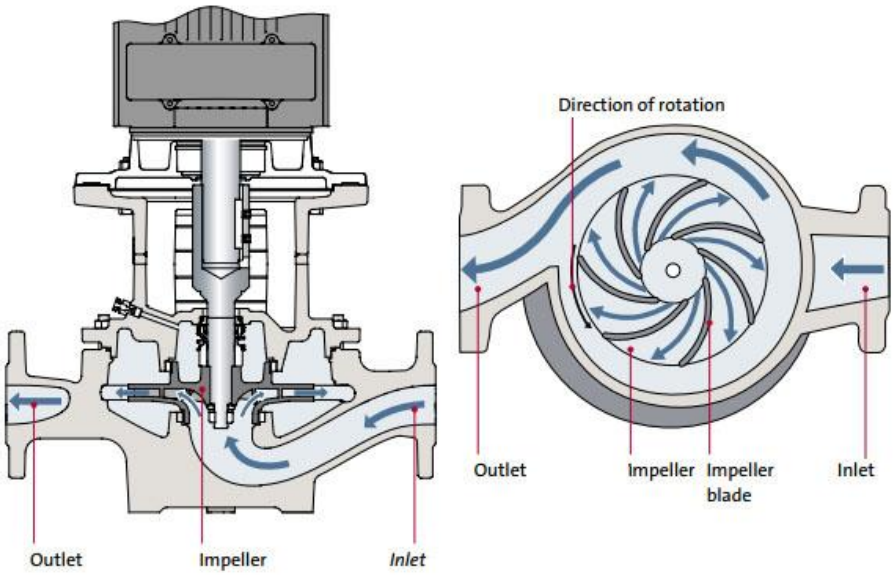

Figure 38: The working principle of a centrifugal water pump

- *A dynamic pump* uses rotating blades or impellers to develop high liquid velocity and pressure in the pumping system. By either rotating the impellers in a clockwise or anticlockwise direction, the water is pumped from one point to another. A centrifugal water pump is a common type of dynamic water pump. It uses the centrifugal force

created by rotating impellers to suck the water and the casing then directs the water to the outlets whilst the impellers are rotating.

- *A positive displacement water pump* operates by varying the volume in a closed system. It forces a fixed amount of water from the inlet section to the discharge section of the pump driven by different mechanisms like screws, pistons, diaphragm and gears. By reducing the volume, the pressure increases and increasing the volume reduces the pressure of water. So the changes in pressure cause the water to be sucked into the pumping system and then pushed out to the desired destination. Examples of positive displacement pumps include rotary, piston, reciprocating, diaphragm and screw pumps.

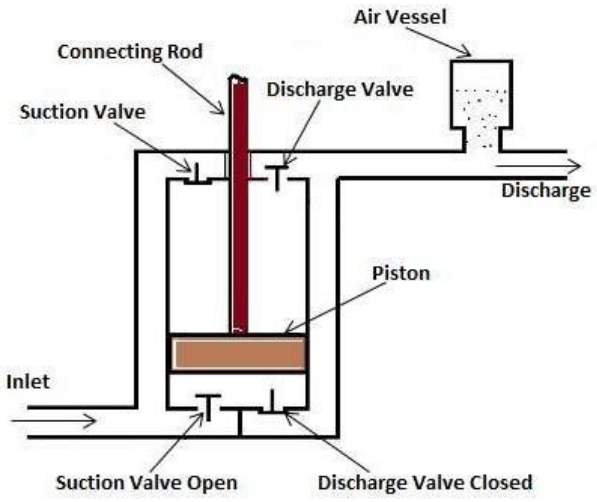

Figure 39: A typical positive displacement water pump

3.2 Solar water pumping system configurations

There are several types of configurations for solar water pumping systems. Every configuration has its advantages and disadvantages. Several factors should be considered when selecting the optimum configuration for a certain application. Listed below are some common setups for solar water pumping systems.

3.2.1 Configuration basing on energy storage

1) Battery connected solar water pumping systems

Battery connected water pumping systems are made up of solar modules, charge controllers, pump controllers, batteries and a water pump. The system may or not include a water storage tank depending on the application and the water pump can also be powered by DC or AC. The batteries are charged using excess energy from the PV modules and they discharge to power the pump during the night or periods of low solar insolation. However, the use of batteries can

increase the system costs, complexity and even the overall efficiency of the system. In most cases, the pump controllers are used to boost battery voltage supplied to the pump thereby improving the system efficiency.

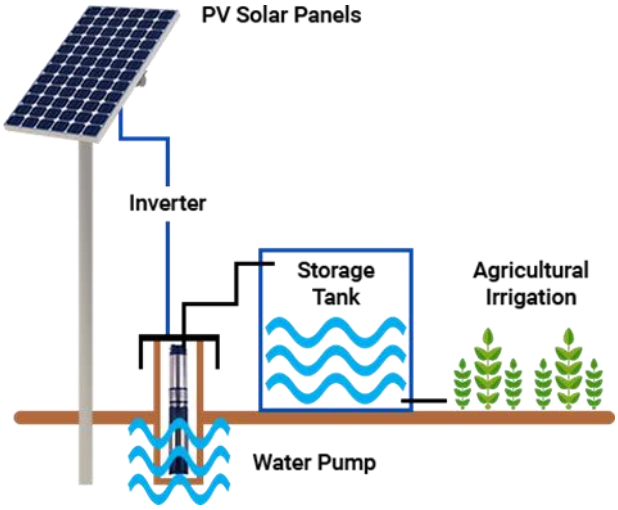

Figure 40: A diagram of a battery connected solar water pumping system.

2) Direct connected solar water pumping system

For a direct connected solar water pumping system, the power from PV modules is directed straight to the pump.

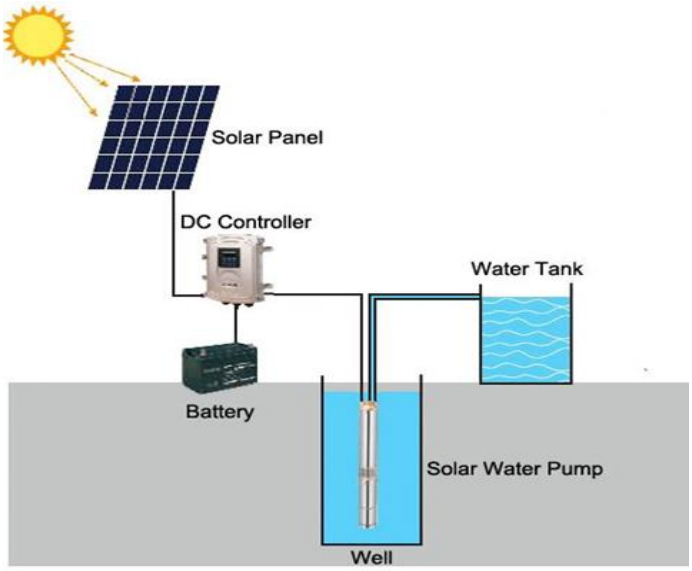

Figure 41: A diagram of a direct connected solar water pumping system.

The amount of water pumped is directly proportional to the solar irradiation hitting the PV panels. The advantages of this system are that it is simple and cheap as compared to the battery connected solar water pumping system. However, since there are no batteries, the pump only works during the day when there is enough solar insolation. A water storage tank is usually

incorporated in this system to ensure the availability of water on cloudy days and at night. Direct connected solar water pumps cannot operate at the maximum power point because the solar radiation varies during the day and to improve the performance a maximum power point tracking controller is included [166].

3.2.2 Configuration basing on the form of the electric power unit

1) DC solar water pumping systems.

In this type of solar water pumping system, DC motors are used to drive the water pump. DC motors are commonly used for low power solar water pumping systems. There are two types of DC motors which are (a) conventional DC motor that has brushes (b) Brushless DC motor (BLDC). The conventional DC motors use carbon brushes for transferring power to the motor shaft. Because of the continuous operation of the pump, these brushes wear out and they should be replaced regularly. Therefore, using conventional DC motors causes high operational and maintenance costs. Brushless DC motors utilize the principle of magnetic induction to transfer the power to the motor shaft. Another type of brushless DC motor is a permanent magnet DC motor (PMBLDC) which is now a popular choice for solar water pumping with a submersible solar water pump being a typical example. The absence of brushes makes the system to be more efficient, reliable and has a low maintenance requirement.

2) Alternating current solar water pumping systems.

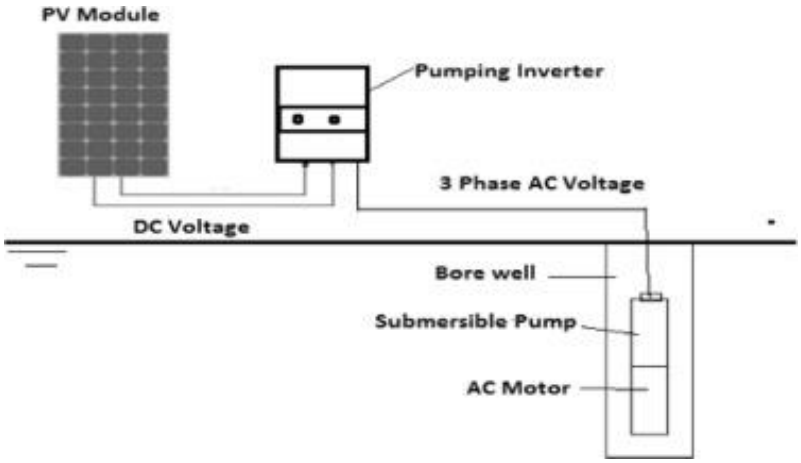

Figure 42: Typical AC solar water pumping system.

In this system, an AC motor is used to drive the water pump. Induction and synchronous AC motors can be used for this application. A suitable power inverter is included to convert DC from PV modules to AC which is needed by the motor pump. However, inverters reduce the

efficiency of the pumping system. An AC solar water pumping system can run on grid electricity in the case when there is no PV power which is their main advantage.

4.0 SYSTEM DESIGN, SIZING AND MODELLING

The solar/diesel hybrid water pumping system is made up of PV modules, MPPT charge controllers, a battery bank, a VSDG, an Energy Management Controller (EMC) and the DC water pump. The main aim of this hybrid system is to deliver uninterrupted power to the water pump at minimum diesel generator runtime and fuel consumption. The detailed design, sizing and modelling of the system components is given in this Chapter.

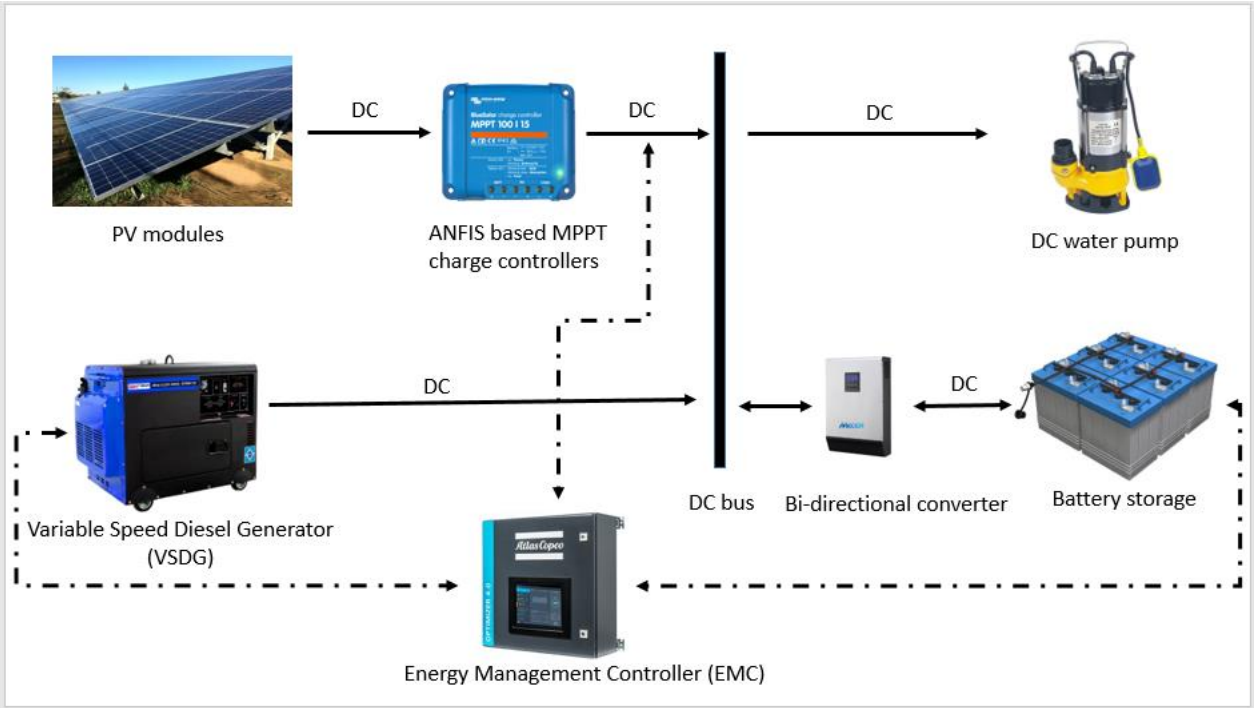

Figure 43: The proposed solar/diesel hybrid water pumping system.

4.1 PV system

Photovoltaic modules convert the energy coming from the sun into electricity using the photovoltaic effect. The most common types of solar panels include polycrystalline, monocrystalline, and thin film. These modules vary in performance, costs, appearance, and installation. In this solar/diesel hybrid water pumping system, PV modules are the main power source. They are sized to power the water pump and also to charge the batteries if there is excess energy.

Each component within a PV system has a certain percentage of power loss which will affect the overall power output of the system. There are also other factors, which affect the performance of a PV array, and these are reflection, shading, module mismatch, and

temperature effects. The percentage losses vary from one system design to the other depending on the specific characteristics of a site and design specifications of the PV components.

4.1.1 PV array sizing

Currently, farmers of the Makarepo irrigation scheme use a Honda WB 30 fuel-powered water pump with a maximum hydraulic power rating of 5Hp. By comparing the specifications, a Tata 5Hp DC – submersible solar water is selected for this application. To get the power required by the motor to drive the pump, the motor-pump efficiency has to be considered. According to the study [168], the motor-pump efficiency ranges between 70% to 96%. The motor power is given by,

$$P_m = \frac{P_H}{\eta_{mp}} \tag{27}$$

where P_m is the required power for the motor; P_H is the hydraulic power of the centrifugal pump and η_{mp} is the motor-pump efficiency. In this study, η_{mp} is estimated to be 85%. Thus,

$$P_m = \frac{3728.5}{0.85}$$
$$= 4386.471W$$

Therefore, the PV array is sized to power the 4386.471W motor pump. There are several proposed methods for sizing PV arrays and in this study, the Peak Sun Hours (PSH) method given in [169-171] is going to be adopted. The PSH method is given below.

1) Determining the total power consumption demand.

When designing a PV system, the first step is to estimate the total power consumed by all the appliances to be connected to the PV system. The step by step procedure is given below:

- *Calculating the total Watt-hours per day of every appliance to be used.*

The Watt-hours of all the appliances to be connected are added together to get the total Watt-hours per day. The water pump is estimated to work from 10 am to 3 pm, which is 5 hours a day. So the total Watt-hours per day for the system is shown in **Table 1**.

Table 1: Calculation of total Watt-hours per day of the system

Appliance	Power rating	Working hours/day.	Total Watt-hours/day
Water pump	4386.471W	× 5hrs	21932.355
			21932.355Watt-hrs/day

- *Calculating the total Watt-hours per day that are needed from solar modules.*

Multiply the appliances' Watt-hours per day by the energy lost in the system. The energy lost in the system is generally taken as 30% [171].

The total Watt-hours needed from solar modules $= 21932.355 \times 1.3$

$$= \mathbf{28512.062}\ \textbf{Watt-hours/day.}$$

2) Sizing the PV array.

To get the size of the PV array, the total peak watt must be calculated. Since the peak-watt (Wp) generated depends on the environmental conditions of the site and the sizes of the PV modules, there is a need to determine the PSH which is the average daily amount of solar energy received on the site. The worst-case PSH is considered for the sizing of the PV array. For Zimbabwe, the worst recorded PSH was 4.5 which was recorded in winter [172]. In some contexts, this value is referred to as the panel generation factor. To calculate the number of the PV modules, the calculations are as follows:

- *Calculating the total Watt-peak rating that is needed for solar modules*

To get the total Watt-peak rating needed for the PV array to operate the appliances, the total Watt-hours per day value is divided by the PSH. Therefore, the total Watt-peak rating is determined as follows:

$$\text{Total Watt-peak rating} = \frac{\mathbf{28512.062}}{\mathbf{4.5}}$$

$$= \mathbf{6336.013}\ \boldsymbol{Wp}$$

- *Calculating the number of solar modules of the system*

To get the number of solar modules, the total Watt-peak rating calculated above is divided by the rated Watt-peak output of the selected solar modules. The answer from this calculation

gives the minimum number of solar modules to be used. If more than calculated solar modules are installed, the system performs better and it improves the battery life. If fewer solar modules are installed, the system may fail to sufficiently supply the load and the battery life might be compromised. The selected panel for this application has the following specifications: ART solar - 360Wp, 39.0 V Si-monocrystalline type module.

Electrical Data @ STC							Electrical Data @ NOCT					
Design	Pmax(Wp)	Vmp	Imp	Voc	Isc	Eff	Design	Pmax(wp)	Vmp	Imp	Voc	Isc
72 Cell	360 Wp	39.0V	9.24A	47.5V	9.71A	18.6%	72 Cell	271 Wp	36.3V	7.46A	44.0V	7.90A
60 Cell	300 Wp	32.6V	9.21A	39.7V	9.77A	18.5%	60 Cell	221 Wp	29.7V	7.43A	36.8V	7.78A

STC - Irradiance 1000 W/m2, cell temp @ 25°C
NOCT - Irradiace 800 W/m2, cell temp @ 20°C
KEY
Pmax(Wp) - maximum power, **Vmp -** voltage at max power, **Voc -** open circuit voltage, **Isc -** short circuit current
Imp - max power current, **Eff -** module efficiency (%)
STC - Standard Test Conditions
NOCT - Nominal Operating Cell Temperature
*** Figures are typical values of performance. Slight variances do occur, exact specifications available with each module,**

Temperature Ratings		Maximum Ratings	
Nominal Operating Cell Temp	45°C (±2°C)	Operational Temp	-40 to +85°C
Temp coefficient of Pmax	-0.39%/°C	Max system Voltage	1000V DC (IEC)
Temp coefficient of Voc	-0.30%/°C	Max Series Fuse Rating	15A
Temp coefficient of Isc	0.050%/°C	Mechanical Load	5400pa

Figure 44: Specifications of a chosen solar module-360Wp [173].

So the total number of solar modules needed = $\mathbf{6336.013/360}$

$$= 17.6.$$

Therefore, the total number of PV modules required in this system is **18** solar panels. Thus, the PV array then consists of 3 parallel strings having 6 modules connected in series per string. Each solar module has its MPPT charge controller to improve the efficiency of solar modules and to minimize the impact of voltage mismatch problems.

4.1.2 PV modelling

The general model of a solar cell can be derived from the physical characteristics of a diode, which is usually called the single diode model. The diagram below illustrates the circuit of a single diode model.

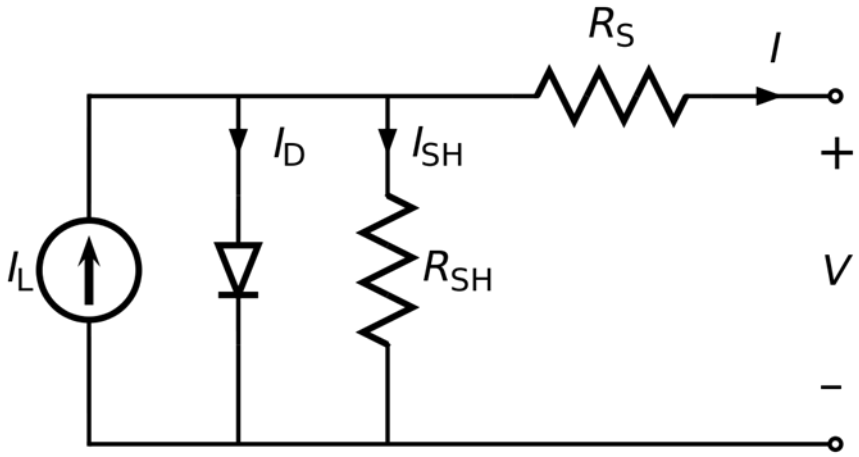

Figure 45: A single diode model of a PV cell

From the diagram above, the current source, I_L represents the flow of electrons when solar radiation hits the surface of a solar PV cell. And the diode represents the characteristic behaviour of the *PN* junction of the solar PV cell. The model has two resistances namely series resistance and parallel resistance. The series resistance, R_s, represents current losses due to metal contacts within the solar PV cells and the parallel resistance, R_{SH}, accounts for current leakages through the resistive path in parallel with the intrinsic device. Several solar cells have to be connected to form a solar PV module. The output current of the solar PV module is given as,

$$I = I_{ph} - I_o\left[e^{\frac{q(V+IR_S)}{nKN_ST}} - 1\right] - I_{sh} \quad \textbf{(28)}$$

where I_{ph} is the photo-current; I_o is the saturation current; q is the electron charge; V is the output voltage of the PV module; n is the ideality factor of the diode; K is the Boltzmann constant; N_s represents the number of solar cells connected in series; T is the solar cell temperature; I_{SH} is the current through the shunt resistor. The current generated from the incidence of radiation at a given temperature is expressed as,

$$I_{ph} = \left[I_{sc} + k_i(T - 298)\frac{G}{1000}\right] \quad \textbf{(29)}$$

where I_{sc} represents the short circuit current; k_i is the temperature coefficient of the I_{sc} at Standard Test Conditions (STC); G is the solar irradiance. The reverse saturation current of the diode is given by,

$$I_{rs} = \frac{I_{sc}}{e^{\left(\frac{q\,V_{oc}}{n\,N_s K\,T}\right)} - 1} \quad \textbf{(30)}$$

where V_{oc} is the open-circuit voltage. The module's saturation current at any given temperature is given by,

$$I_o = I_{rs}\left(\frac{T}{T_n}\right)^3 e^{\left[\frac{q\,E_{go}\left(\frac{1}{T_n}-\frac{1}{T}\right)}{n\,K}\right]} \quad \textbf{(31)}$$

where, T_n = 298 K; E_{go} is the bandgap energy. In this study, the ART solar module - 360Wp, 39.0 V Si-monocrystalline type module is used. The parameters of the module at STC as per the manufacturer's datasheet are given in **Table 2**.

Table 2: ART solar -360 Wp module parameters

Quantity	**Single module**	**PV array (18 modules)**
Maximum power, P_{MPP}	360 W_p	6480 W_p
The voltage at maximum power, V_{MPP}	39.0 V	234 V
The current at maximum power, I_{MPP}	9.24 A	27.7 A
V_{oc}	47.5 V	285 V
I_{sc}	9.71 A	29.1 A

By using the parameters presented in **Table 2**, the MATLAB/Simulink model of the solar module is created. After modelling, the MATLAB/Simulink PV module model must be verified or validated to check if resembles the characteristics of the actual module.

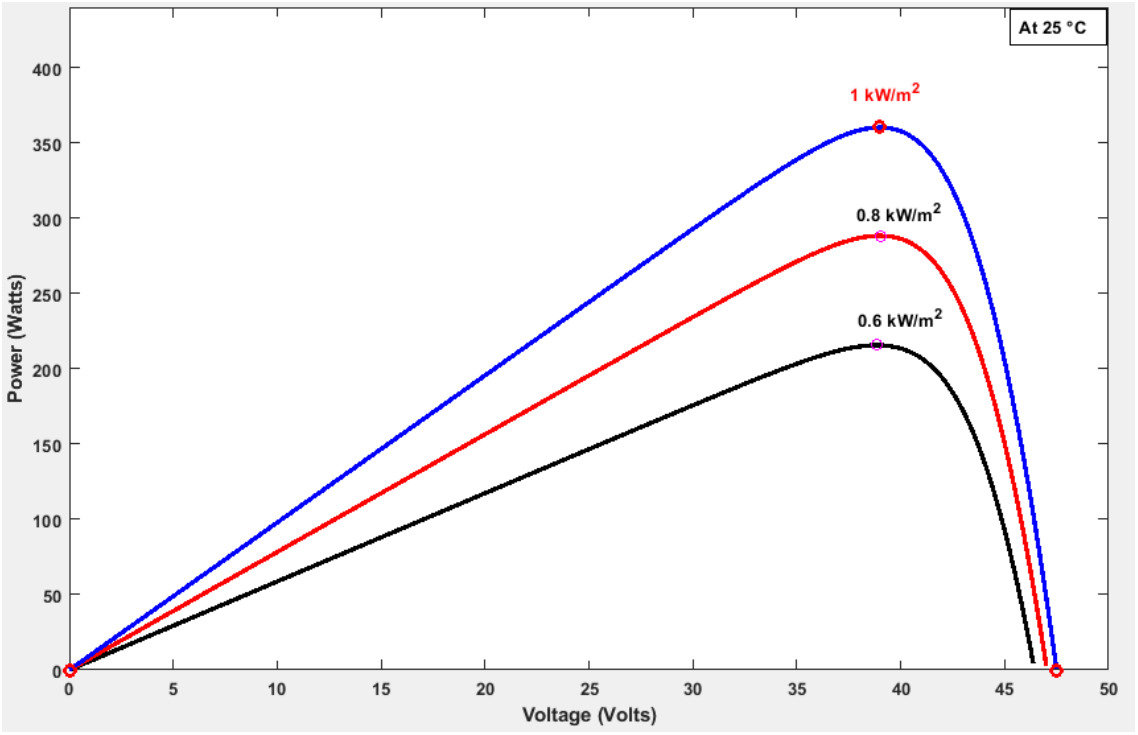

Figure 46:P-V curves of the MATLAB model.

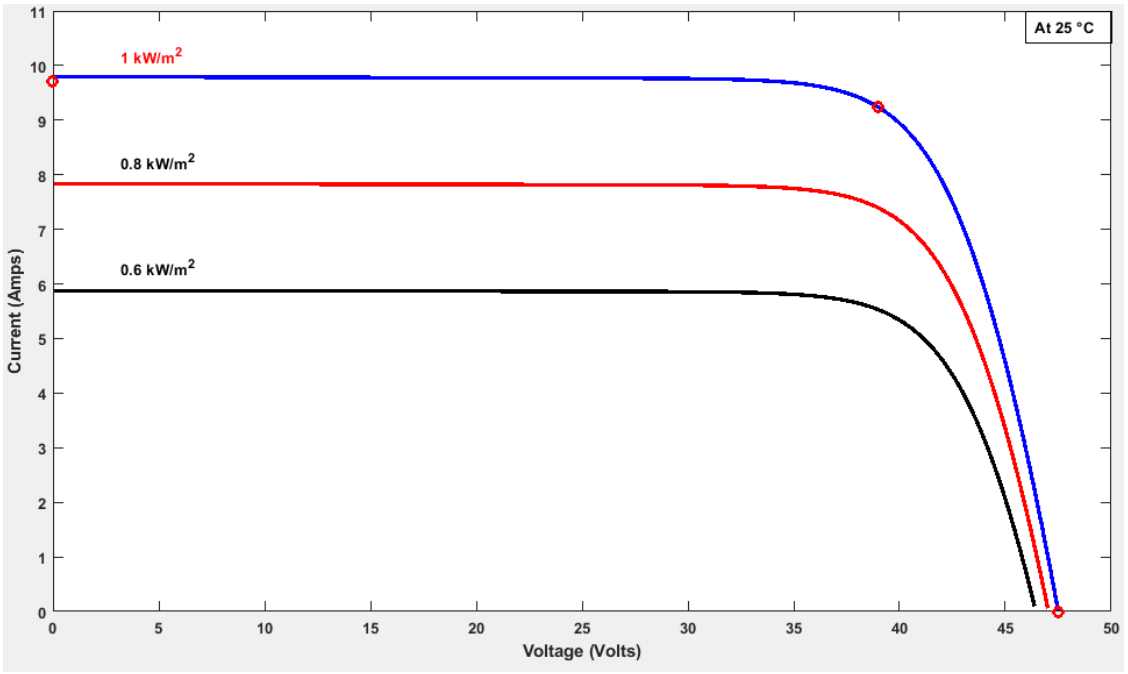

Figure 47: I-V curves of the MATLAB model.

To test it, the model is simulated to calculate its peak-watt power (Wp). The model is simulated under Standard Test Conditions (STC). STC is a testing condition for manufacturers to check the performance of solar modules and it specifies that the module must be tested under a solar cell temperature of 25° C, the irradiance of 1000W/$m^2$and an air mass of 1.5 (AM1.5) [174]. The peak power point of the simulated MATLAB/Simulink model was 360 W_p which is given

in the manufacturer's datasheet. **Fig 46 & 47** show the I-V and P-V curves of the simulated MATLAB model of the PV module at 25 $°C$ and different solar irradiance.

4. 2 Variable speed diesel generator

The concept of variable speed engines in diesel generators has emerged as a solution for low-load operation problems of constant speed diesel generators. The engine of a Variable Speed Diesel Generator (VSDG) can select the optimum speed for a specific load. The proposed VSDG is comprised of a diesel engine and a double-fed induction generator (DFIG). The speed of the VSDG is controlled according to the state of charge (SOC) of the battery storage, the power from the PV modules, and the load demand. The VSDG only starts when the battery storage reaches its maximum discharge level (SOC_{min}) and it has to run to power the load and charging the batteries to a float level. The speed of the diesel engine and the fuel injection to the engine is controlled according to the power demand. The configuration of the VSDG based on the DFIG is shown in **Fig. 48**.

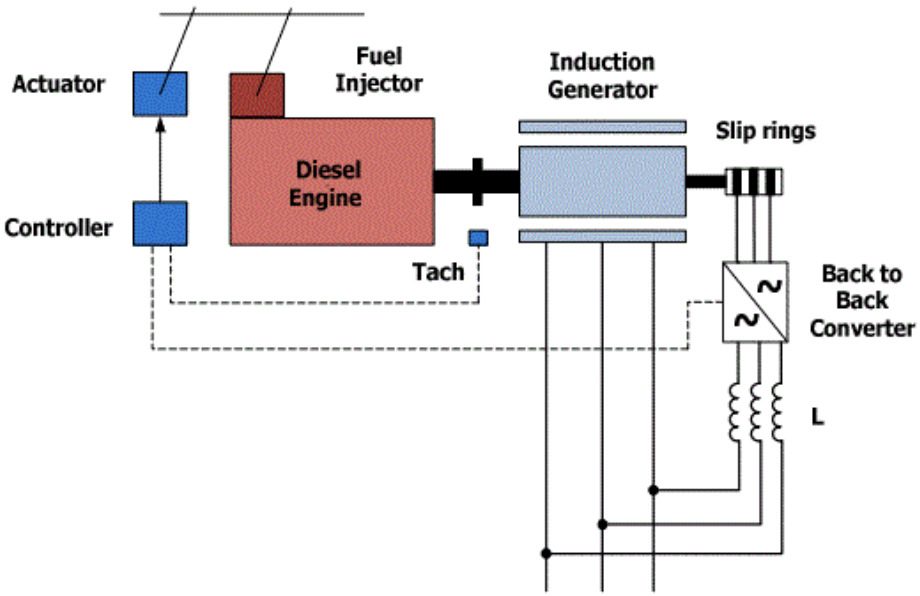

Figure 48: DFIG based VSDG

4.2.1 Variable speed diesel generator specifications

The main purpose of using a VSDG in this study is to increase the PV energy penetration in the hybrid system. The following procedure is followed for sizing the VSDG:

1) **Calculating total power requirement**

The first step is to list all appliances to be powered by the generator. The total power requirement is determined by adding up the total wattage of all the equipment to be powered. In this study, the water pump is only the appliance with a wattage rating of 4.386 kW.

2) Converting kW to kVA

The maximum required wattage of the system is given kilowatts (kW). Kilowatts represent the actual power required by the load to give a useful working output. Generators are normally rated in kilo-volt-amperes (kVA). Kilo-volt-amperes measure the apparent power which is the total amount of power in use in the system. For 100% efficient systems, kVA is equal to kW. However, electrical systems can't be 100% efficient due to electrical losses. In generators, the efficiency of the system is stated as a power factor. The international standards require generators to have a power factor of at least 0.8. Therefore, kilowatts are converted to kilo-volt-amperes using the equation given below:

$$Power\ in\ kVA = \frac{Power\ in\ kW}{Power\ Factor}. \quad \textbf{(32)}$$

Thus, the power rating of the VSDG for this application is given by,

$$VSDG_{rating} = \frac{4.386}{0.8}$$

$$= 5.483\ kVA.$$

Table 3: Kohler - 6kW Variable Speed Direct Current (DC) Generator.

Manufacturer	Kohler Generators
Rated output power	6kW
Engine RPM	Variable (2300-2900)
Starting system	Automatic starting
Generator type	Standby
Engine size	725 cc
Alternator type	Brushless

The generator must be at least 10-20% larger in capacity than the load. The selected VSDG for this application is the Kohler - 6kW Variable Speed Direct Current (DC) Generator. The specifications of the generator are given in **Table 3**.

The Kohler 6kW variable speed DC generator is specially designed for renewable energy applications and some other remote applications. Advantages of this generator include extended engine life and lower fuel consumption as compared to constant speed diesel generators and the variable speed operation also reduces maintenance requirements.

4.2.2 Modelling of a variable speed diesel generator

The mathematical model of the DFIG with the d-q synchronous rotating reference frame is expressed as follows [175]:

$$\begin{cases} V_{ds} = R_s i_{ds} - w_s \lambda_{qs} + \dfrac{d\lambda_{ds}}{dt} \\ V_{qs} = R_s i_{qs} + w_s \lambda_{ds} + \dfrac{d\lambda_{qs}}{dt} \end{cases} \quad \textbf{(33)}$$

$$\begin{cases} V_{dr} = R_r i_{dr} - (w_s - w_r)\lambda_{qr} + \dfrac{d\lambda_{dr}}{dt} \\ V_{qr} = R_r i_{qr} + (w_s - w_r)\lambda_{qr} + \dfrac{d\lambda_{qr}}{dt} \end{cases} \quad \textbf{(34)}$$

$$\begin{cases} \lambda_{ds} = L_s i_{ds} + L_m i_{dr} \\ \lambda_{qs} = L_s i_{qs} + L_m i_{qr} \end{cases} \quad \textbf{(35)}$$

$$\begin{cases} \lambda_{dr} = L_r i_{dr} + L_m i_{ds} \\ \lambda_{qr} = L_r i_{qr} + L_m i_{qs}, \end{cases} \quad \textbf{(36)}$$

where R is resistance, V is voltage, i represents the current, w is the angular velocity, L is the inductance, L_m represents the mutual inductance, i_{ms} is excitation current and λ is the flux linkage. The direct and quadrature components from the reference are represented by d and q respectively. The rotor and stator variables are represented by the subscripts r and s respectively. The differential of the stator flux is zero under the constant-state operation of the generator. And neglecting the stator resistance, the stator will be only calculated from stator flux which is indicated in equation 34. The stator flux is determined by regulating the rotor current. Therefore, if we align the q-axis of synchronous rotating reference frame on the stator flux vector, we get $\lambda_{ds} = 0, \lambda_{qs} = L_m i_{ms}$. Then from equation 34, we get:

$$\begin{cases} i_{ds} = -\dfrac{L_m}{L_s} i_{dr} \\ i_{qs} = -\dfrac{L_m}{L_s}\left(i_{qr} - i_{ms}\right) \end{cases} \quad \textbf{(37)}$$

And substituting equation 36 into 33, we get:

$$i_{qr} = \frac{L_m}{\tau}\frac{di_{ms}}{dt} + i_{ms} - \frac{1}{\tau}u_{qs} \quad \textbf{(38)}$$

Where,

$$\tau = \frac{R_s L_m}{L_s} \quad \textbf{(39)}$$

Equation 33 is determined by excitation current whilst ignoring u_{qs} which is reasonable due to its small value. Equation 38 is preferred for the determination of the d-axis component of the rotor current, i_{dr}:

$$i_{dr} = -\frac{L_s}{L_m} i_{qs} \quad \textbf{(40)}$$

The stator flux angle can be determined by integrating the reference value of the stator voltage synchronous speed, w_e :

$$\theta_s = \int w_e dt \quad \textbf{(41)}$$

The control of the $dq - axis$ rotor current can be done by controlling the $dq - axis$ rotor voltage to give:

$$\begin{cases} V_{dr} = R_r i_{dr} + \sigma L_r \dfrac{di_{dr}}{dt} - w_{slip}\sigma L_r i_{qr} \\ V_{qr} = R_r i_{qr} + \sigma L_r \dfrac{di_{qr}}{dt} + w_{slip}\sigma L_r i_{dr} + w_{slip}\dfrac{L_m^2}{L_s} i_{ms} \end{cases} \quad \textbf{(42)}$$

Where,

$$w_{slip} = w_s - w_r \quad \textbf{(43)}$$

$$\sigma = 1 - \frac{L_m^2}{L_s L_r}. \quad \textbf{(44)}$$

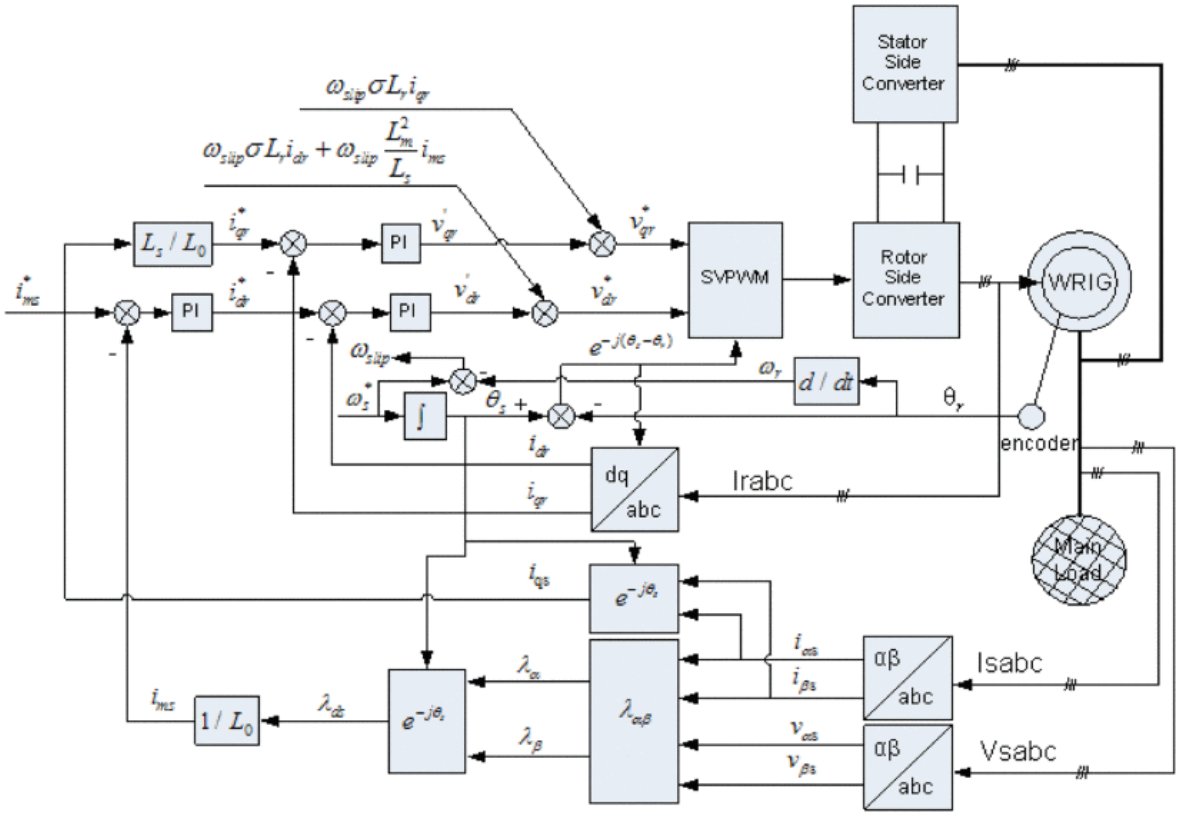

Figure 49: Control structure of a stand-alone DFIG

The main objective of the rotor side converter is to excite the flux as well as maintaining constant frequency and voltage output. And the stator side converter is used to stabilize the DC bus. For grid-connected applications, reactive and active power is controlled and decoupled by both the rotor and stator side converter. In this research work, the VSDG is modelled in the MATLAB/Simulink environment as a controlled voltage source as shown in **Fig. 50**. The operating range of the VSDG is between 2300 rpm to 2900 rpm and it is connected to a boost converter to give a voltage output of 240V at rated speed.

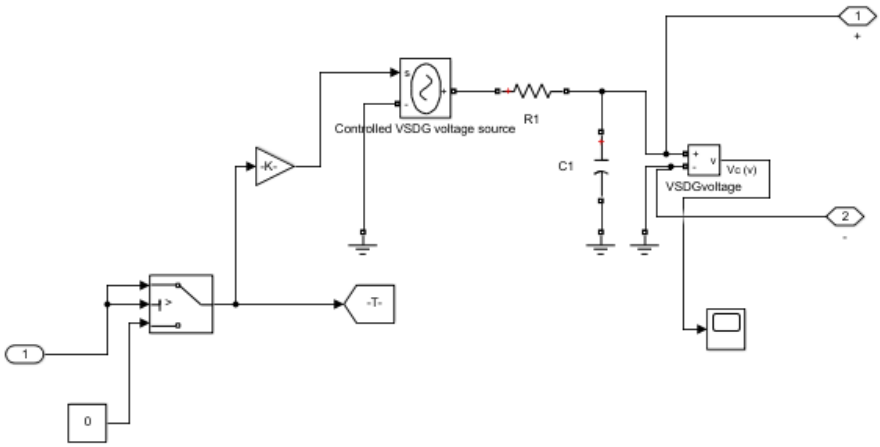

Figure 50: Matlab/Simulink model of the VSDG.

4.3 Battery storage

To make the best use of the solar energy available and to reduce the use of the VSDG, batteries must be incorporated. Batteries enable the continuous power supply to the water pump in the event of power failure or under cloudy weather. In some applications, the battery storage is connected directly to the DC-bus without using a power converter. This configuration doesn't give a better efficiency as compared to using a converter and it requires more batteries. Also, the absence of any control strategy for regulating the battery storage voltage and current may result in a degraded life expectancy of the batteries. In this study, a bi-directional converter is used to connect the battery storage to the DC bus. The types of batteries which can be used for solar energy systems include lead-acid, gel, lithium-ion, and nickel-based batteries. Lead-acid batteries are considered the best option for solar systems because of their low cost, high power, and easy recyclability. In this hybrid system, lead-acid batteries were used.

4.3.1 Battery sizing

The battery type recommended for PV systems is a deep cycle battery such as a lead-acid battery. Lead-acid batteries are specially designed to be discharged at lower energy levels and then rapidly recharged day after day for years [176]. The battery size must be large such that it can be able to store enough energy to power the appliances at night and under cloudy weather conditions. To find out the size of the battery, the procedure given in [169, 170, 172, 176] is going to be followed.

$$\boldsymbol{Battery\ capacity(Ah) = \frac{Total\ Watt - hours\ per\ day\ \times Days\ of\ Autonomy}{0.85\ \times 0.6\ \times normial\ system\ voltage}}, \quad \textbf{(45)}$$

where given in [172], 0.85 is for battery losses, 0.6 is the depth of discharge. Days of autonomy refers to the number of days the battery bank can power the appliances without being charged. In this study, considering that the water pump only works 5hours/day, the number of days of autonomy is 1.

$$Battery\ bank\ capacity(Ah) = \frac{21932.355 \times 1}{0.85 \times 0.6 \times 12}$$

$$= \mathbf{3583.718\ Ah.}$$

The battery in the market which is selected for this application is a 12 V, 300Ah AGM lead-acid, deep cycle solar battery. To get the number of batteries required, the battery bank capacity is divided by the rating of each battery (300Ah).

$$Number\ of\ batteries = \frac{\mathbf{3583.718}}{300}$$

$$= \mathbf{11.9}.$$

Therefore, **12** batteries will be used in this solar system. The number of series-connected batteries is calculated by dividing the nominal voltage of the system by the rating of one of the batteries used,

$$N_s = \frac{48}{12}$$

$$= 4.$$

Then, parallel paths, N_p are calculated by dividing the total number of batteries by the number of series-connected batteries,

$$N_p = \frac{12}{4}$$

$$= 3$$

4.3.2 Lead-acid battery modelling

A lead-acid battery is made up of two electrodes immersed in a sulphuric acid electrolyte. The positive electrode is made up of metallic lead oxide (PbO_2) and the negative electrode is made up of sponge lead (Pb). There are two modes of operation in a lead-acid battery namely the charge mode and discharge mode. The charging and discharging are based on the following chemical reactions:

Anode: $Pb + H_2SO_4 \leftrightharpoons PbSO_4 + 2H^+ + 2e^-$

Cathode: $PbO_2 + H_2SO_4 + 2e^- \rightleftharpoons PbSO_4 + 2OH^-$

Overall reaction: $Pb + PbO_2 + 2H_2SO_4 \rightleftharpoons 2PbSO_4 + 2H_2O$.

The lead-acid battery is modelled mathematically using a modified Thevenin battery model given in [177]. The electric equivalent circuit of this model is shown in **Fig. 51** where, E_m is the open-circuit voltage of the battery, R_o is the battery internal resistance, the $R_1 - C_1$ the network represents the transient behaviour of the battery, I is the discharge current of the battery, and V is the output voltage of the battery. The dynamic equations of the circuit model for discharging and charging are given by:

$$\frac{dV_p}{dt} = -V_p \frac{1}{R_d C} + V_o \frac{1}{R_d C} - I_b \frac{1}{C}, \qquad V_p \leq V_o \tag{46}$$

$$\frac{dV_p}{dt} = -V_p \frac{1}{R_c C} + V_o \frac{1}{R_c C} - I_b \frac{1}{C}, \qquad V_p > V_o \tag{47}$$

where,

$$I_b = \frac{V_p - V_0}{R_b} \tag{48}$$

and, V_{oc} is the open-circuit voltage, V_p is the capacitor voltage, V_t is the terminal voltage of the battery. R_c , R_d and R_b are the charging, discharging, and internal resistance of the battery respectively. C is the capacitance of the battery and I_b is the current of the battery.

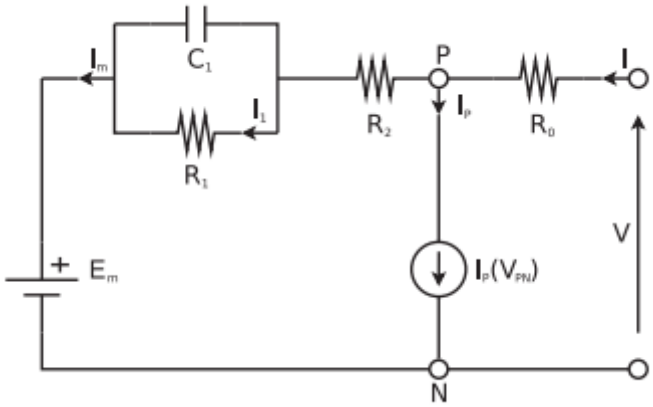

Figure 51: Mathematical model of a lead-acid battery.

Fig. 52 shows the MATLAB/Simulink model of the battery bank connected to the bi-directional converter.

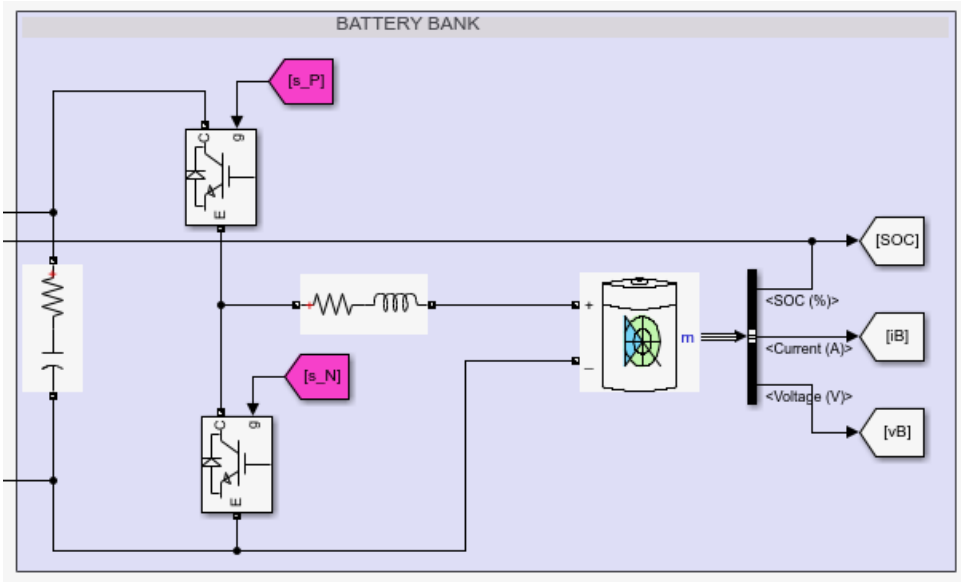

Figure 52: Bi-directional converter and the battery bank.

4.4 Maximum Power Point Tracking charge controllers

To maximize the energy from PV modules, Maximum Power Point Tracking (MPPT) charge controllers are used. Generally, an MPPT controller is a highly efficient DC-DC power converter that is controlled by an algorithm to extract the maximum available power from a PV module. The charge controller is normally connected between the PV module and the battery or load. It also regulates the voltage and current coming from the PV module thereby preventing battery overcharging and reverse current flow. Adaptive Neuro-Fuzzy Inference System (ANFIS) based MPPT controllers are used for maximum power point tracking in this research. Basically, the ANFIS method uses FL for transforming system inputs into desired outputs through interconnected neural networks. Therefore, this method combines the benefits offered by FL and ANNs into a single technique.

4.4.1 Modelling of the maximum power point tracking controller

To describe the ANFIS architecture, two IF-THEN fuzzy rules are considered:

$$Rule_{(1)} = IF\ x\ is\ A_1\ AND\ y\ is\ B_1, THEN$$

$$f_1 = p_1 x + q_1 y + r_1$$

$$Rule_{(2)} = IF\ x\ is\ A_2\ AND\ y\ is\ B_2, THEN$$

$$f_2 = p_2 x + q_2 y + r_2$$

where,

$$x\ and\ y\ are\ inputs,$$

$$A_i\ and\ B_i\ are\ the\ fuzzy\ sets,$$

$$f_i\ are\ the\ outputs\ within\ the\ fuzzy\ rule,$$

$$p_i, q_i\ and\ r_i\ are\ the\ design\ parameters\ that\ are\ determined\ during\ the\ training\ process.$$

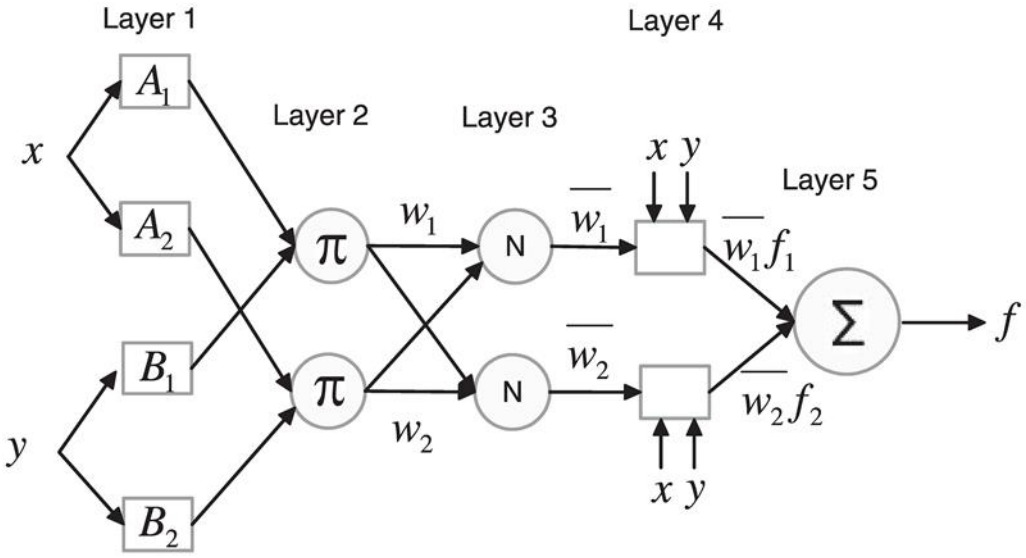

Figure 53: ANFIS architecture.

Fig. 53 illustrates the ANFIS architecture which is used to implement the two rules explained above. The ANFIS architecture is made up of 5 layers.

- For layer (1), the nodes are adaptive and the outputs are the fuzzy membership grades given by:

$$O_{1,i} = \mu_{Ai}(x), i = 1,2$$

$$O_{1,i} = \mu_{Bi-2}(y), i = 3,$$

where x and y represent the inputs to the node i , and A_i and B_i represent linguistic labels. $\mu_{Ai}(x)$ and $\mu_{Bi-2}(y)$ can be of any fuzzy membership function. If a bell-shaped membership function is used, $\mu_{Ai}(x)$ is given as:

$$\mu_{Ai} = \frac{1}{1 + \left[\left(\frac{x - c_i}{a_i}\right)^2\right] b_i}; \;\; i = 1,2 \qquad \textbf{(49)}$$

where $a_i, b_i, and\ c_i$ being variables for the membership function.

- For layer (2), all nodes are fixed. In this layer, the fuzzy operators are involved and the AND operator is used to fuzzify the inputs. The layer is labelled with π to indicate that it performs as a simple multiplier. The output of layer (2) is called the firing strength and is given by:

$$O_2, i = w_i = \mu_{Ai}(x) * \mu_{Bi}(y), i = 1,2.$$

- For layer (3), the nodes are also fixed. This layer is labelled N indicating that its role is to normalize firing strengths from layer (2). The output of layer (3) is called normalized firing strength and is represented as:

$$O_3, i = \overline{w_i} = \frac{w_i}{w_1 + w_2}, i = 1,2.$$

- For layer (4), the nodes are adaptive. The output of this layer is a product of the first-order polynomial (first-order Sugeno model) and normalized firing strength from layer (3). The output of layer (4) is given by:

$$O_4, i = \overline{w_i} f_i = \overline{w_i}(p_i x + q_i y + r_i); i = 1,2$$

where $\overline{w}$ is the layer (3) output and p_i, q_i and r_i are the subsequent parameters.

- For layer (5), there is one fixed node denoted by $\sum x$. This layer sums all the incoming signals of the model. The output of layer (5) is given by:

$$O_5, i = \sum_i \overline{w}\, f_i = \frac{\sum_i w_i f_i}{\sum_i w_i}$$

The proposed MPPT technique must be able to extract the maximum power from PV modules quickly and effectively with minimum power oscillations. The ANFIS controller has to work as a reference model of PV modules for computing the maximum power from input variables which are the temperature and irradiance.

4.4.2 Adaptive neuro-fuzzy inference system model

The proposed ANFIS based MPPT controller is made up of the ANFIS reference model, FL power controller and a DC-DC boost converter as shown in **Fig. 54**. This MPPT controller is based on the fact that by knowing the maximum possible power output of a PV module for a given set of solar irradiance and temperature, the real-time MPP of the solar module can be perfectly tracked.

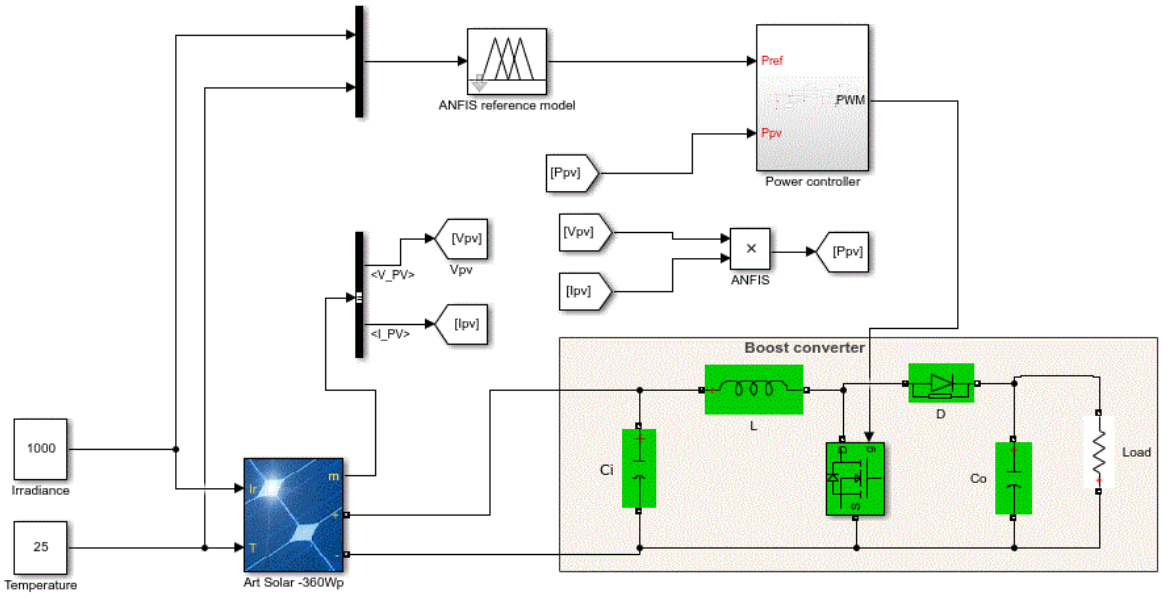

Figure 54: ANFIS based MPPT controller.

The ANFIS reference model provides the system with a reference value of the maximum possible power output from a solar module at a certain temperature and irradiance. At the same irradiance and temperature, the actual power output which is coming from PV modules is measured and compared to the reference value from the ANFIS model. The difference between the two power values is calculated to give an error, which is then fed to the FL power controller to generate a control signal. The signal generated by the FL power controller is given to the Pulse Width Modulator (PWM). The PWM generates a signal at a high level of frequency to control the duty cycle of the DC-DC power converter and force PV modules to operate at the MPP. It should be noted that most of the ANFIS based MPPT controllers that have been presented in the literature rely on the PI(D) controller for generating the duty cycle for the DC-DC power converter as given in [178-181]. Thus, the use of the FL power controller for generating the duty cycle makes this research work unique. The proposed model has two inputs (solar irradiance and temperature) and one output which is the reference maximum power output of the PV modules. The temperature and irradiance values for the particular site used in this study have been obtained from the PVGIS website. And the reference maximum power output values are obtained from simulating the MATLAB/Simulink model of the ART solar-360Wp solar array without connecting any load. Therefore, the ANFIS is trained with 145 data sets of temperature and irradiance as inputs and the reference maximum power as the output. The power controller is used to track the maximum power point by varying the duty cycle of the boost converter basing on the data stored in the ANFIS reference model. The design of the

ANFIS is based on the Sugeno inference model, 5 triangular membership functions are chosen for solar irradiance and 3 triangular membership functions for temperature. The structure of the ANFIS is shown in the figure below:

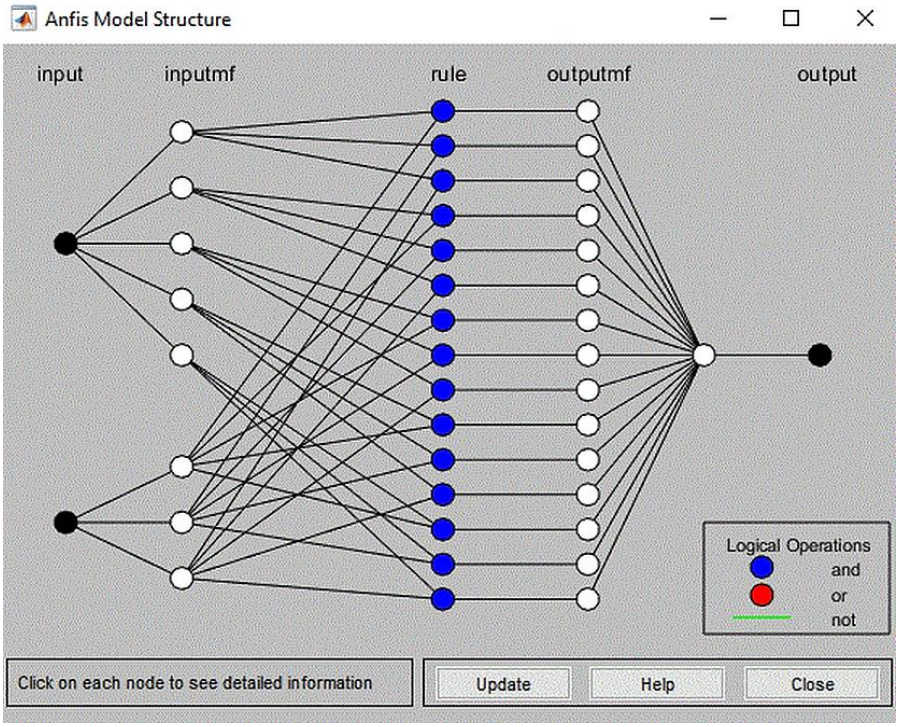

Figure 55: ANFIS reference model structure

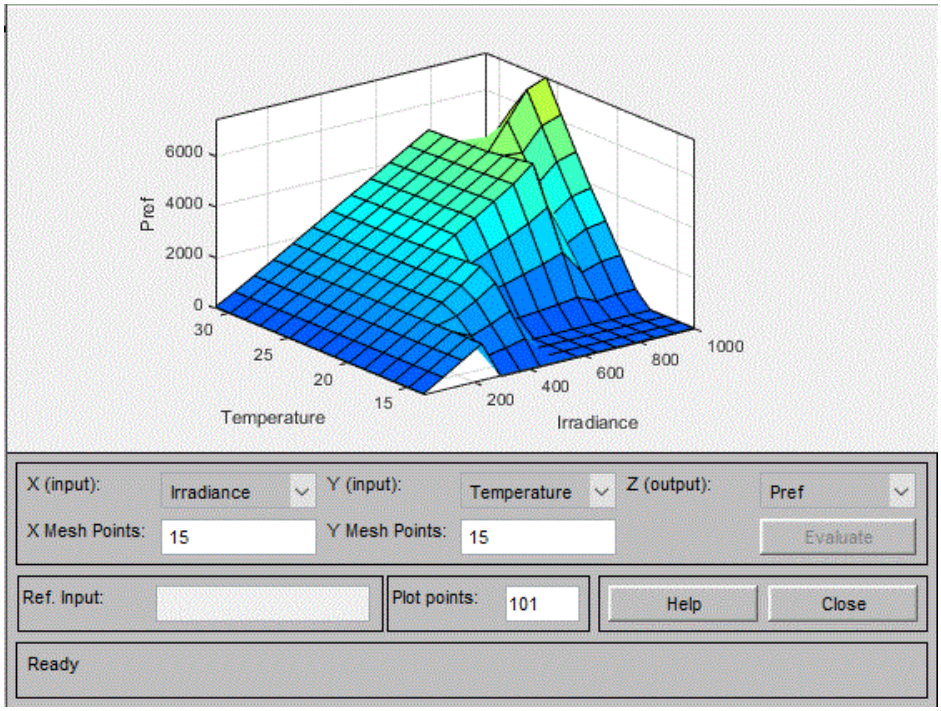

Figure 56: Surface view of the ANFIS reference model showing the mapping of inputs and outputs.

4.4.3 DC-DC Boost converter

MPPT algorithms are implemented using highly efficient DC-DC power converters. There are several topologies of DC-DC power converters which can be used for maximum power point tracking and these include the boost converter, buck converter, Cùk converter and SEPIC converter. Because of its simplicity and ability to step up the voltage, the boost converted is adopted in this study. In this study, a boost converter is used due to its simplicity and high reliability as compared to other converters [182]. A boost converter is made up of two semiconductor switches (diode and Mosfet), an inductor and a capacitor as shown in the diagram below.

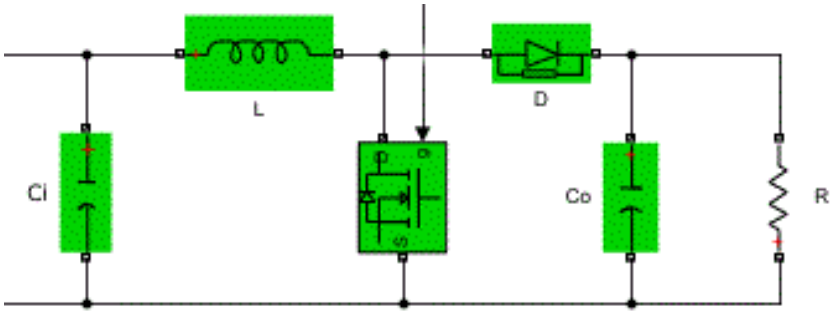

Figure 57:DC-DC boost converter

The converter utilizes the maximum power transfer theory to be able to track the MPP of solar modules. According to the theory, the maximum power is only transferred from the source to the load when the source impedance matches the load impedance (load matching). In other words, the input to the DC-DC boost converter as seen by the PV module must match the load impedance for the maximum power to be transferred to the load. The load matching is achieved by using an ANFIS algorithm to adjust the duty cycle of the DC-DC converter. The duty cycle, D, is defined as the ratio between the period the switch is on to the total switching period. A boost converter is made up of two semiconductor switches (Mosfet and diode), an inductor, and a capacitor. The working principle of the boost converter is based on that, the inductor, L, resist sudden changes in input current. Assuming continuous conduction mode of operation, the converter has two states of operation which are given below.

a) ON state

During this state, the MOSFET switch, S, will be on and the diode switch, D, will be off. The diode will be open-circuited because the n side of the diode will be higher compared to the p side which will be shorted to the ground. The current flow through the inductor and then to the MOSFET. The inductor stores energy in the form of a magnetic field. On the other side of the

circuit, the current flows from the capacitor to the load. The ON state duration is given by $T_{ON} = D + T$, where D is the duty cycle and T is the switching frequency.

b) OFF state

In this state, the control signal turns off the MOSFET and the diode is turned on. The inductor discharges and the current flows through the diode to the filter capacitor and the load. The capacitor stores energy in the form of charge. The filter capacitor in the output circuit is assumed to be large such that the Resistor-Capacitor (RC) time constant is higher than the switching frequency to ensure constant output voltage.

The boost converter is designed at STC of the solar module. The PV array specifications are given in **Table 2**. Thus, the PV output current, $I_{PV} = I_{MPP}$, output voltage, $V_{PV} = V_{MPP}$ and output power, $P_{PV} = P_{MPP}$. Therefore, the input/output voltage and current relationships of a DC-DC boost converter are given by,

$$V_o = \frac{V_{MPP}}{1 - D} \tag{50}$$

$$I_o = (1 - D) I_{MPP} \tag{51}$$

where V_o is the output voltage of the converter, V_{MPP} is the input voltage to the converter, I_o is the output current of the converter, I_{MPP} is the input current to the converter. The relationship between the load resistance (R) and optimal internal resistance of the PV module (R_{MPP}) is given as,

$$R = \frac{R_{MPP}}{(1 - D_{MPP})^2} \tag{52}$$

where $R = \frac{V_o}{I_o}$, $R_{MPP} = \frac{V_{MPP}}{I_{MPP}}$ and D_{MPP} is the duty cycle at MPP at STC. Since the range of the duty cycle is between 0 and 1, the load resistance must be equal to or greater than the optimal internal resistance of the PV module $(R \geq R_{MPP})$. At STC, $R_{MPP} = \frac{V_{MPP}}{I_{MPP}}$. Using the load resistance of 10Ω and assuming a lossless converter $(P_o = P_{PV} = P_{MPP})$, the output voltage of the converter is determined as,

$$V_o = \sqrt{P_o R} = 60\ V. \tag{53}$$

The duty cycle at MPP at STC is determined as,

$$D_{MPP} = 1 - \frac{V_{PV}}{V_0} = 0.35.$$

The PV module's voltage varies with the current and to minimize ripples, the minimum value of the inductor has to be designed for 1% current ripples (ΔI_{PV}) at a high-frequency value of 20 kHz as given below [183],

$$L \geq \frac{V_{PV} \times D_{MPP}}{2 \times \Delta I_{PV} \times f} = 3.7\ mH.$$

The minimum value of the input capacitor has to be designed for 1% of the voltage ripples as given below [183],

$$C \geq \frac{D_{MPP}}{2 \times \Delta V_o \times f \times R} = 87.5\ nF.$$

In this study, the input capacitor, C_i, is incorporated to reduce the ripples of the input voltage as well as to deliver alternating current to the inductor. The selected design parameters of the DC-DC boost converter are given in the table below.

Table 4: Selected parameters of the boost converter

Parameter	Symbol	Value
Input voltage	V_{MPP}	39 V
Input current	I_{MPP}	9.24 A
Duty ratio	D_{MPP}	0.35
Inductor	L	3.7 mH
Load resistance	R	10 Ω
Output capacitor	C_o	87.5 μF
Input capacitor	C_i	4000 μF
Switching frequency	f	20 kHz

4.4.4 Design of the power controller

The power controller is based on FL and it is used to generate the control signal for the converter. The signal is generated based on the error between the actual power output of the PV array and the reference power output given by the ANFIS reference model. The FL power controller has two input variables (error, E, and change in error, CE) and one output variable (duty cycle increment, ΔD).

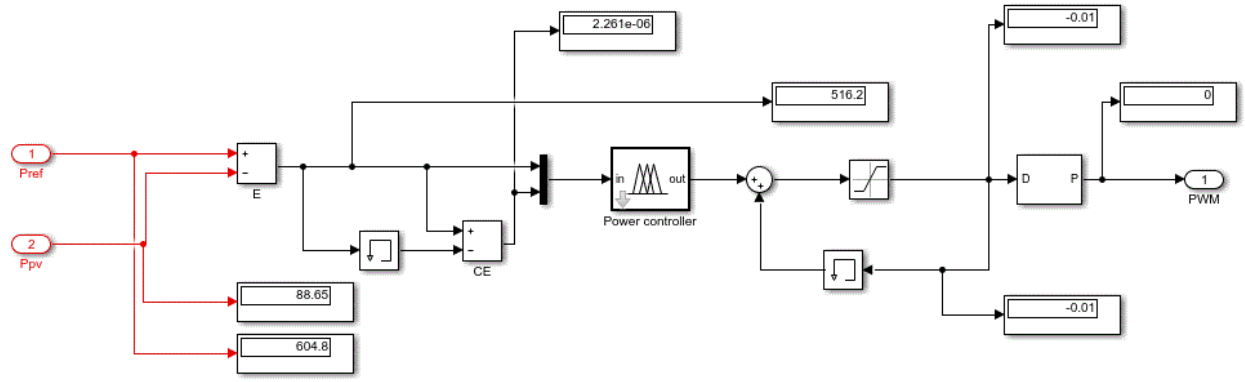

Figure 58: FL power controller model

Triangular membership functions were used for each variable in the design of the FL controller. Five membership functions were chosen for each variable and defined as: Very Low (VL), Low (L), Neutral (N), High (H) and Very High (VH). The ranges of the variables are given as E $(-100\ to\ 100)$, CE $(-10\ to\ 10)$ and D $(-0.1\ to\ 0.1)$.

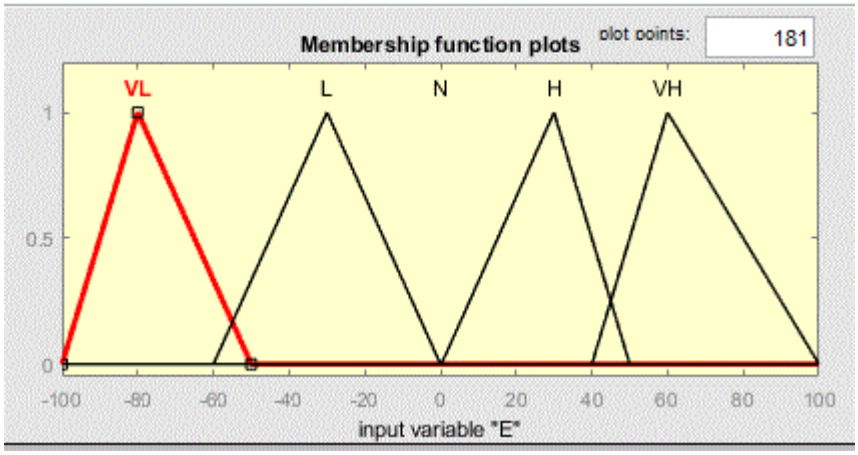

Figure 59: Membership functions of the error, E.

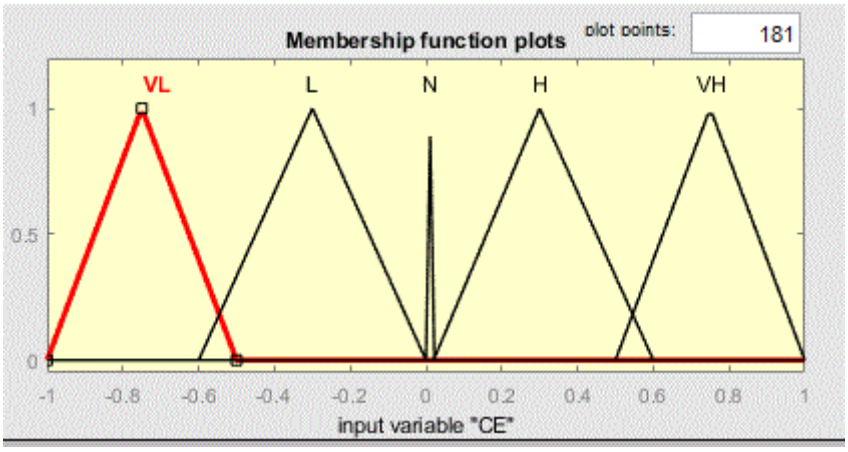

Figure 60:Membership functions of the change in error, CE.

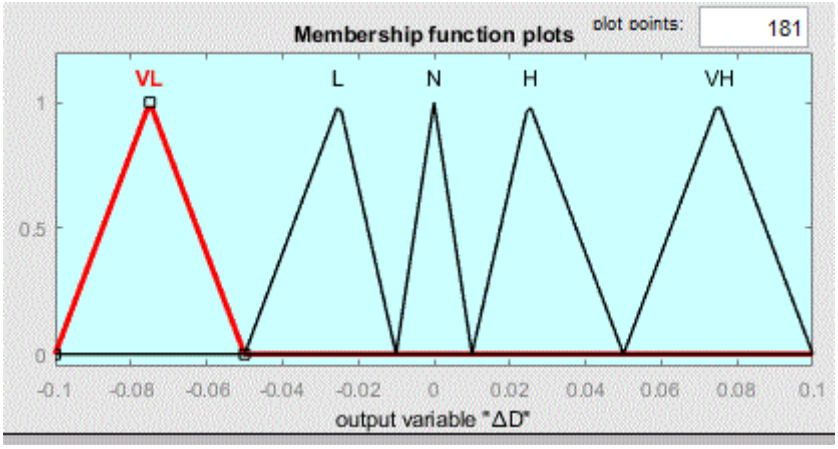

Figure 61: Membership functions of the duty cycle increment, ΔD.

Thus, the FL power controller is designed with 25 fuzzy rules shown in **Table 5**. Rows and columns represent the input variables (E) and (CE) and the output variable (ΔD) is located at the intersection of the row and the column.

Table 5:Fuzzy rules of the FL power controller

E/CE	Very Low	Low	Neutral	High	Very High
Very Low	VH	VH	H	VL	VL
Low	H	H	H	VL	L
Neutral	H	H	N	L	L
High	H	H	L	L	VL
Very High	H	H	L	L	VL

4.5 Energy management controller

The Energy Management Controller (EMC) must satisfy the load demand regardless of the variation of the power coming from the renewable energy source. Thus, the EMC must select the appropriate energy source or a combination of energy sources at each instant to maintain a constant DC bus voltage to power the water pump. The DC bus is supplied by the PV array, VSDG, and the battery bank. As mentioned before, the PV system is the main source of energy and the VSDG constantly fills up the gap between the energy generated by the PV system and the required load value. The EMC is based on fuzzy logic. Fuzzy logic control is an adaptive control that gives a robust performance for both linear and non-linear control systems. The controller is used to control the power generated by the PV modules, battery bank, and the VSDG. Depending on the available power and the load demand, the fuzzy logic controller

selects either a single power source or a combination of power sources that can meet the load demand. The controller also regulates the charging and discharging of the battery bank by activating the charging switch when the power from PV modules is in excess and activating the discharging switch when the PV modules do not meet the load demand. The following are the modes of operation of the energy management controller.

Mode 1: Total generated power from PV modules (P_{PV}) is equal to or greater than the load demand (P_L).

In this scenario, the controller must first check the SOC of the battery bank. If the SOC is less than the maximum state of charge of the battery (SOC_{max}), the controller must direct excess energy to charge the battery bank until it reaches SOC_{max}. When the battery bank reaches it SOC_{max}, the controller must terminate the charging to avoid overcharging of the battery bank. The power balance equation is given by,

$$P_{PV} = P_B + P_L.$$

where P_B is the power from the battery bank.

Mode 2: Total generated power from PV modules is less than the load demand.

In this mode, the controller has to also first check the SOC of the battery bank. If the SOC is greater than the minimum discharge limit, SOC_{min}, the controller must discharge the battery to meet the load demand until the battery bank reaches SOC_{min}. The power balance equation is given by,

$$P_L = P_{PV} + P_B$$

Mode 3: Total power produced by the PV modules plus the battery storage is less than the load demand.

The VSDG must be started when the sum of power from the PV modules & battery bank do not meet the load demand. The VSDG must operate to constantly fill up the gap between the power produced by the PV modules & battery and the load demand. If the solar irradiance increases, the power from the PV modules also increases thereby charging the battery bank. When the battery bank charges and reaches the float level, SOC_{fl}, and if the sum of the power from the PV modules & battery bank meets the load demand, the VSDG is switched off.

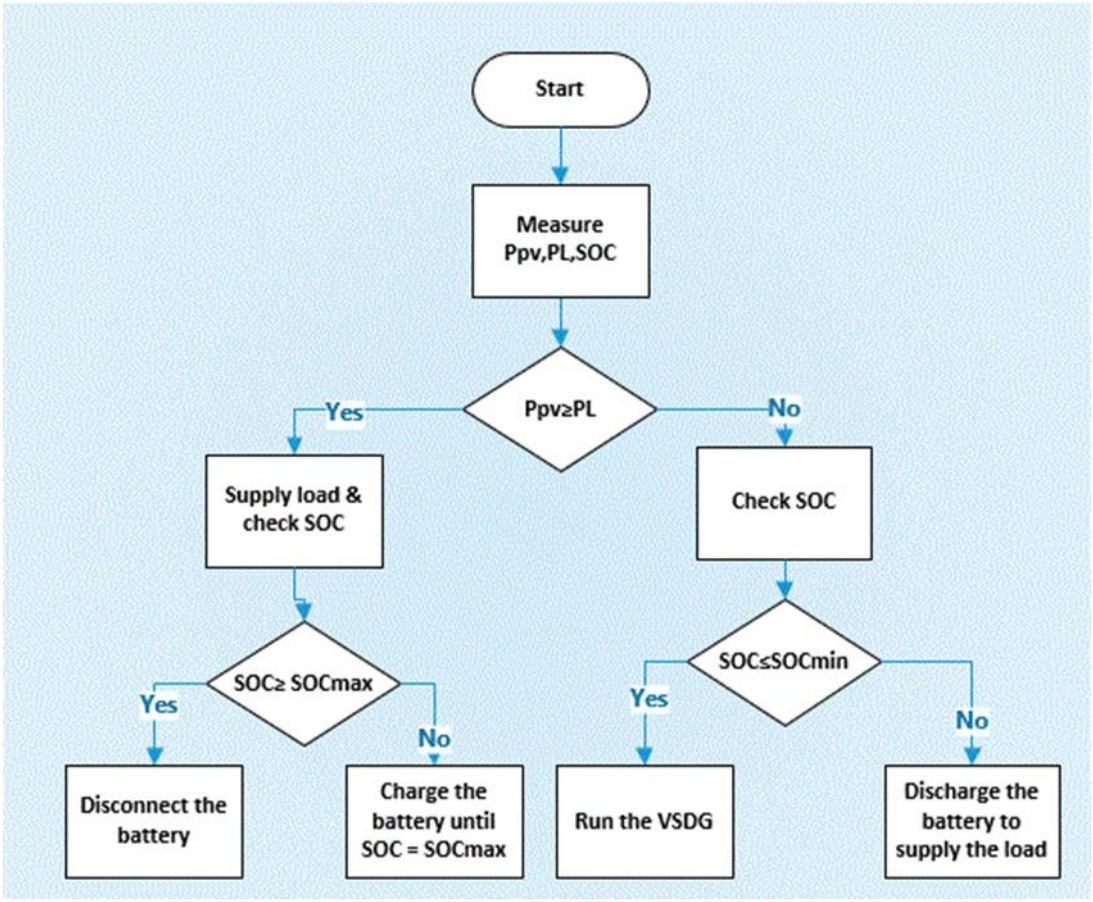

Figure 62: Flow chart of the EMC.

4.5.1 Design of the fuzzy logic controller

The IF-THEN rules of the Fuzzy Logic Controller (FLC) relate the inputs to the outputs variables of the system. In this research, the fuzzy input variables are P_{PV} & SOC and output variables are the VSDG status ($VSDG_{status}$), VSDG speed ($VSDG_{rpm}$) and battery bank status (B_{status}) as shown in **Fig. 63**. The FLC is modelled and implemented in MATLAB/Simulink environment.

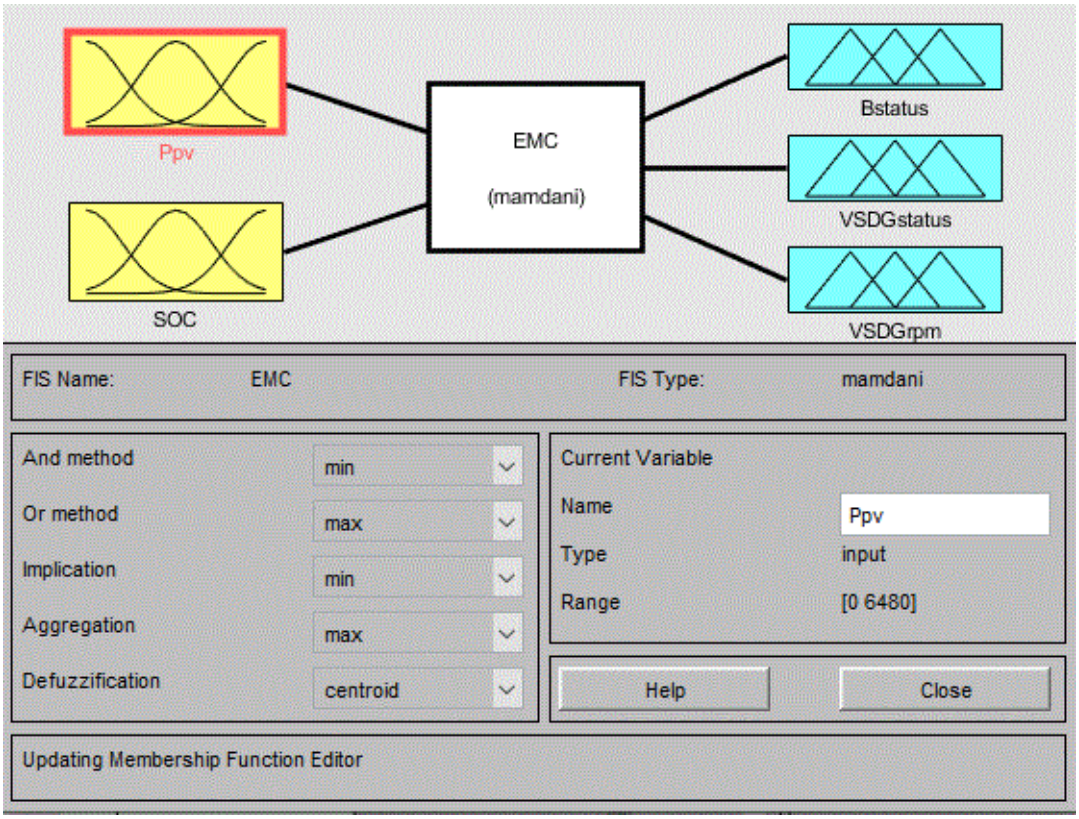

Figure 63: Fuzzy logic designer of the EMC.

The battery bank state of charge has 3 triangular membership functions which are described as LOW (0-20%), MEDIUM (20-80%) and HIGH (80-100%). The maximum power the PV array can produce at STC is 6480W (18 modules × 360Wp). Therefore, the membership functions of P_{PV} are described as LOW (0-2160W), MEDIUM (2160-4320W) and HIGH (4320-6480W) as shown in **Table 6**.

Table 6: The ranges of the input variables membership functions

Input variables	**LOW**	**MEDIUM**	**HIGH**
SOC	0 - 20	20 - 80	80 - 100
P_{PV}	0 - 2160	2160 - 4320	4320 - 6480

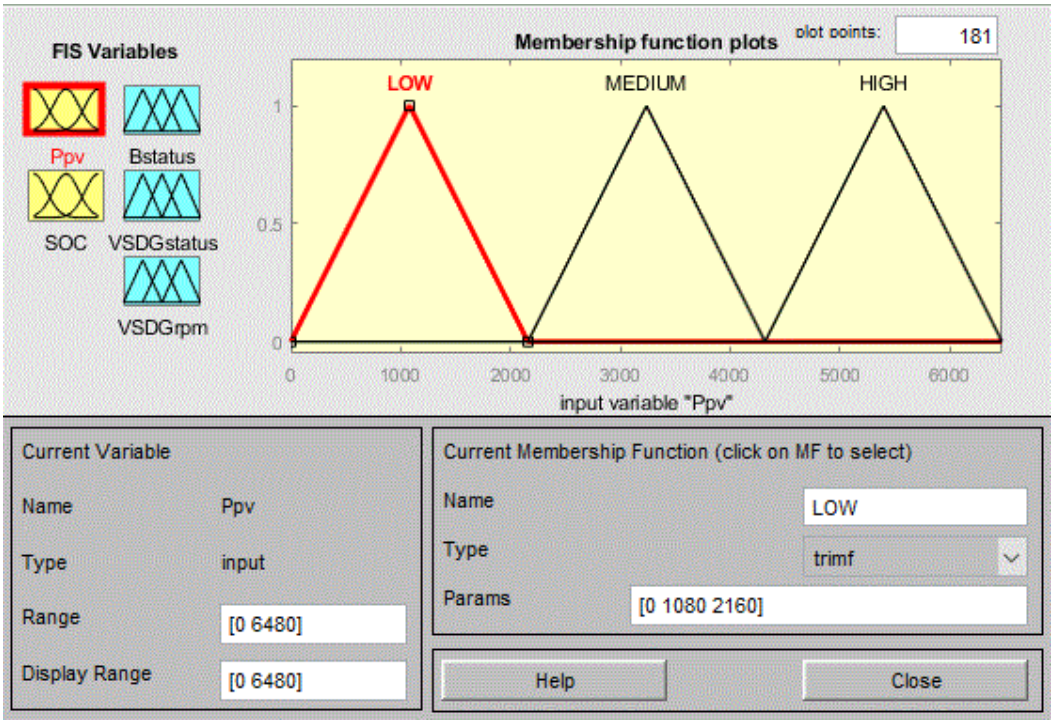

Figure 64: Membership functions of the PV array power output.

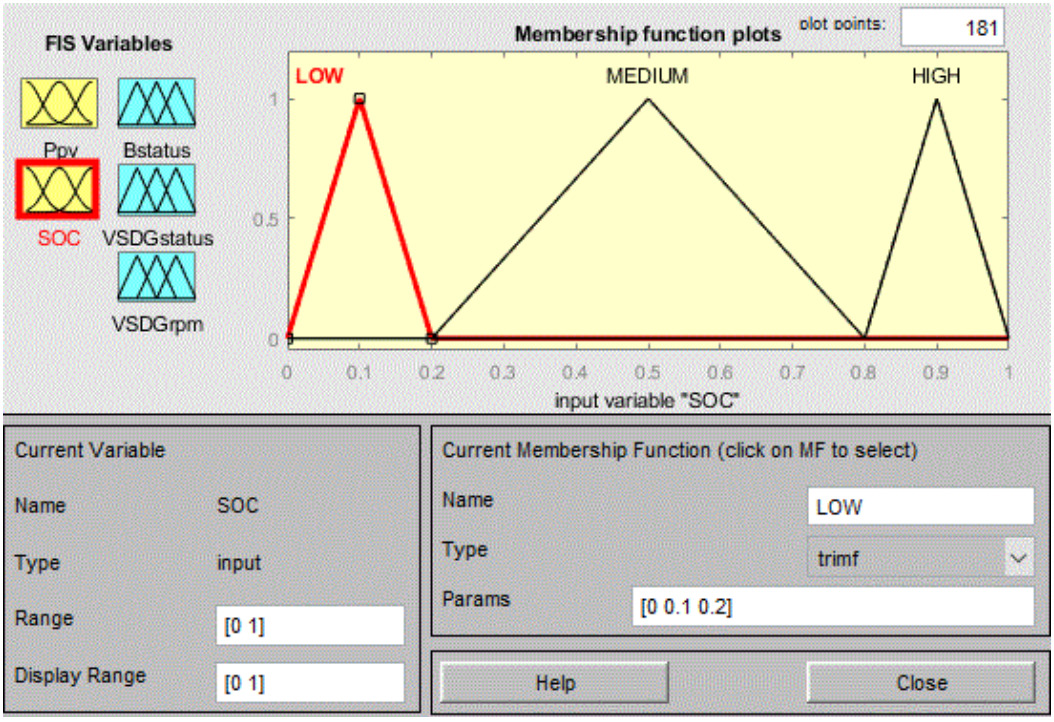

Figure 65: Membership functions of the battery bank state of charge.

For the output variables, the battery bank control has 3 membership functions namely, charging (0-0.2), discharging or charging (0.2-0.8) and discharging (0.8-1.0). These membership functions have to control the battery bank status such that when the battery's SOC exceeds 80 %, the charging control is terminated and the battery bank will only be able to discharge to

complement the power from the PV array to meet the load demand. When the SOC is between 20% to 80%, the status of the battery bank will be either charging or discharging depending on the PV array power output. And when the SOC is below 20%, the battery bank control will be charging as shown in **Table 7**.

Table 7: The ranges of the membership functions of the battery bank status

Output variable	**Charging**	**Discharging/ Charging**	**Discharging**
B_{status}	0 – 0.2	0.2 – 0.8	0.8 – 1.0

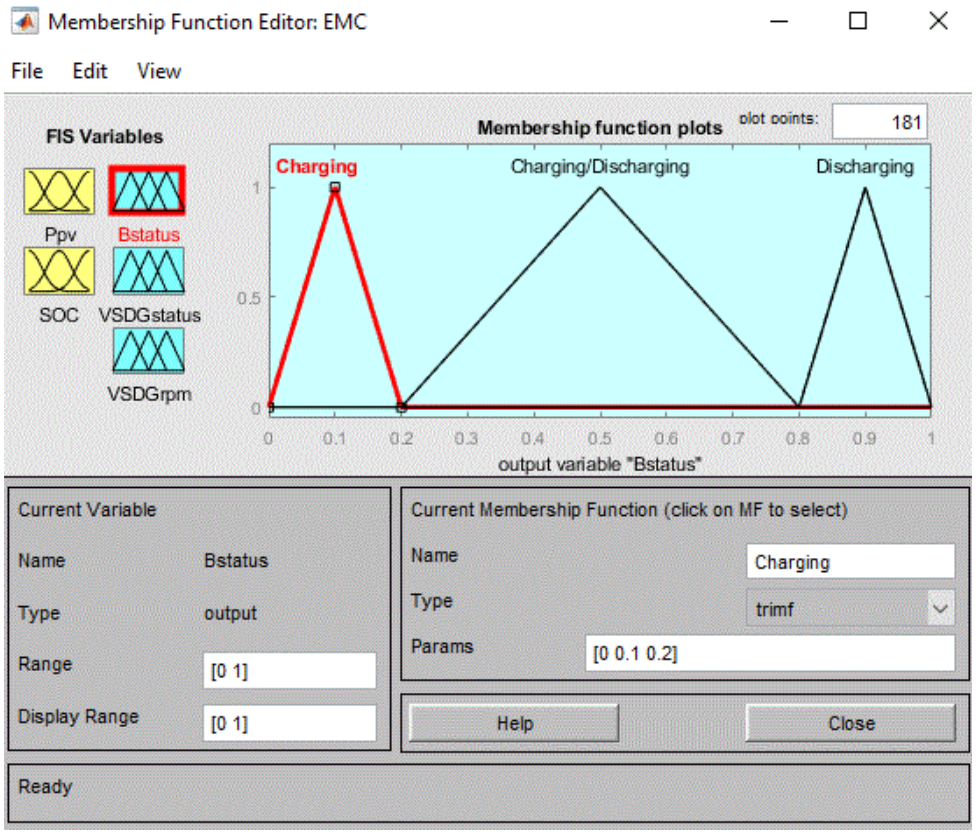

Figure 66: Membership functions of the battery bank status.

The VSDG has an operating range of 2300 rpm to 2900 rpm. At maximum speed, the VSDG generates a maximum power output of 6 kW. The membership functions of the VSDG control are designed in such a way that the speed of the generator has to be adjusted to generate the power that adds up to the PV array's output to meet the load demand when the power from the PV system is not enough to power the load as shown in **Table 8**.

Table 8: The ranges of the membership functions of the VSDG speed.

Output variable	**LOW**	**MEDIUM**	**HIGH**
$VSDG_{rpm}$	2300 - 2500	2500 - 2700	2700 - 2900

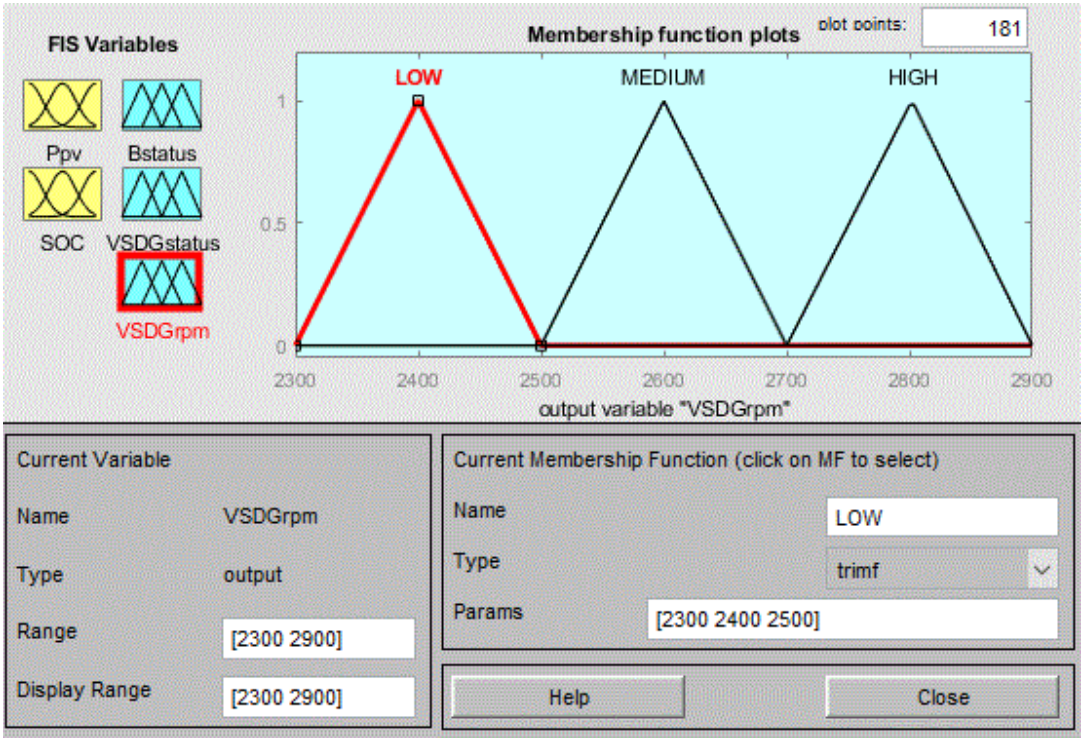

Figure 67: Membership functions of the VSDG speed.

The last output variable of the FLC is the VSDG status which is described as OFF (0-0.5) and ON (0.5-1.0). The membership functions of this variable are designed to start the generator when the primary sources (PV array & battery bank) do not meet the load demand. The membership functions of VSDG status are shown in **Table 9.**

Table 9: The ranges of the membership functions of the VSDG status.

Output variable	**OFF**	**ON**
$VSDG_{status}$	0 – 0.5	0.5 - 1

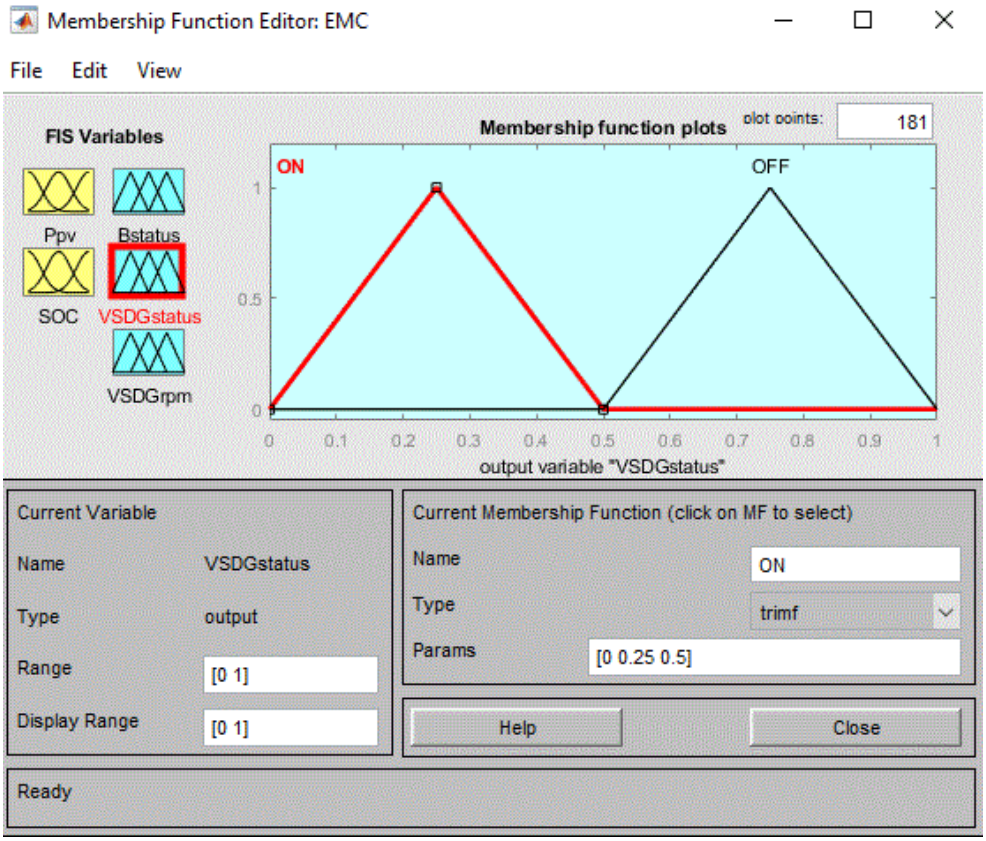

Figure 68: Membership functions of the VSDG status.

Using the membership functions of different variables designed above, the IF-THEN rules of the FLC are created. **Table 10** shows nine different rules for different operational conditions of the hybrid system. In MATLAB/Simulink, the IF-THEN rules can be represented using the Rule Viewer. The Rule Viewer shows rules that are active or not active and it also indicates how each membership function influence the results of the system. **Fig. 69** shows the Rule Viewer of the designed EMC.

Table 10: Fuzzy rules for the EMC.

1.	**IF** the P_{PV} is HIGH and SOC is HIGH **THEN** B_{status} is Discharging and $VSDG_{rpm}$ is ZERO.
2.	**IF** the P_{PV} is HIGH and SOC is MEDIUM **THEN** B_{status} is Charging/Discharging and $VSDG_{rpm}$ is ZERO.
3.	**IF** the P_{PV} is HIGH and SOC is LOW **THEN** B_{status} is Charging and $VSDG_{rpm}$ is ZERO.
4.	**IF** the P_{PV} is MEDIUM and SOC is HIGH **THEN** B_{status} is Discharging and $VSDG_{rpm}$ is ZERO.

5.	**IF** the P_{PV} is MEDIUM and SOC is MEDIUM **THEN** B_{status} is Charging/Discharging and $VSDG_{rpm}$ is LOW.
6.	**IF** the P_{PV} is MEDIUM and SOC is LOW **THEN** B_{status} is Charging and $VSDG_{status}$ is ON and $VSDG_{rpm}$ is MEDIUM.
7.	**IF** the P_{PV} is LOW and SOC is HIGH **THEN** B_{status} is Discharging and $VSDG_{rpm}$ is ZERO.
8.	**IF** the P_{PV} is LOW and SOC is MEDIUM **THEN** B_{status} is Charging/Discharging and $VSDG_{rpm}$ is MEDIUM.
9.	**IF** the P_{PV} is LOW and SOC is LOW **THEN** B_{status} is Charging and $VSDG_{rpm}$ is HIGH.

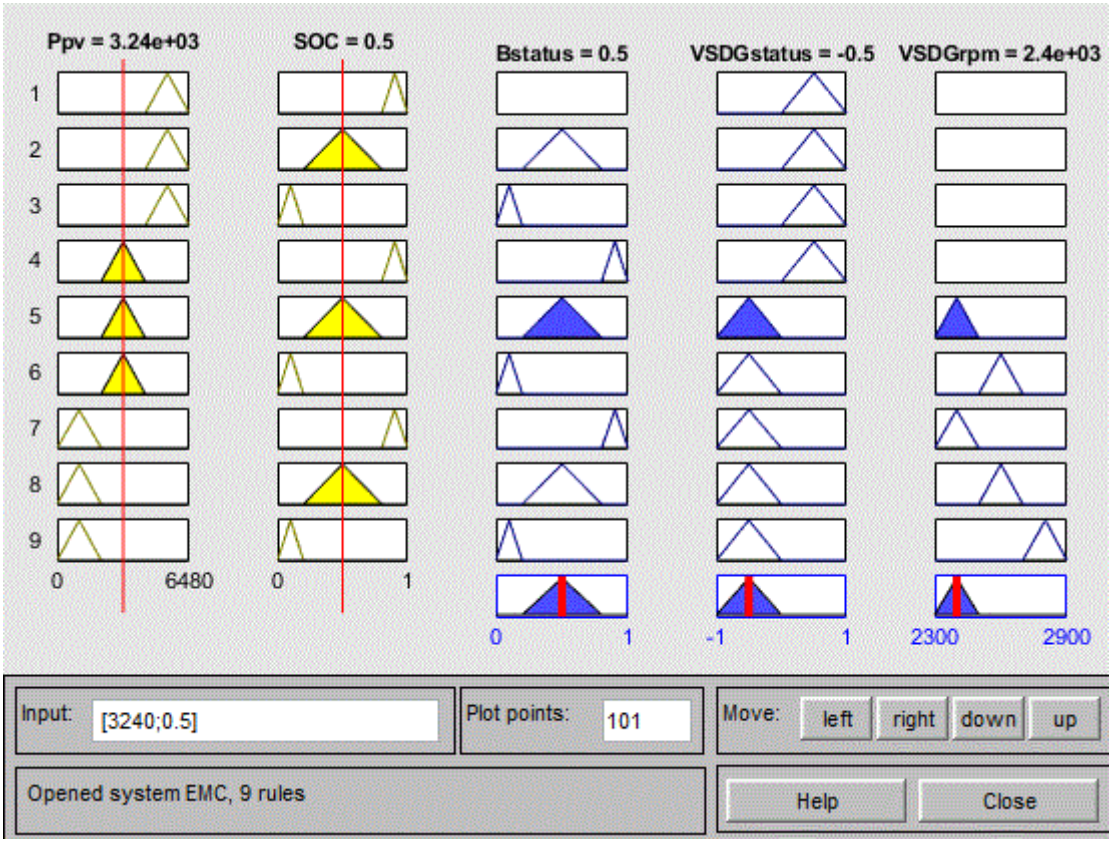

Figure 69: Rule viewer of the FL based EMC.

To show how each output depends on one or two of the inputs, the Surface Viewer is utilized. The Surface Viewer generates input/output surface mapping of the system as shown in **Fig. 70, 71 and 72.**

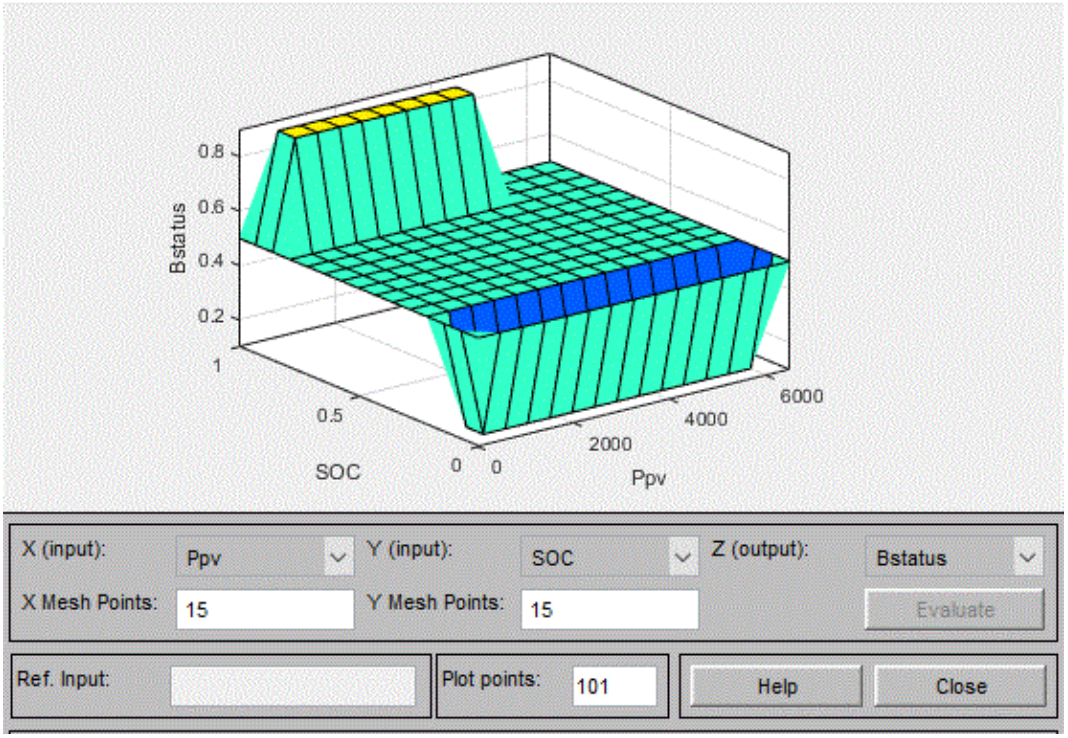

Figure 70: Surface viewer of P_{PV}, SOC and B_{status}.

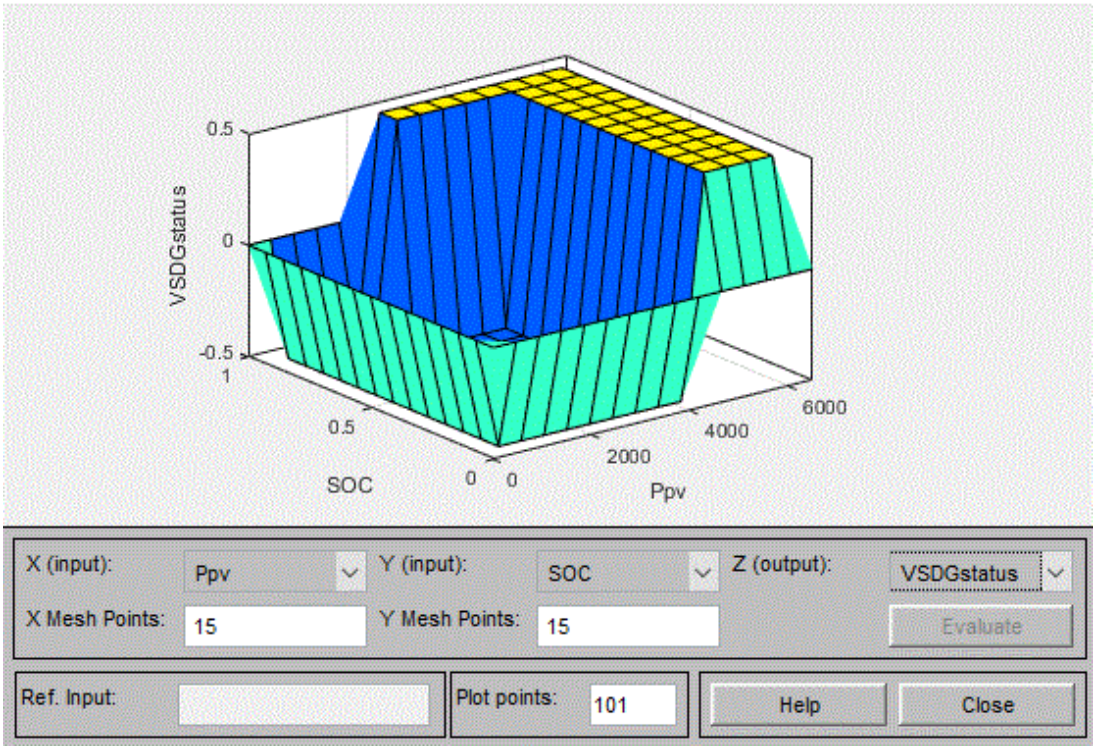

Figure 71: Surface viewer of P_{PV}, SOC and $VSDG_{status}$.

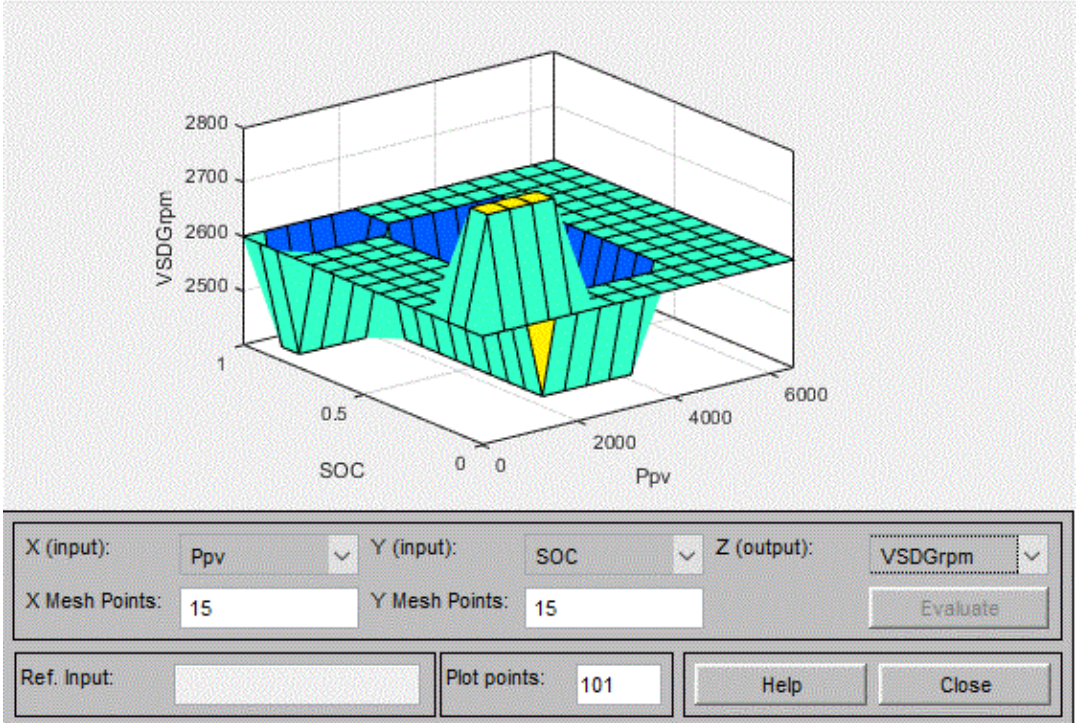

Figure 72: Surface viewer of P_{PV}, SOC and $VSDG_{rpm}$.

4.6 DC water pumping unit

The water pumping unit is made up of a Permanent Magnet DC (PMDC) motor and a submersible pump. Submersible pumps can be described as multi-stage centrifugal pumps that operate in a vertical position. The specifications of the solar water pump for this application are given below.

Table 11: Solar water pump specifications [184].

Brand	Tata
Model	5 Hp – DC Submersible
Pump capacity	5 Hp
Maximum pump head	50 m
Motor type	Permanent Magnet Direct Current (PMDC) motor
Module capacity	≥ 4800Wp
Rated speed	3600rpm

4.6.1 DC motor modelling

DC motors are electrical machines that convert DC electrical power to mechanical power. In a PMDC motor, the field winding is a permanent magnet and no external excitation is needed. The diagram below shows an equivalent circuit of the PMDC motor.

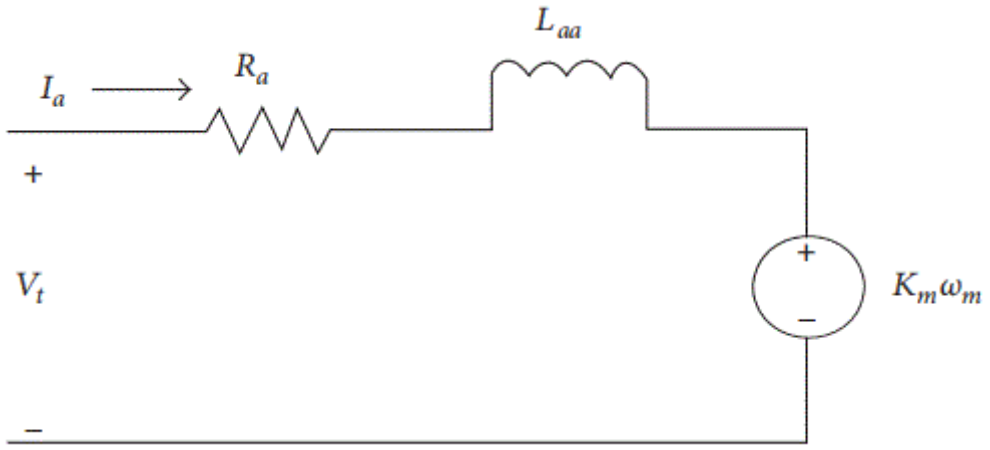

Figure 73: Equivalent circuit of a PMDC motor

The terminal voltage (V_t) is given by,

$$V_t = I_a R_a + L_{aa}\frac{dI_a}{dt} + k_m w_m \tag{54}$$

where I_a is the armature current, R_a is the armature resistance, L_{aa} represents the inductance, k_m is the motor torque constant and w_m is the angular speed of the motor.

The electrical torque (T_e) is given as,

$$T_e = k_m I_a \tag{55}$$

and the motor speed is written as a function of the electrical torque and the load torque (T_L) as

$$J\frac{dw_m}{dt} = T_e - T_L - B_m w_m \tag{56}$$

where J is the inertia constant, B_m is the viscous friction coefficient. Therefore, rearranging equations **54**, **55** and **56**, the dynamic behaviour of the PMDC is given by,

$$\begin{cases} \dfrac{dI_a}{dt} = \dfrac{1}{L_{aa}}(V_t - I_a R_a - k_m w_m) \\ \dfrac{dw_m}{dt} = \dfrac{1}{J}(T_e - T_L - B_m w_m) \end{cases} \tag{57}$$

The MATLAB/Simulink model of the DC water pump is shown in **Fig. 74**.

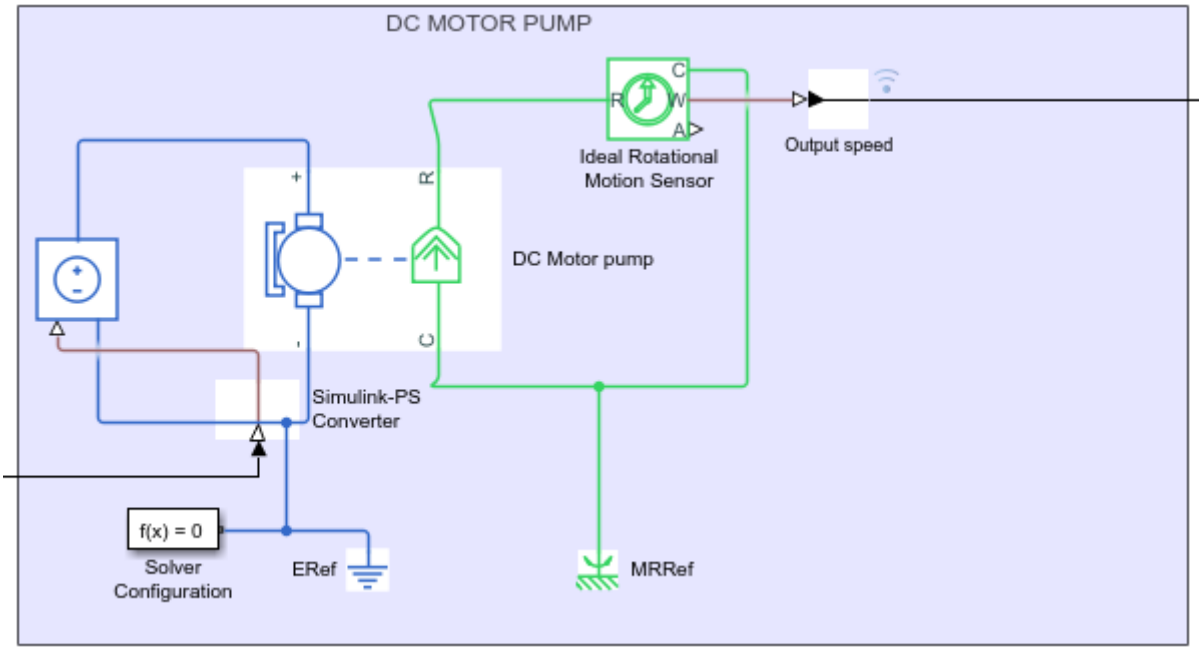

Figure 74:MATLAB/Simulink model of the DC water pump.

5.0 SYSTEM TESTING AND RESULTS ANALYSIS.

The modelling of the AI-based solar-diesel hybrid water pumping system is described in detail in Chapter 4. To verify the performance of the proposed hybrid water pumping system, several case studies are presented in this chapter. The performance of the proposed ANFIS based MPPT controller as well as the EMC is tested through simulations in the MATLAB/Simulink environment.

5.1 ANFIS based MPPT controller simulations

As stated before, if the PV module is connected directly to the load, its operating point is rarely at the MPP. MPPT techniques are employed to match the internal resistance of the PV module to the load resistance for maximum power to be transferred to the load. To analyse the dynamic behaviour of the proposed ANFIS based MPPT controllers and to find out if the maximum possible power is being extracted, different scenarios are considered and simulated in the MATLAB/Simulink environment.

Scenario 1: At STC, with and without the proposed MPPT controller.

The proposed MPPT controller is simulated at STC (1000W/ m^2 & 25 ℃) and then compared to the simulation of the same circuit but without the MPPT controller.

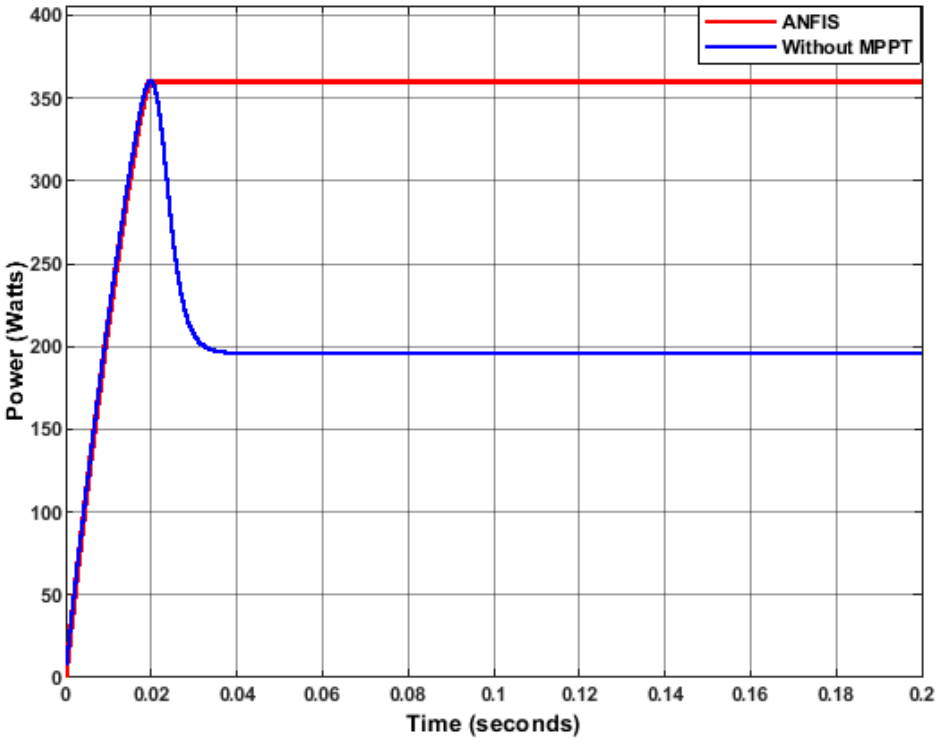

Figure 75: At STC, with and without the proposed MPPT controller.

Fig. 75 shows the PV module power output with the proposed MPPT (red line) and without the MPPT controller (blue line). In both graphs, the PV power output rises sharply from zero up to about the MPP (360 W) after a time of 20 ms. For the system with the MPPT controller, the power output settles at MPP since the MPPT controller will be continuously forcing the PV module to operate at the MPP. For the system without the controller, the PV power output drops and settles at around 200 W. This is because the load resistance doesn't match the internal resistance of the module and there is no external circuit that can force the PV to find its MPP.

Scenario 2: Under varying irradiance, with and without the proposed MPPT.

In this case, the proposed controller is evaluated at 25 ℃ and with sudden changes in solar irradiance levels (1000W/m^2, 850W/m^2 500W/m^2, and 50W/m^2).

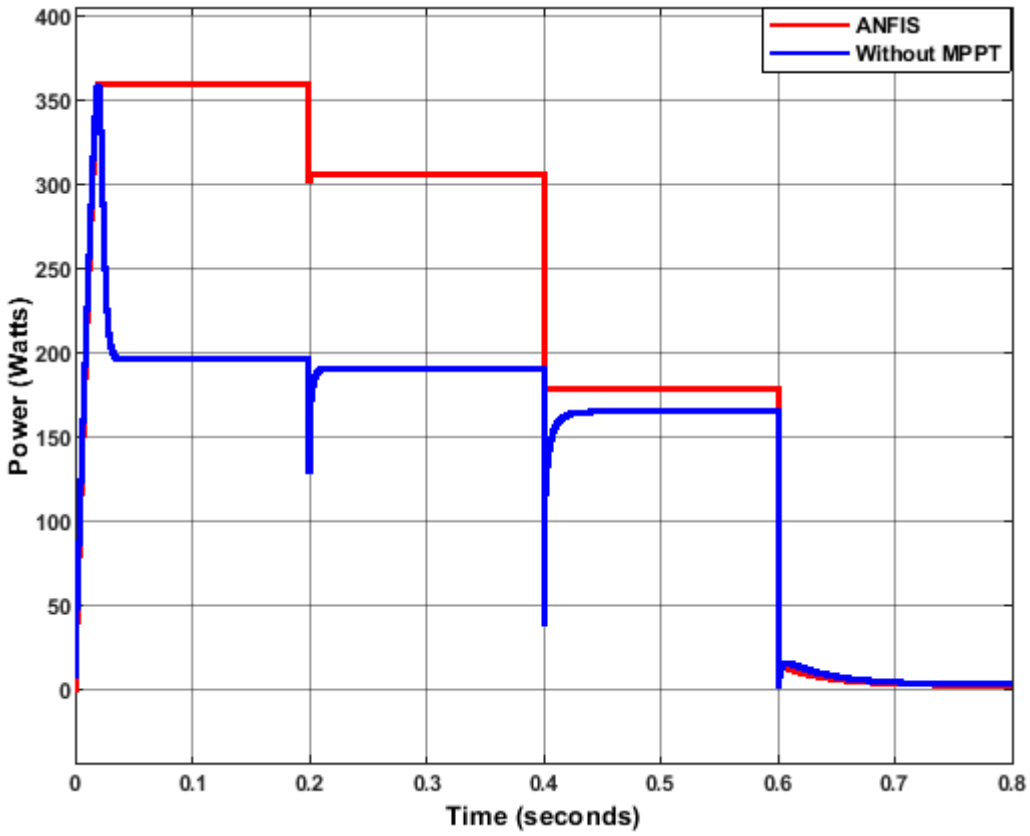

Figure 76: Under varying solar irradiance, with and without the proposed MPPT controller.

Fig. 76 shows the PV power output curves for the two systems. It can be noted that the proposed MPPT controller presents a good performance under varying solar irradiance since it perfectly tracks the MPP for different solar irradiances levels. For the PV module without the MPPT controller, the system does not operate at the MPP. However, it should be noted that between 0.4 seconds and 0.8 seconds, the system without the controller operates around the MPP. This

is because, during that period, the optimal internal resistance of the solar module is almost equal to the load resistance of the circuit.

At 25 ℃, 500W/m^2 the optimal internal resistance of the PV module is given by,

$$R_{MPP} = \frac{{V_{MPP}}^2}{P_{MPP}} = 8.5\Omega,$$

which is almost equal to the load resistance of 10 Ω. Because of that, the PV module can operate at almost MPP without the inclusion of any controller to control its operating point.

Scenario 3: At STC, comparing with the P&O MPPT controller.

The performance of the proposed ANFIS based MPPT controller is also evaluated by comparing it with the P&O MPPT technique at STC. It can be noted from **Fig. 77** that for both MPPT controllers, the PV module power output rises sharply up to the MPP with the rise time of 20 ms. For the system with the ANFIS based MPPT controller, the power output settles and maintains that value. However, for the system with the P&O MPPT controller, the power output oscillates about the MPP before settling down. The power output of the P&O technique settles at the MPP after 80 ms as shown in **Fig. 77.**

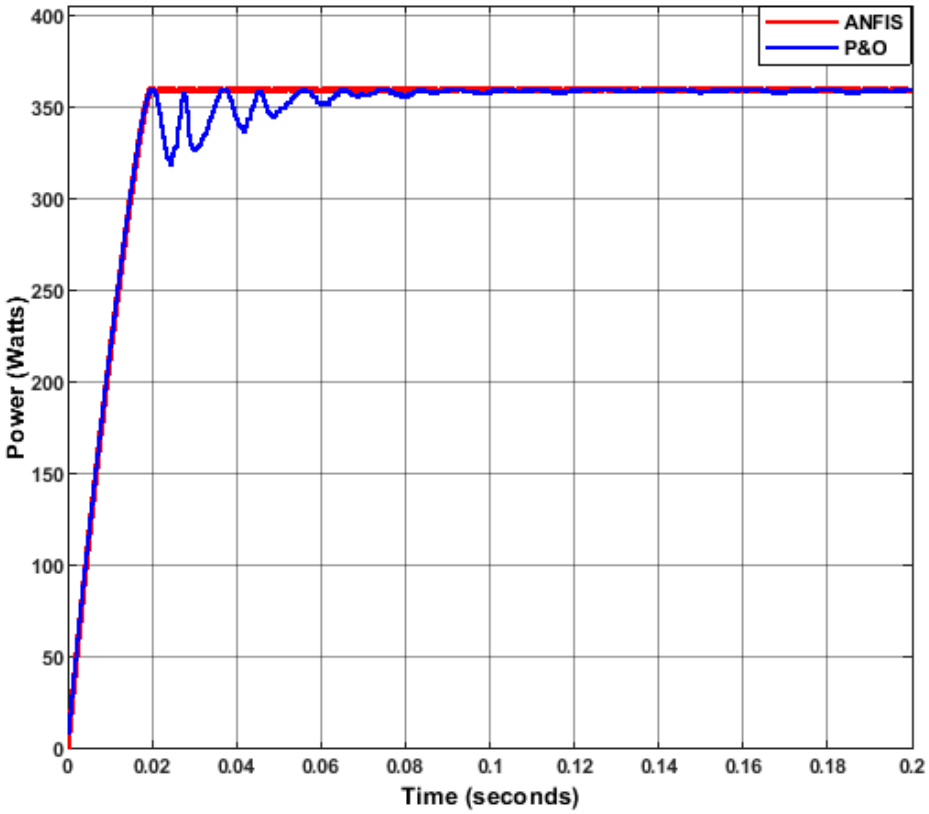

Figure 77: At STC, comparing with the P&O MPPT controller.

Scenario 4: Under varying solar irradiance, comparing with the P&O MPPT controller.

At this point, the performance of the proposed MPPT controller is evaluated by comparing it with the P&O MPPT controller under varying solar irradiance levels (1000W/m^2, 850W/m^2 500W/m^2, and 50W/m^2). Both controllers exhibit satisfactory tracking performance, but the degree of accuracy is different as shown in **Fig. 78.**

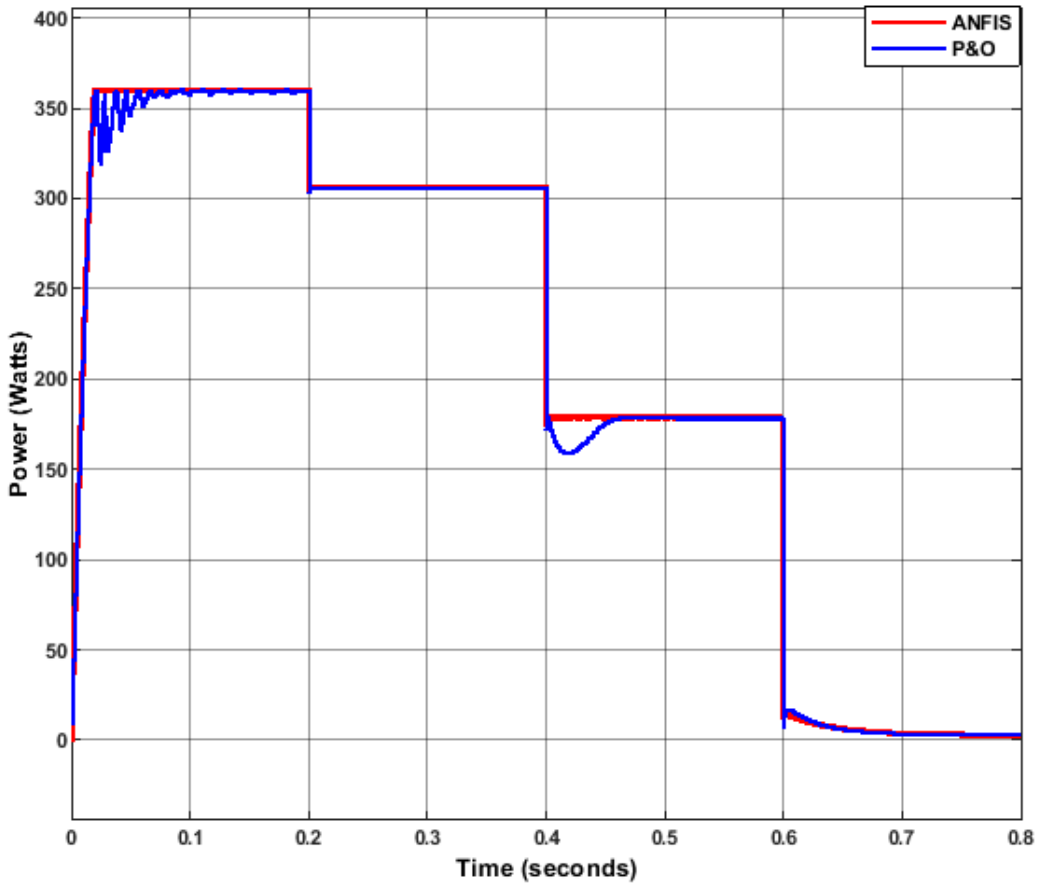

Figure 78: Under varying solar irradiance, comparing with the P&O MPPT controller.

The ANFIS based MPPT controller displays a fast response to sudden changes in solar irradiance levels with small oscillations about the MPPT. For the P&O MPPT controller, the tracking speed is lower and oscillations are much higher. The P&O MPPT controller also exhibits the drift phenomenon (caused by the incorrect decision to either decrease or increase the duty cycle for fast-changing irradiance levels). It must be also noted that the efficiency of the P&O MPPT technique is very poor for lower solar irradiance levels (at $500W/m^2$) as illustrated in **Fig. 78** (between 40 and $60ms$). This is because the P&O method uses a fixed step to either decrease or increase the duty cycle (non-adaptive) but for the ANFIS based MPPT controller, ΔD changes (from -0.1 to 0.1 as shown in **Fig. 61**) depending on the error given

to the FL power controller, which makes the proposed MPPT technique efficient for any given solar irradiance level and temperature.

Scenario 5: Under varying solar irradiance, varying temperature and comparing with the P&O MPPT controller.

The performance of the proposed ANFIS based MPPT is also evaluated under varying solar irradiance and temperature by comparing it with the P&O MPPT technique. In general, the efficiency of PV modules decreases with an increase in solar cell temperature. Four real environmental data sets of solar irradiance and temperature are used. **Table 12** shows these data sets. **Fig. 79** shows the power output curves of the two controllers.

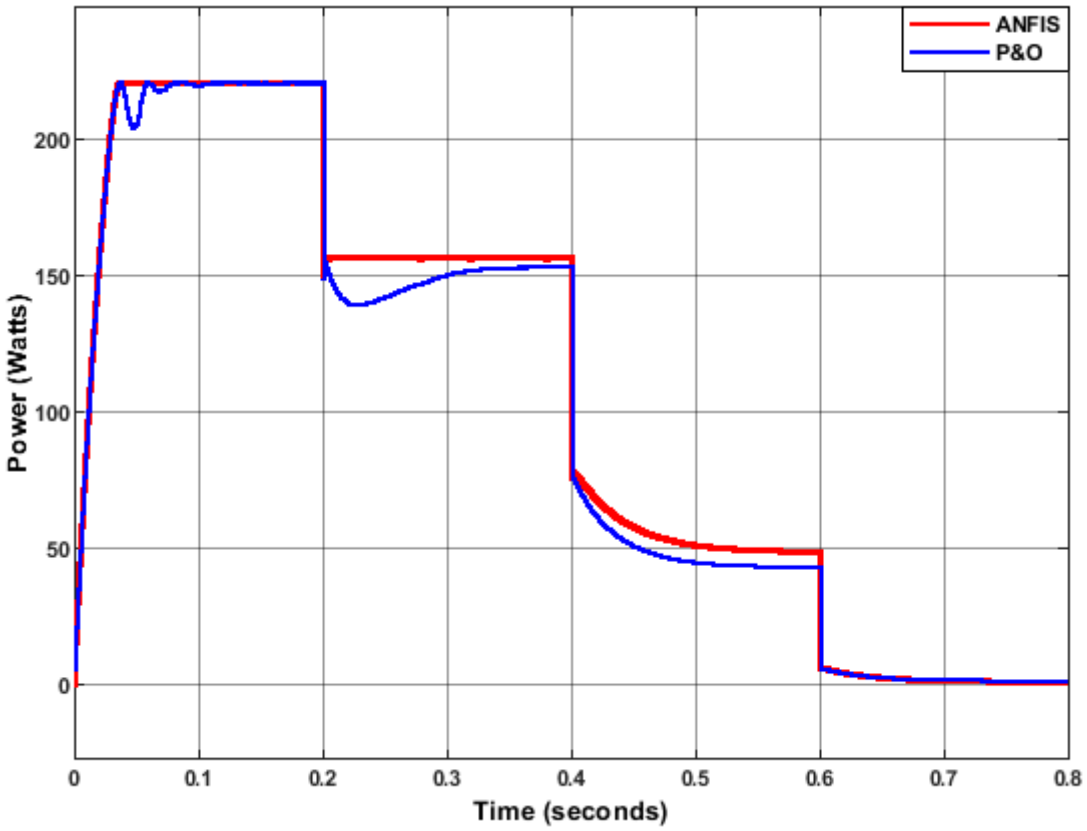

Figure 79: Under varying solar irradiance, varying temperature comparing with the P&O MPPT controller.

The proposed ANFIS based MPPT shows a better response for changing solar irradiance and temperature. For the P&O MPPT controller, the accuracy and tracking speed is slower and this results in power wastages since the SPV system won't be operating at the MPP.

Table 12: Data sets of solar irradiance and temperature

Solar Irradiance	Temperature
633 W/m^2	30.6 ℃
440 W/m^2	25.2 ℃
222 W/m^2	20.1 ℃
30 W/m^2	15.2 ℃

The reason for this poor performance is because the P&O technique relies on fixed steps to update the duty cycle of the DC-DC boost converter and it takes time for this controller to locate the new MPP for rapidly changing environmental conditions.

5.2 Energy management controller simulations

As mentioned before, the EMC must select the appropriate energy source or a combination of energy sources at each instant whilst maintaining a constant DC bus voltage at 240V. Three case studies are simulated and studied to analyze the performance of the proposed system. In every case study, the P_{PV} is varied from HIGH (0 – 0.2) seconds, MEDIUM (0.2 – 0.4) seconds and LOW (0.4 – 0.6) seconds as shown in **Fig. 80.** The P_{PV} is varied by varying the solar irradiance input to the PV array.

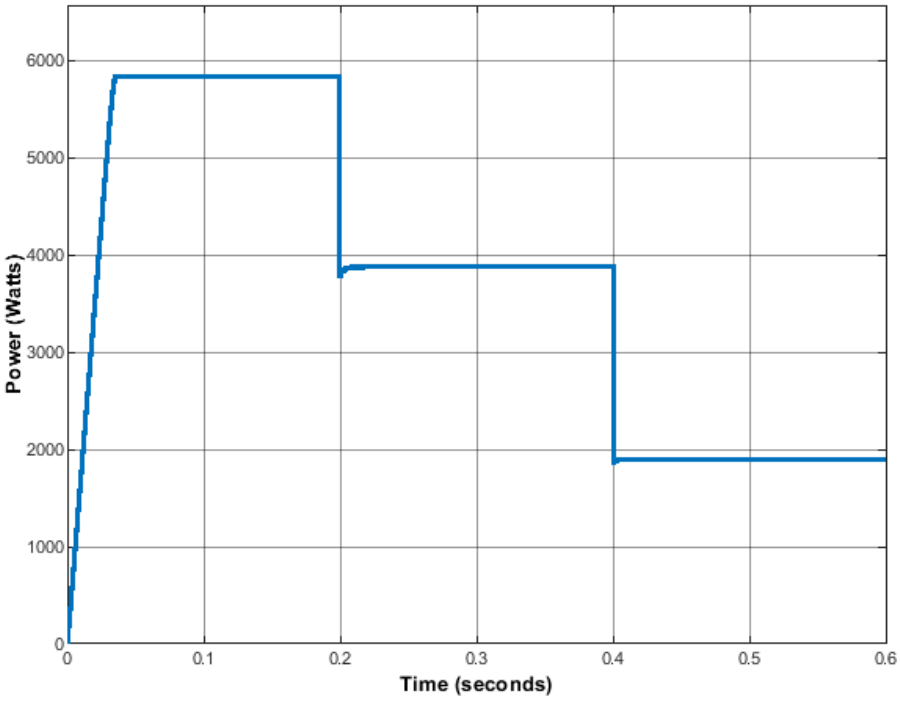

Figure 80: P_{PV} variation from HIGH to LOW.

Case 1: The P_{PV} is varied from HIGH, MEDIUM and LOW whilst the initial SOC is LOW.

In this case, the power from PV modules is varied from HIGH to LOW whilst the initial SOC is LOW. The results of the simulations are given below which include the DC bus voltage, VSDG speed and water pump speed. **Fig. 81** shows the results of the DC bus voltage. The blue line represents the actual DC bus voltage of the system whilst the red line represents the target which is 240V. It can be seen that the DC bus voltage rises from 0V to just above 250V. Since the power from PV modules is high between 0 to 0.2 seconds, the EMC selects solar modules as the only source of energy for this time frame. The status of the VSDG is off/zero between 0 – 0.2 seconds as shown in **Fig. 82**. Moreover, the EMC also makes sure that there is no further discharge of the batteries when the SOC is LOW. **Fig. 83** shows simulation results for the speed of the water pump. The speed of the water pump rises to around 4000 rpm before it goes down to its optimum speed of 3600 rpm. Kindly note that, since the P_{PV} rises from zero to maximum as shown in **Fig. 80**, the EMC controller read that small rising time as the P_{PV} is LOW and that's why the VSDG status shows the speed of between 2800 rpm to 2600 rpm before it goes to zero as shown in **Fig. 82**.

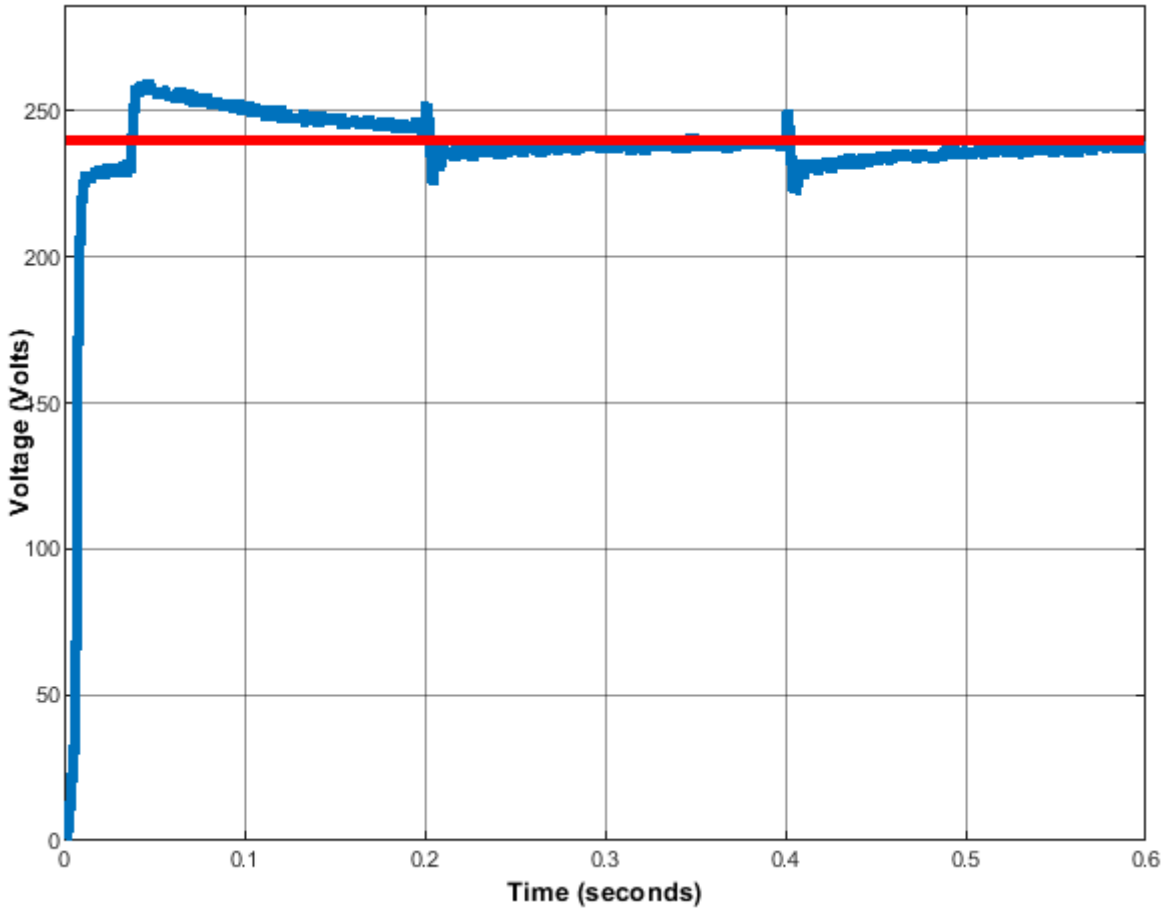

Figure 81: DC bus voltage of case study 1.

From 0.2 to 0.4 seconds, the P_{PV} is reduced to MEDIUM. At this point, the EMC activates the VSGD to operate at a medium speed of around 2600 rpm as shown in **Fig. 82**. The water pump will be powered by the sum of the energy from the PV modules and VSDG to meet its power requirement. The EMC also makes sure that the DC bus voltage is kept around 240V as shown in **Fig. 81**.

From 0.4 to 0.6 seconds, the P_{PV} is further reduced and the EMC makes the VSDG increase its operating speed to make up for the reduced power from the PV modules. The water pump will be powered by both the VSDG and PV modules. Because of the LOW P_{PV}, the speed of the VSDG is HIGH at 2800 rpm as shown in **Fig. 82**.

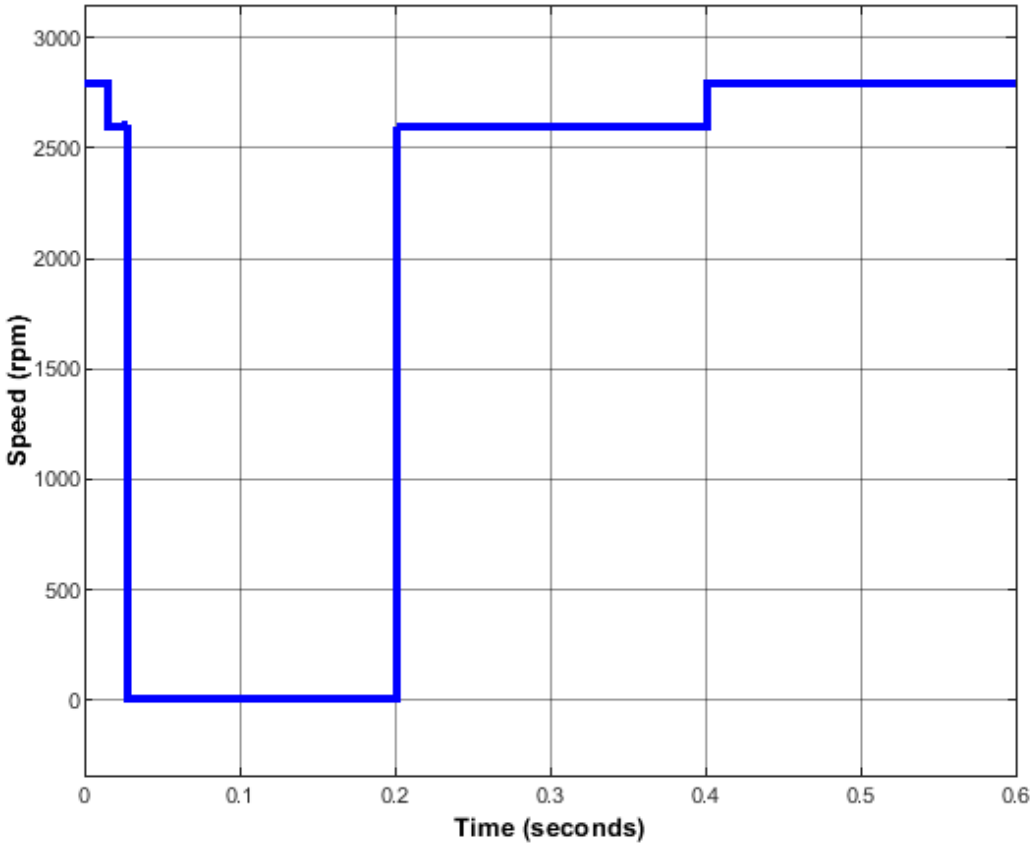

Figure 82: VSDG speed case study 1.

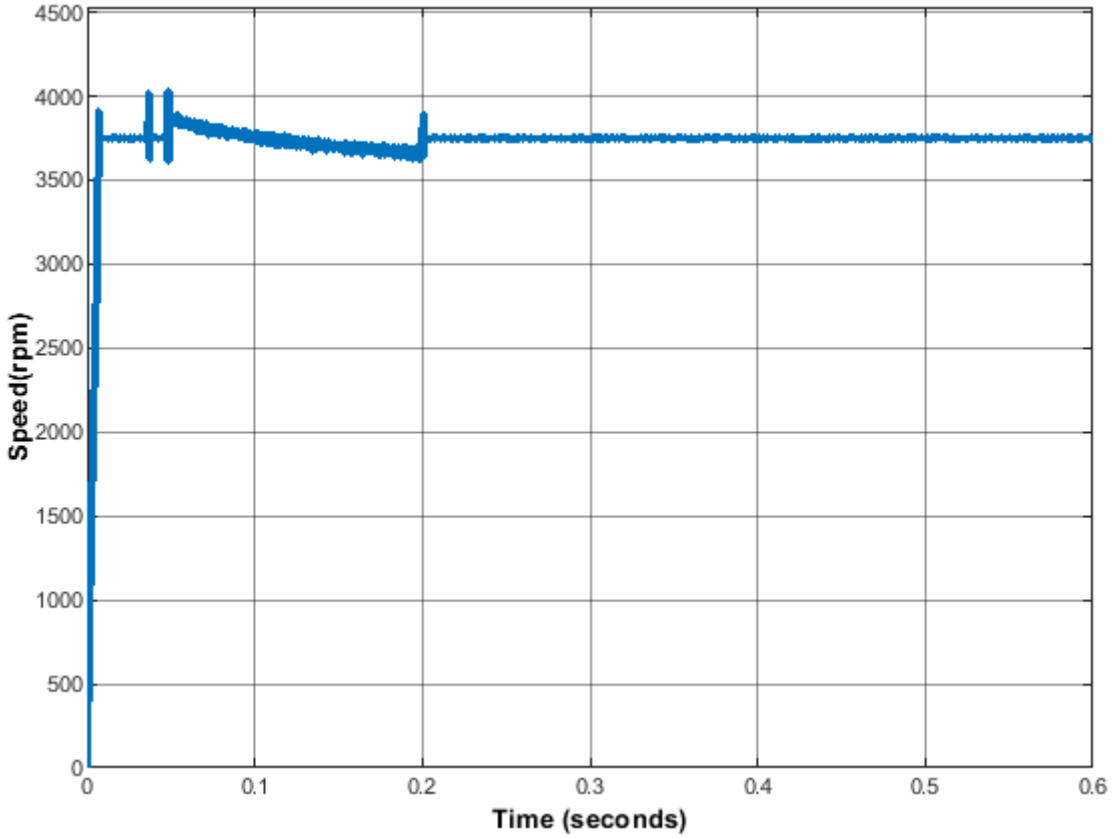

Figure 83: Water pump speed of case study 1.

Case 2: The P_{PV} is varied from HIGH, MEDIUM and LOW whilst the initial SOC is MEDIUM.

In this case, the power from the PV modules is varied from HIGH to LOW whilst the initial SOC is MEDIUM. From 0 to 0.2 seconds, the EMC activates the charging/discharging of the battery bank and the water pump will be powered by the PV modules and batteries. The VSDG status will be zero/off since the power from the batteries and solar modules will be enough to power the water pump as shown in **Fig. 85**. The EMC also regulates the DC bus voltage to operate at 240V despite variations of P_{PV} as shown in **Fig. 84**.

From 0.2 to 0.4 seconds, the VSDG start to run to add some power to the system since the power from the batteries and solar modules won't be enough to power the water pump. The VSDG operates at a lower speed of around 2400 rpm to make the hybrid system meet the power requirement of the water pump as shown in **Fig. 85**.

From 0.4 to 0.6 seconds, the P_{PV} is LOW. The EMC makes the VSDG increase its power output by increasing its speed from 2400 rpm to 2600 rpm as shown in **Fig. 85.** The water pump will be powered by the VSDG, PV modules and batteries. **Fig. 86** shows the speed of the water

pump. Between 0 to 0.2 seconds the speed of the water pump is not that consistent since the power from the PV array always vary. The inclusion of the VSDG between 0.2 to 0.6 seconds improves the power quality of the system and the speed of the water pump is almost constant as shown in **Fig. 86**.

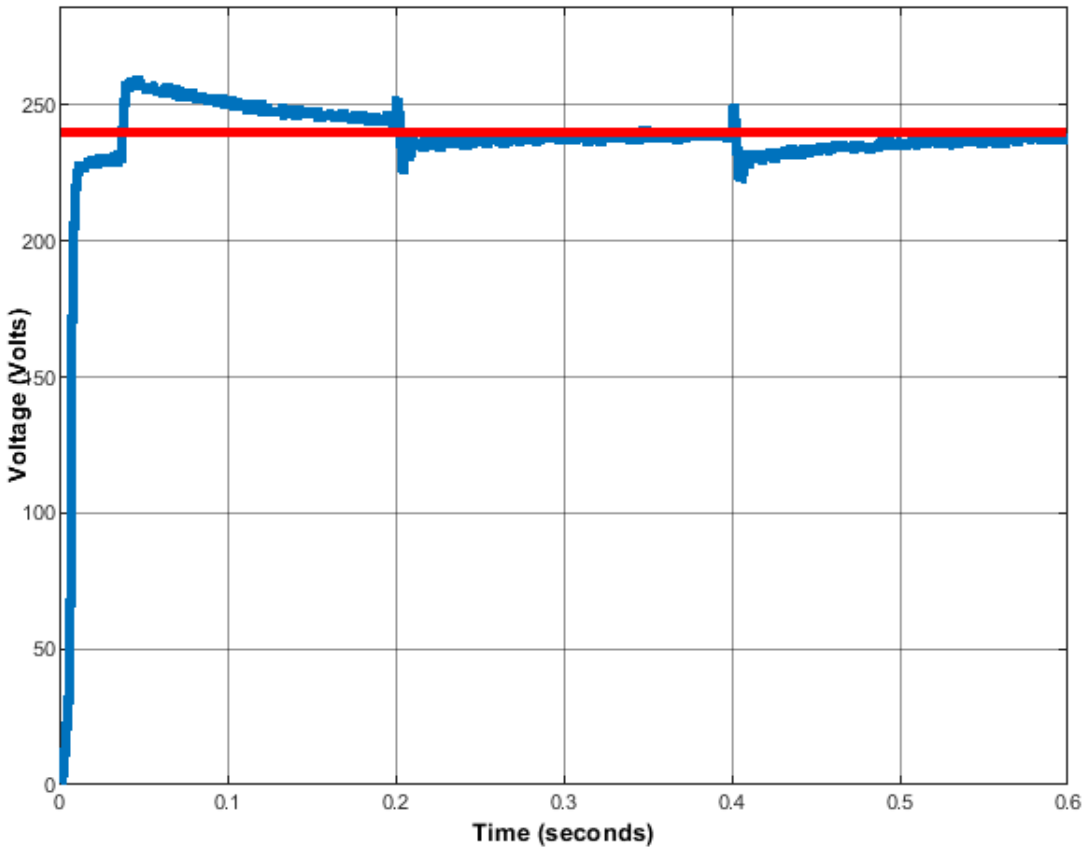

Figure 84: DC bus voltage for case study 2.

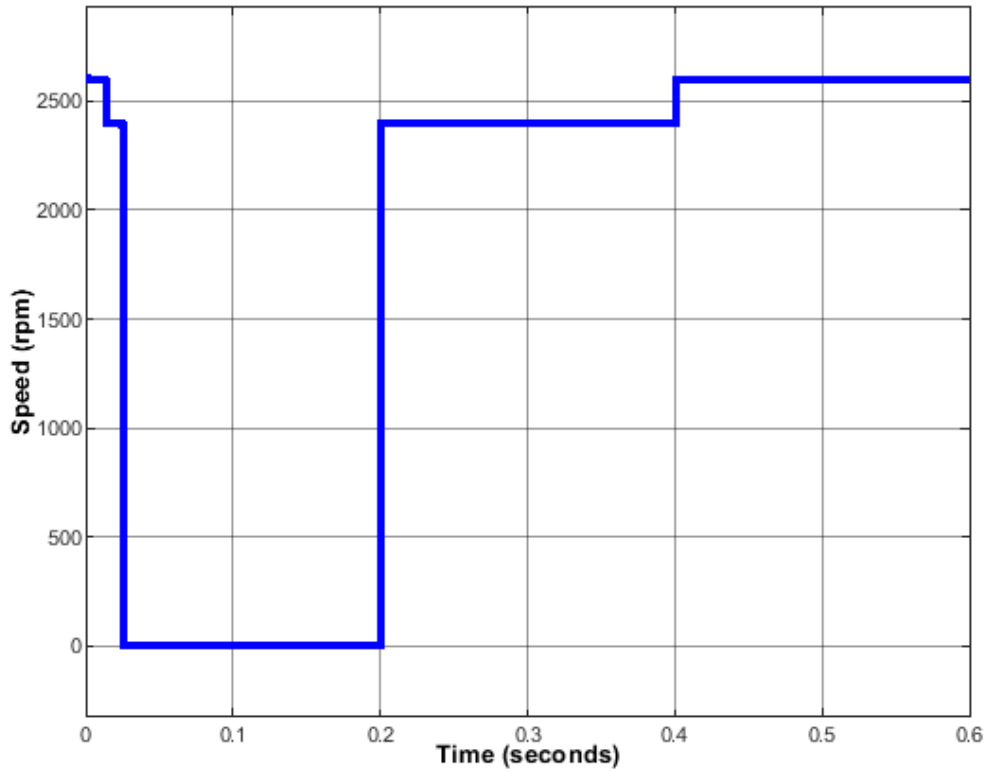

Figure 85: VSDG speed for case study 2.

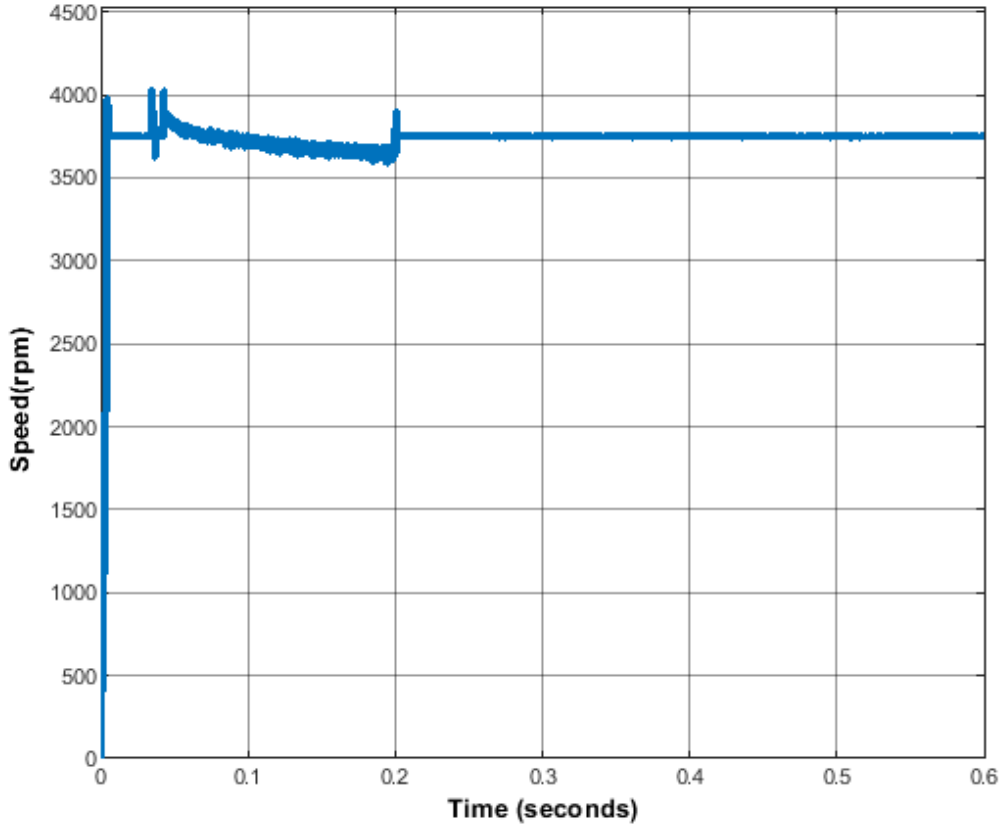

Figure 86: Water pump speed for case study 2.

Case 3: The P_{PV} is varied from HIGH, MEDIUM and LOW whilst the initial SOC is HIGH.

In this case, the power from PV modules is varied from HIGH to LOW whilst the initial SOC of the battery bank is HIGH. From 0 to 0.2 seconds, the P_{PV} is HIGH and the EMC selects PV modules and batteries as the power source of the hybrid system and the VSDG is off as shown in **Fig. 88**.

From 0.2 to 0.4 seconds, the P_{PV} becomes MEDIUM and the power from PV modules and battery is still enough to power the water without the inclusion of the VSDG. The EMC can maintain constant DC bus voltage despite changes in P_{PV} as shown in **Fig. 87**. The speed of the water pump for this timeframe is just above 3500 rpm because of the reduced power from the PV array.

From 0.4 to 0.6 seconds, the P_{PV} becomes LOW. The EMC activates the VSDG to operate at a slower speed to make up for the reduced power from the PV modules as shown in **Fig. 88**. The water pump will be powered with PV modules, a battery bank and the VSDG. The speed of the water pump increases to around 3600 rpm when the VSDG is introduced as shown in **Fig. 89**.

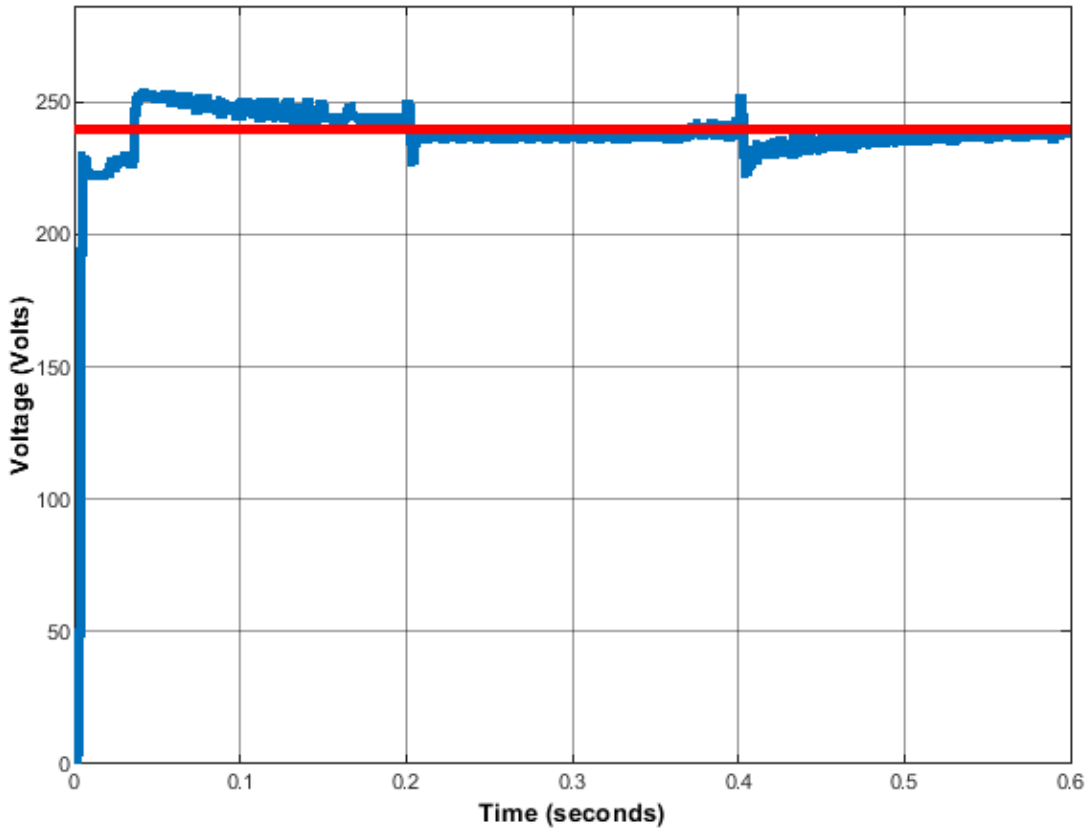

Figure 87 : DC bus voltage of case study 3.

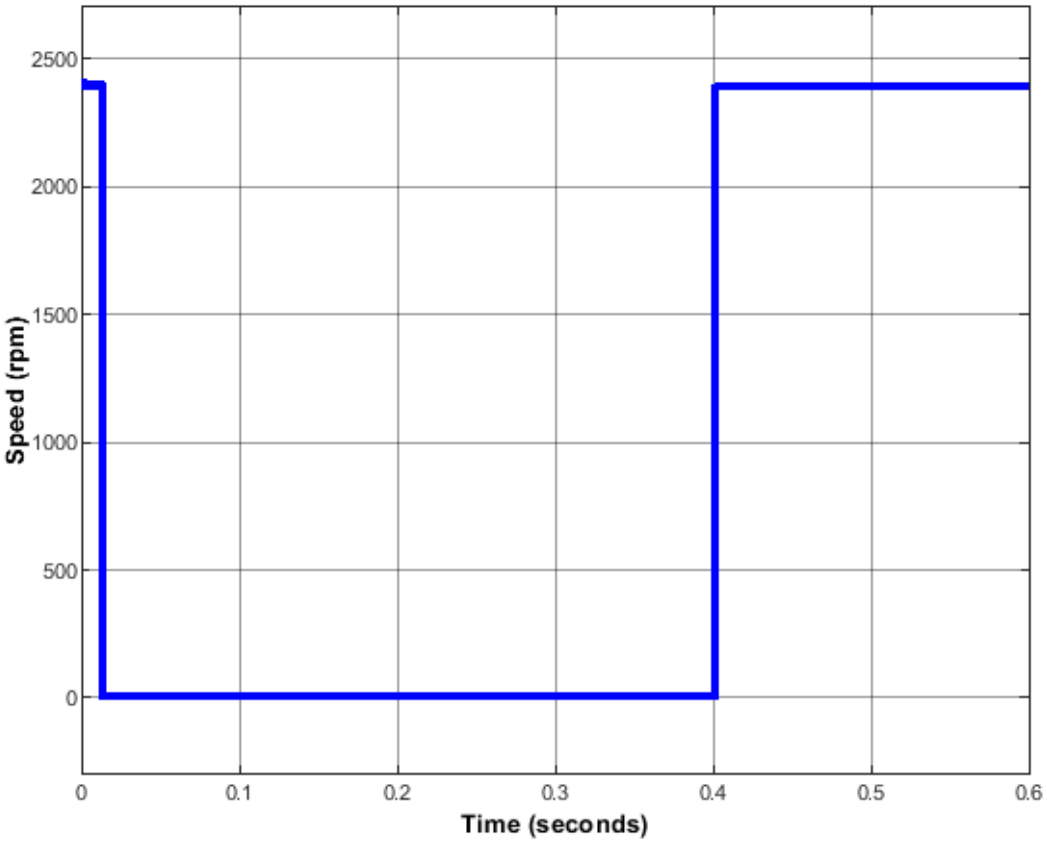

Figure 88: VSDG speed for a case study 3.

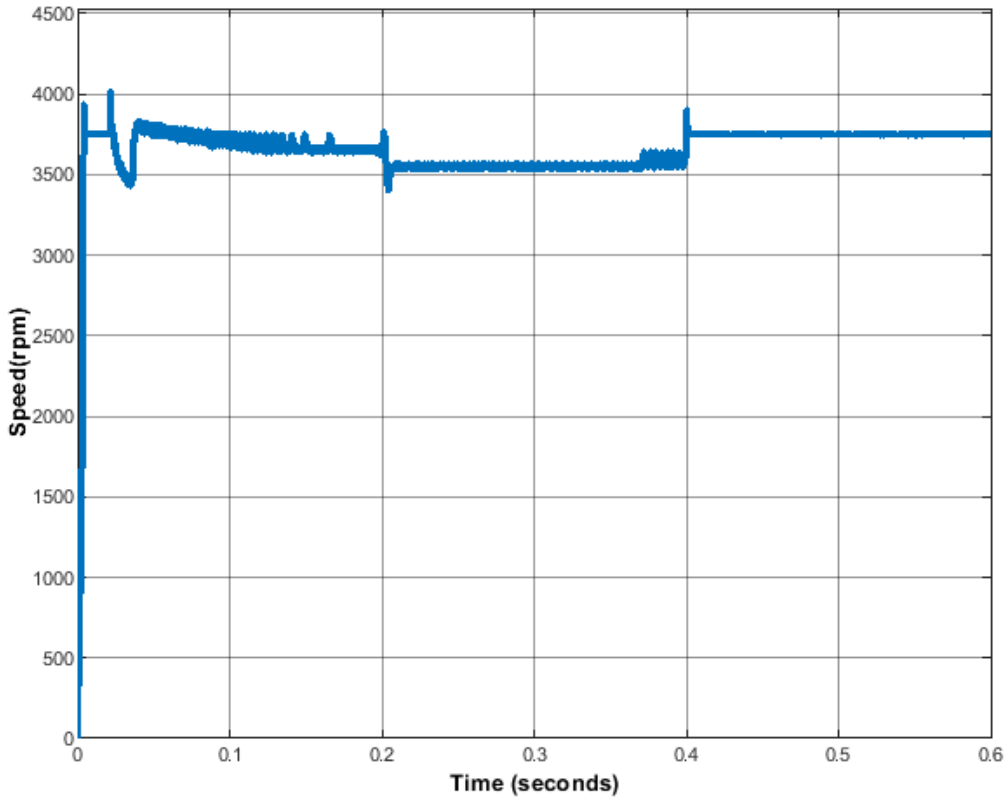

Figure 89:Water pump speed for case study 3.

6.0 CONCLUSION AND FUTURE WORK

This chapter gives the overall summary of the developed, modelled and simulated solar-diesel hybrid water pumping system. The future work on this topic is discussed, giving recommendations that can be considered to enhance the performance of the proposed system.

6.1 Conclusions

This research work focuses on the use of AI techniques in solar energy technologies. The Adaptive Neuro-Fuzzy Inference System (ANFIS) was utilized for Maximum Power Point Tracking (MPPT) of solar modules. The Fuzzy Logic (FL) concept is adopted for energy management within the hybrid system. All the components of the hybrid system were modelled in the MATLAB/Simulink environment.

The hybrid water pumping system is comprised of PV modules, batteries, ANFIS based MPPT charge controllers, FL based EMC, VSDG and a 5Hp DC water pump. Solar modules are the main source of energy and the batteries are utilized when the power from solar modules is not enough to power the load. The VSDG is activated when both the power from the PV array and the battery bank is not enough to power the water pump. The VSDG is proposed in this research work for achieving higher solar energy penetration in the hybrid system since the VSDG has a flexible operating range as compared to constant speed generators.

After modelling hybrid system components, several case studies were considered and simulated in the MATLAB/Simulink environment to evaluate the performance of the proposed system. Five different scenarios were simulated and studied to evaluate the performance of the ANFIS based MPPT charge controllers. Simulation results proved that the ANFIS based MPPT controllers are efficient and can maximize the power output of the solar modules for steady-state and varying environmental weather conditions. For the EMC, three case studies were simulated and analyzed. The EMC was able to manage the power distribution in the hybrid system, maintaining a constant DC bus voltage. It should be noted that the EMC was also able to manage the battery bank charging and discharging. In conclusion, this research work was a great success and it creates a knowledge base on ways to integrate a solar energy source with other energy sources.

6.2 Future work

Correct modelling of HRES is of prime importance in this research work. During the modelling stage, there are some assumptions considered and some components are presented in a simplified form. For further evaluation of the proposed system, a hardware implementation

of the system remains an important aspect for future research. This may include the use of micro-processors and micro-controllers to see the dynamic response of the proposed system. Lastly, for future work, the techno-economic analysis for this hybrid system should also be explored.

REFERENCES

[1] P. A. Owusu and S. Asumadu-Sarkodie, "A review of renewable energy sources, sustainability issues and climate change mitigation," *Cogent Engineering*, vol. 3, no. 1, 04/04/ 2016, doi: 10.1080/23311916.2016.1167990.

[2] I. R. E. Agency. "Renewable Capacity Statistics 2019." International Renewable Energy Agency https://irena.org/publications/2019/Mar/Renewable-Capacity-Statistics-2019 (accessed 2020).

[3] D. o. Energy. "Integrated Resource Plan for Electricity." Department of Energy. http://www.energy.gov.za/IRP/irp%20files/IRP2010_2030_Final_Report_20110325.pdf (accessed 2020).

[4] SOLAGIS. "Solar resource maps of South Africa." SOLAGIS. https://solargis.com/maps-and-gis-data/download/south-africa (accessed 2020).

[5] M. Ahmadi *et al.*, "Solar power technology for electricity generation: A critical review," *Energy Science & Engineering*, vol. 6, no. 5, pp. 340-361, 09/28 2018, doi: 10.1002/ese3.239.

[6] R. T. Moyo, P. Y. Tabakov, and S. Moyo, "THE EFFICACY OF THE MAXIMUM POWER TRANSFER THEOREM IN IMPROVING THE EFFICIENCY OF PHOTOVOLTAIC MODULES: A REVIEW," presented at the Southern African Solar Energy Conference, East London, South Africa, 25-27 November 2019, 2019.

[7] T. Hove and J. Göttsche, "Mapping global, diffuse and beam solar radiation over Zimbabwe," *Renewable Energy*, vol. 18, no. 4, pp. 535-556, 1999/12/01/ 1999, doi: https://doi.org/10.1016/S0960-1481(98)00782-4.

[8] L. Bokopane, K. Kusakana, and H. Vermaark, "Hybrid System Configurations and Charging Strategies for Isolated Electric Tuk-Tuk Charging Station in South Africa," *International Journal of Electrical and Computer Engineering*, vol. 8, no. 11, pp. 1671-1676, 2014.

[9] D. Zhou and Abdullah, "The acceptance of solar water pump technology among rural farmers of northern Pakistan: A structural equation model," *Cogent Food & Agriculture*, vol. 3, no. 1, p. 1280882, 2017/01/01 2017, doi: 10.1080/23311932.2017.1280882.

[10] I. Staffell and S. Pfenninger, "The increasing impact of weather on electricity supply and demand," *Energy*, vol. 145, pp. 65-78, 2018/02/15/ 2018, doi: https://doi.org/10.1016/j.energy.2017.12.051.

[11] M. Ghofrani and N. N. Hosseini, "Optimizing hybrid renewable energy systems: a review," *Sustainable energy-technological issues, applications and case studies*, pp. 161-176, 2016.

[12] J. Kartite and M. Cherkaoui, "Study of the different structures of hybrid systems in renewable energies: A review," *Energy Procedia*, vol. 157, pp. 323-330, 2019/01/01/ 2019, doi: https://doi.org/10.1016/j.egypro.2018.11.197.

[13] Y.-K. Wu and S.-M. Chang, "Review of the Optimal Design on a Hybrid Renewable Energy System," *MATEC Web of Conferences*, vol. 55, p. 06001, 01/01 2016, doi: 10.1051/matecconf/20165506001.

[14] P. Bajpai and V. Dash, "Hybrid renewable energy systems for power generation in stand-alone applications: A review," *Renewable and Sustainable Energy Reviews*, vol. 16, 06/01 2012, doi: 10.1016/j.rser.2012.02.009.

[15] M. K. Deshmukh and S. S. Deshmukh, "Modeling of hybrid renewable energy systems," *Renewable and Sustainable Energy Reviews*, vol. 12, no. 1, pp. 235-249, 2008/01/01/ 2008, doi: https://doi.org/10.1016/j.rser.2006.07.011.
[16] V. Khare, S. Nema, and P. Baredar, "Solar–wind hybrid renewable energy system: A review," *Renewable and Sustainable Energy Reviews*, vol. 58, pp. 23-33, 2016/05/01/ 2016, doi: https://doi.org/10.1016/j.rser.2015.12.223.
[17] M. Fadaee and M. A. M. Radzi, "Multi-objective optimization of a stand-alone hybrid renewable energy system by using evolutionary algorithms: A review," *Renewable and Sustainable Energy Reviews*, vol. 16, no. 5, pp. 3364-3369, 2012/06/01/ 2012, doi: https://doi.org/10.1016/j.rser.2012.02.071.
[18] I. Pvps, *Task 9: User Guide Monitoring PV Diesel Hybrid Systems*. 2015.
[19] H. Tazvinga and T. Hove, *Photovoltaic/Diesel/Battery Hybrid Power Supply System*. VDM Publishers, 2010.
[20] S. Mandal, H. Yasmin, M. R. I. Sarker, and M. Beg, *Prospect of Solar-PV/Biogas/Diesel Generator Hybrid Energy System of an Off-Grid area in Bangladesh*. 2017.
[21] N. Phuangpornpitak and S. Kumar, "PV hybrid systems for rural electrification in Thailand," *Renewable and Sustainable Energy Reviews*, vol. 11, no. 7, pp. 1530-1543, 2007.
[22] P. Kruangpradit and W. Tayati, "Hybrid renewable energy system development in Thailand," *Renewable Energy*, vol. 8, no. 1-4, pp. 514-517, 1996.
[23] P. Peerapong and B. Limmeechokchai, "Optimal electricity development by increasing solar resources in diesel-based micro grid of island society in Thailand," *Energy Reports*, vol. 3, pp. 1-13, 2017.
[24] C. Nayar, M. Tang, and W. Suponthana, "Wind/PV/diesel micro grid system implemented in remote islands in the Republic of Maldives," in *2008 IEEE international conference on sustainable energy technologies*, 2008: IEEE, pp. 1076-1080.
[25] W. Van Sark *et al.*, "The first PV-diesel hybrid system in the Maldives installed at Mandhoo Island," in *21st European photovoltaic solar energy conference*, 2006, pp. 4-8.
[26] A. A. Setiawan and C. V. Nayar, "Design of Hybrid Power System for a Remote Island in Maldives," *The Proceedings of the HOMER Webcast-NREL USA*, pp. 1-5, 2006.
[27] T. Y. Jung, Y. T. Kim, and J. H. Hyun, "An Economic Analysis of a Hybrid Solar PV-Diesel-ESS System for Kumundhoo, Maldives," *Korea and the World Economy*, vol. 18, no. S1, pp. 109-134, 2017.
[28] L.-q. Liu and Z.-x. Wang, "The development and application practice of wind–solar energy hybrid generation systems in China," *Renewable and Sustainable Energy Reviews*, vol. 13, no. 6, pp. 1504-1512, 2009/08/01/ 2009, doi: https://doi.org/10.1016/j.rser.2008.09.021.
[29] Y. Shivrath, P. B. Narayana, S. Thirumalasetty, and E. L. Narsaiah, "Design & integration of wind-solar hybrid energy system for drip irrigation pumping application," *International Journal of Modern Engineering Research (IJMER)*, vol. 2, no. 4, pp. 2947-2950, 2012.
[30] J. Tianjun and Y. Minghao, "Hybrid household generation and supply system with wind-solar-hydro power for rural areas [J]," *Transactions of the Chinese Society of Agricultural Engineering*, vol. 8, 2008.
[31] M. A. M. Ramli, A. Hiendro, and Y. A. Al-Turki, "Techno-economic energy analysis of wind/solar hybrid system: Case study for western coastal area of Saudi Arabia,"

Renewable Energy, vol. 91, pp. 374-385, 2016/06/01/ 2016, doi: https://doi.org/10.1016/j.renene.2016.01.071.

[32] Z. Ding, H. Hou, G. Yu, E. Hu, L. Duan, and J. Zhao, "Performance analysis of a wind-solar hybrid power generation system," *Energy conversion and management,* vol. 181, pp. 223-234, 2019.

[33] S. Szewczuk, "Hybrid mini-grid systems-distributed generation systems for communities based on renewable energy resources," 2009.

[34] S. M. Zahraee, M. Khalaji Assadi, and R. Saidur, "Application of Artificial Intelligence Methods for Hybrid Energy System Optimization," *Renewable and Sustainable Energy Reviews*, vol. 66, pp. 617-630, 2016/12/01/ 2016, doi: https://doi.org/10.1016/j.rser.2016.08.028.

[35] F. Huneke, J. Henkel, J. A. Benavides González, and G. Erdmann, "Optimisation of hybrid off-grid energy systems by linear programming," *Energy, Sustainability and Society,* vol. 2, no. 1, p. 7, 2012/04/16 2012, doi: 10.1186/2192-0567-2-7.

[36] S. Ashok, "Optimised model for community-based hybrid energy system," *Renewable energy,* vol. 32, no. 7, pp. 1155-1164, 2007.

[37] T. Das, D. Chakraborty, and S. Seth, "Energy consumption and prospects for renewable energy technologies in an Indian village," *Energy*, vol. 15, no. 5, pp. 445-449, 1990.

[38] R. T. Moyo, P. Y. Tabakov, and S. Moyo, "THE EFFICACY OF THE MAXIMUM POWER TRANSFER THEOREM IN IMPROVING THE EFFICIENCY OF PHOTOVOLTAIC MODULES: A REVIEW."

[39] P. García, J. P. Torreglosa, L. M. Fernandez, and F. Jurado, "Optimal energy management system for stand-alone wind turbine/photovoltaic/hydrogen/battery hybrid system with supervisory control based on fuzzy logic," *International Journal of Hydrogen Energy,* vol. 38, no. 33, pp. 14146-14158, 2013.

[40] O. Erdinc, B. Vural, and M. Uzunoglu, "A wavelet-fuzzy logic based energy management strategy for a fuel cell/battery/ultra-capacitor hybrid vehicular power system," *Journal of Power sources,* vol. 194, no. 1, pp. 369-380, 2009.

[41] K.-S. Jeong, W.-Y. Lee, and C.-S. Kim, "Energy management strategies of a fuel cell/battery hybrid system using fuzzy logics," *Journal of power sources,* vol. 145, no. 2, pp. 319-326, 2005.

[42] A. Al-Alawi, S. M Al-Alawi, and S. M Islam, "Predictive control of an integrated PV-diesel water and power supply system using an artificial neural network," *Renewable Energy*, vol. 32, no. 8, pp. 1426-1439, 2007/07/01/ 2007, doi: https://doi.org/10.1016/j.renene.2006.05.003.

[43] R. Hossain, A. M. T. Ooa, and A. S. Alia, "Historical weather data supported hybrid renewable energy forecasting using artificial neural network (ANN)," *Energy Procedia,* vol. 14, pp. 1035-1040, 2012.

[44] V. K. Soni and R. Khare, "Optimal sizing of HRES for small sized institute using HOMER," in *2014 IEEE 2nd International Conference on Electrical Energy Systems (ICEES)*, 7-9 Jan. 2014 2014, pp. 77-81, doi: 10.1109/ICEES.2014.6924145.

[45] R. Khare and Y. Kumar, "Application of GA on size optimization of solar-DG-battery storage HRES with reliability and CO 2," in *2014 Annual IEEE India Conference (INDICON)*, 2014: IEEE, pp. 1-7.

[46] M. Abu-Aligah, "Design of Photovoltaic Water Pumping System and Compare it with Diesel Powered Pump," *Jordan Journal of Mechanical & Industrial Engineering,* vol. 5, no. 3, 2011.

[47] S. A. Kalogirou, "Environmental benefits of domestic solar energy systems," *Energy conversion and management,* vol. 45, no. 18-19, pp. 3075-3092, 2004.

[48] G. Rzevski, "A new direction of research into Artificial Intelligence," *SRI LANKA ASSOCIATION FOR ARTIFICIAL INTELLIGENCE,* p. 11, 2008.
[49] A. M. TURING, "I.—COMPUTING MACHINERY AND INTELLIGENCE," *Mind,* vol. LIX, no. 236, pp. 433-460, 1950, doi: 10.1093/mind/LIX.236.433.
[50] R. D. Sriram, "Artificial intelligence in engineering: Personal reflections," 2006.
[51] S. Russell and J. Bohannon, "Artificial intelligence. Fears of an AI pioneer," (in eng), *Science (New York, N.Y.),* vol. 349, no. 6245, p. 252, 2015/07// 2015, doi: 10.1126/science.349.6245.252.
[52] M. Haenlein and A. Kaplan, "A brief history of artificial intelligence: On the past, present, and future of artificial intelligence," *California Management Review,* vol. 61, no. 4, pp. 5-14, 2019.
[53] K. D. Foote. "A Brief History of Artificial Intelligence." DATAVERSITY Education, LLC. https://www.dataversity.net/brief-history-artificial-intelligence/ (accessed 2002).
[54] H. Tan, "A brief history and technical review of the expert system research," *IOP Conference Series: Materials Science and Engineering,* vol. 242, p. 012111, 2017/09 2017, doi: 10.1088/1757-899x/242/1/012111.
[55] S. Schuchmann, "Analyzing the Prospect of an Approaching AI Winter," 2019.
[56] K. Miyazaki and R. Sato, "Analyses of the Technological Accumulation over the 2nd and the 3rd AI Boom and the Issues Related to AI Adoption by Firms," in *2018 Portland International Conference on Management of Engineering and Technology (PICMET)*, 19-23 Aug. 2018 2018, pp. 1-7, doi: 10.23919/PICMET.2018.8481822.
[57] S. Oke, "A literature review on artificial intelligence," *International Journal of Information and Management Sciences,* vol. 19, pp. 535-570, 12/01 2008.
[58] S. Kalogirou and A. Sencan, "Artificial intelligence techniques in solar energy applications," *Solar Collectors and Panels, Theory and Applications,* vol. 15, pp. 315-340, 2010.
[59] S. Kalogirou, *Artificial intelligence in energy and renewable energy systems*. Nova Publishers, 2007.
[60] E. M. Sharma, *A Survey in fuzzy Logic: An Introduction*. 2014.
[61] L. Bin-Da, C. Chuen-Yau, and T. Ju-Ying, "Design of adaptive fuzzy logic controller based on linguistic-hedge concepts and genetic algorithms," *IEEE Transactions on Systems, Man, and Cybernetics, Part B (Cybernetics)*, vol. 31, no. 1, pp. 32-53, 2001, doi: 10.1109/3477.907563.
[62] T. point. "Artificial Intelligence - Fuzzy Logic Systems." Tutorials point. https://www.tutorialspoint.com/artificial_intelligence/artificial_intelligence_fuzzy_logic_systems.htm (accessed 2020).
[63] G. Klir and B. Yuan, *Fuzzy sets and fuzzy logic*. Prentice hall New Jersey, 1995.
[64] M. Kochen, "APPLICATIONS OF FUZZY SETS IN PSYCHOLOGY," in *Fuzzy Sets and their Applications to Cognitive and Decision Processes*, L. A. Zadeh, K.-S. Fu, K. Tanaka, and M. Shimura Eds.: Academic Press, 1975, pp. 395-408.
[65] P. Bonissone, "Fuzzy Logic and Soft Computing: Technology Development and Applications by Piero P. Bonissone," 10/29 1999.
[66] L. A. Zadeh, "Fuzzy sets," *Information and Control*, vol. 8, no. 3, pp. 338-353, 1965/06/01/ 1965, doi: https://doi.org/10.1016/S0019-9958(65)90241-X.
[67] T. J. Ross, *Fuzzy logic with engineering applications*. John Wiley & Sons, 2005.
[68] D. Dubois and H. Prade, "Gradual elements in a fuzzy set," *Soft Comput.*, vol. 12, pp. 165-175, 01/01 2008, doi: 10.1007/s00500-007-0187-6.
[69] R. Czabanski, M. Jezewski, and J. Leski, "Introduction to Fuzzy Systems," in *Theory and Applications of Ordered Fuzzy Numbers: A Tribute to Professor Witold Kosiński*,

P. Prokopowicz, J. Czerniak, D. Mikołajewski, Ł. Apiecionek, and D. Ślęzak Eds. Cham: Springer International Publishing, 2017, pp. 23-43.
[70] S. Mabuchi, "An interpretation of membership functions and the properties of general probabilistic operators as fuzzy set operators. (II). Extension to three-valued and interval-valued fuzzy sets," *Fuzzy Sets and Systems*, vol. 92, no. 1, pp. 31-50, 1997/11/16/ 1997, doi: https://doi.org/10.1016/S0165-0114(96)00163-7.
[71] A. P. Engelbrecht, *Computational intelligence: an introduction*. John Wiley & Sons, 2007.
[72] L. Vanneschi and M. Castelli, "Multilayer Perceptrons," in *Encyclopedia of Bioinformatics and Computational Biology*, S. Ranganathan, M. Gribskov, K. Nakai, and C. Schönbach Eds. Oxford: Academic Press, 2019, pp. 612-620.
[73] M. Santamouris, *Advances in building energy research*. Earthscan, 2012.
[74] R. Belu, "Artificial intelligence techniques for solar energy and photovoltaic applications," in *Handbook of Research on Solar Energy Systems and Technologies*: IGI Global, 2013, pp. 376-436.
[75] S. A. Kalogirou, "Artificial neural networks in energy applications in buildings," *International Journal of Low-Carbon Technologies*, vol. 1, no. 3, pp. 201-216, 2006.
[76] S. Agatonovic-Kustrin and R. Beresford, "Basic concepts of artificial neural network (ANN) modeling and its application in pharmaceutical research," *Journal of Pharmaceutical and Biomedical Analysis*, vol. 22, no. 5, pp. 717-727, 2000/06/01/ 2000, doi: https://doi.org/10.1016/S0731-7085(99)00272-1.
[77] M. Landin and R. C. Rowe, "2 - Artificial neural networks technology to model, understand, and optimize drug formulations," in *Formulation Tools for Pharmaceutical Development*, J. E. Aguilar Ed.: Woodhead Publishing, 2013, pp. 7-37.
[78] A. Konar, *Artificial intelligence and soft computing: behavioral and cognitive modeling of the human brain*. CRC press, 2018.
[79] A. K. Jain, M. Jianchang, and K. M. Mohiuddin, "Artificial neural networks: a tutorial," *Computer*, vol. 29, no. 3, pp. 31-44, 1996, doi: 10.1109/2.485891.
[80] G. Piccinini, "The First Computational Theory of Mind and Brain: A Close Look at Mcculloch and Pitts's "Logical Calculus of Ideas Immanent in Nervous Activity"," *Synthese*, vol. 141, 08/01 2004, doi: 10.1023/B:SYNT.0000043018.52445.3e.
[81] J. A. Hertz, *Introduction to the theory of neural computation*. CRC Press, 2018.
[82] F. Rosenblatt, "The perceptron: a probabilistic model for information storage and organization in the brain," *Psychological review*, vol. 65, no. 6, p. 386, 1958.
[83] M. Marvin and A. P. Seymour, "Perceptrons," ed: MIT Press, 1969.
[84] A. Van Ooyen and B. Nienhuis, "Improving the convergence of the back-propagation algorithm," *Neural Networks*, vol. 5, no. 3, pp. 465-471, 1992/01/01/ 1992, doi: https://doi.org/10.1016/0893-6080(92)90008-7.
[85] A. Krenker, J. Bešter, and A. Kos, "Introduction to the artificial neural networks," *Artificial Neural Networks: Methodological Advances and Biomedical Applications. InTech*, pp. 1-18, 2011.
[86] P. Sibi, S. A. Jones, and P. Siddarth, "Analysis of different activation functions using back propagation neural networks," *Journal of Theoretical and Applied Information Technology*, vol. 47, no. 3, pp. 1264-1268, 2013.
[87] S. Haykin, *Neural networks: a comprehensive foundation*. Prentice Hall PTR, 1994.
[88] V. Chandwani, V. Agrawal, and R. Nagar, "Applications of Artificial Neural Networks in Modeling Compressive Strength of Concrete: A State of the Art Review," *International Journal of Current Engineering and Technology*, vol. 4, pp. 2949-2956, 08/01 2014.

[89] R. Quiza and J. Davim, "Computational Methods and Optimization," 2011, pp. 177-208.
[90] T. P. Lillicrap, D. Cownden, D. B. Tweed, and C. J. Akerman, "Random synaptic feedback weights support error backpropagation for deep learning," (in eng), *Nature communications,* vol. 7, pp. 13276-13276, 2016, doi: 10.1038/ncomms13276.
[91] P. J. Werbos, "Backpropagation through time: what it does and how to do it," *Proceedings of the IEEE,* vol. 78, no. 10, pp. 1550-1560, 1990.
[92] M. Puig-Arnavat and J. C. Bruno, "Chapter 5 - Artificial Neural Networks for Thermochemical Conversion of Biomass," in *Recent Advances in Thermo-Chemical Conversion of Biomass*, A. Pandey, T. Bhaskar, M. Stöcker, and R. K. Sukumaran Eds. Boston: Elsevier, 2015, pp. 133-156.
[93] A. R. A. Ellah, M. H. Essai, and A. Yahya, "Comparison of different backpropagation training algorithms using robust M-estimators performance functions," in *2015 Tenth International Conference on Computer Engineering & Systems (ICCES)*, 23-24 Dec. 2015 2015, pp. 384-388, doi: 10.1109/ICCES.2015.7393080.
[94] J. G. Carney and P. Cunningham, "The epoch interpretation of learning," *IEEE Transaction on Neural Networks,* vol. 8, pp. 111-116, 1998.
[95] K. Arthishri, R. Balasubramanian, P. Kathirvelu, S. P. Simon, and R. Amirtharajan, "Maximum power point tracking of photovoltaic generation system using artificial neural network with improved tracking factor," *Journal of Applied Sciences,* vol. 14, no. 16, pp. 1858-1864, 2014.
[96] B. Tripathy, *Advances in Secure Computing, Internet Services, and Applications*. IGI Global, 2013.
[97] S. Sumathi and L. A. Kumar, *Computational intelligence paradigms for optimization problems using MATLAB®/SIMULINK®*. CRC Press, 2018.
[98] C. McCue, "7 - Predictive Analytics," in *Data Mining and Predictive Analysis*, C. McCue Ed. Burlington: Butterworth-Heinemann, 2007, pp. 117-141.
[99] M. Sazli, "A brief review of feed-forward neural networks," *Communications, Faculty Of Science, University of Ankara,* vol. 50, pp. 11-17, 01/01 2006, doi: 10.1501/0003168.
[100] L. Jin, P. N. Nikiforuk, and M. M. Gupta, "Approximation of discrete-time state-space trajectories using dynamic recurrent neural networks," *IEEE Transactions on Automatic Control*, vol. 40, no. 7, pp. 1266-1270, 1995.
[101] HACKERNOON. "Recurrent Neural Network for Noobs." HACKERNOON. https://hackernoon.com/rnn-or-recurrent-neural-network-for-noobs-a9afbb00e860 (accessed 2020).
[102] T. I. Poznyak, I. Chairez Oria, and A. S. Poznyak, "Chapter3 - Background on dynamic neural networks," in *Ozonation and Biodegradation in Environmental Engineering*, T. I. Poznyak, I. Chairez Oria, and A. S. Poznyak Eds.: Elsevier, 2019, pp. 57-74.
[103] I. R. E. A. (IRENA). "Renewable Energy Capacity." IRENA. https://www.irena.org/publications/2020/Mar/Renewable-Capacity-Statistics-2020 (accessed 2019).
[104] Y.-J. Zheng, S.-Y. Chen, Y. Lin, and W.-L. Wang, "Bio-inspired optimization of sustainable energy systems: a review," *Mathematical Problems in Engineering,* vol. 2013, 2013.
[105] F. Chekired, A. Mahrane, Z. Samara, M. Chikh, A. Guenounou, and A. Meflah, "Fuzzy logic energy management for a photovoltaic solar home," *Energy Procedia,* vol. 134, pp. 723-730, 2017/10/01/ 2017, doi: https://doi.org/10.1016/j.egypro.2017.09.566.

[106] O. Mengi and İ. Altas, "A Fuzzy logic control for a wind/battery renewable energy production system," *Turkish Journal of Electrical Engineering and Computer Sciences*, vol. 20, 03/01 2012, doi: 10.3906/elk-1104-20.
[107] Y. Liu, J. Li, Y. Wu, and F. Zhou, "Coordinated Control of the Energy Router-Based Smart Home Energy Management System," *Applied Sciences*, vol. 7, p. 943, 09/13 2017, doi: 10.3390/app7090943.
[108] F. Rodríguez, A. Fleetwood, A. Galarza, and L. Fontán, "Predicting solar energy generation through artificial neural networks using weather forecasts for microgrid control," *Renewable Energy*, vol. 126, pp. 855-864, 2018/10/01/ 2018, doi: https://doi.org/10.1016/j.renene.2018.03.070.
[109] K. Ronay, D. Bica, and C. Munteanu, "Micro-grid Development Using Artificial Neural Network for Renewable Energy Forecast and System Control," *Procedia Engineering*, vol. 181, pp. 818-823, 2017/01/01/ 2017, doi: https://doi.org/10.1016/j.proeng.2017.02.472.
[110] M. Vakili, S.-R. Sabbagh-Yazdi, K. Kalhor, and S. Khosrojerdi, "Using Artificial Neural Networks for Prediction of Global Solar Radiation in Tehran Considering Particulate Matter Air Pollution," *Energy Procedia*, vol. 74, pp. 1205-1212, 2015/08/01/ 2015, doi: https://doi.org/10.1016/j.egypro.2015.07.764.
[111] S. Jain, "21 - The current and future perspectives of biofuels," in *Biomass, Biopolymer-Based Materials, and Bioenergy*, D. Verma, E. Fortunati, S. Jain, and X. Zhang Eds.: Woodhead Publishing, 2019, pp. 495-517.
[112] F. Perera, "Pollution from Fossil-Fuel Combustion is the Leading Environmental Threat to Global Pediatric Health and Equity: Solutions Exist," (in eng), *International journal of environmental research and public health*, vol. 15, no. 1, p. 16, 2017, doi: 10.3390/ijerph15010016.
[113] S. E. Jorgensen, *Encyclopedia of Environmental Management, Four Volume Set*. CRC Press, 2012.
[114] H. Gunerhan, A. Hepbasli, and U. Giresunlu, "Environmental Impacts from the Solar Energy Systems," *Energy Sources Part A-recovery Utilization and Environmental Effects*, vol. 31, 12/02 2008, doi: 10.1080/15567030701512733.
[115] R. R. Hernandez, M. K. Hoffacker, M. L. Murphy-Mariscal, G. C. Wu, and M. F. Allen, "Solar energy development impacts on land cover change and protected areas," *Proceedings of the National Academy of Sciences*, vol. 112, no. 44, pp. 13579-13584, 2015, doi: 10.1073/pnas.1517656112.
[116] H.-J. Yang, S.-Y. Lim, and S.-H. Yoo, "The environmental costs of photovoltaic power plants in South Korea: A choice experiment study," *Sustainability*, vol. 9, no. 10, p. 1773, 2017.
[117] G. R. E. Ltd. "PV Manufacturing." Green Rhino Energy Ltd. http://www.greenrhinoenergy.com/solar/technologies/pv_manufacturing.php (accessed 2020).
[118] H. J. Tchognia Nkuissi, F. Konan, B. Hartiti, and J. Ndjaka, "Toxic Materials Used in Thin Film Photovoltaics and Their Impacts on Environment," 2019.
[119] S. Wang and S. Wang, "Impacts of wind energy on environment: A review," *Renewable and Sustainable Energy Reviews*, vol. 49, pp. 437-443, 2015/09/01/ 2015, doi: https://doi.org/10.1016/j.rser.2015.04.137.
[120] D. R. Wilburn, *Wind energy in the United States and materials required for the land-based wind turbine industry from 2010 through 2030*. US Department of the Interior, US Geological Survey, 2011.
[121] O. Jianu, M. A. Rosen, and G. Naterer, "Noise pollution prevention in wind turbines: status and recent advances," *Sustainability*, vol. 4, no. 6, pp. 1104-1117, 2012.

[122] M. Edkins, "IMPACTS OF WIND ENERGY DEVELOPMENTS ON BIRDS AND BATS: LOOKING INTO THE PROBLEM," 01/27 2014.
[123] T. D. Allison *et al.*, "Impacts to wildlife of wind energy siting and operation in the United States," *Issues in Ecology*, no. 21, pp. 1-24, 2019.
[124] S. C. Bhatia, "1 - Energy resources and their utilisation," in *Advanced Renewable Energy Systems*, S. C. Bhatia Ed.: Woodhead Publishing India, 2014, pp. 1-31.
[125] ARTsolar. "ARTsolar – 310 Watt Solar Panel – Mono Percium High Efficiency." ARTsolar. https://artsolar.net/product/310-watt-solar-panel-mono-perc/ (accessed 2020).
[126] ARTsolar. "150 Watt Solar Panel – Polycrystalline." ARTsolar. https://artsolar.net/product/150-watt-solar-panel/ (accessed 2020).
[127] A. EXPO. "THIN-FILM PV PANEL." https://www.archiexpo.com/prod/first-solar/product-87503-1541886.html (accessed 2020).
[128] S. Kouro, J. I. Leon, D. Vinnikov, and L. G. Franquelo, "Grid-Connected Photovoltaic Systems: An Overview of Recent Research and Emerging PV Converter Technology," *IEEE Industrial Electronics Magazine*, vol. 9, no. 1, pp. 47-61, 2015, doi: 10.1109/MIE.2014.2376976.
[129] E. Informative. "Grid-Tied Solar System." Energy Informative. https://energyinformative.org/grid-tied-off-grid-and-hybrid-solar-systems/ (accessed 2020).
[130] S. C. Bhatia, "5 - Solar photovoltaic systems," in *Advanced Renewable Energy Systems*, S. C. Bhatia Ed.: Woodhead Publishing India, 2014, pp. 144-157.
[131] A. Fragaki and T. Markvart, "Stand-alone PV system design: results using a new sizing approach," *Renewable Energy*, vol. 33, no. 1, pp. 162-167, 2008.
[132] B. A. a. T. C. Limited. "STAND-ALONE SYSTEM." BKSAT Limited. https://bksystem-hub.com/en/solution/stand-alone-system (accessed 2020).
[133] P. Heinstein, C. Ballif, and L.-E. Perret-Aebi, "Building integrated photovoltaics (BIPV): review, potentials, barriers and myths," *Green*, vol. 3, no. 2, pp. 125-156, 2013.
[134] INHABITAT. "Clean Energy." INHABITAT. https://inhabitat.com/national-laboratory-scales-up-quantum-dot-solar-windows-to-power-entire-buildings/ (accessed 2020).
[135] C. Peng, Y. Huang, and Z. Wu, "Building-integrated photovoltaics (BIPV) in architectural design in China," *Energy and Buildings*, vol. 43, no. 12, pp. 3592-3598, 2011/12/01/ 2011, doi: https://doi.org/10.1016/j.enbuild.2011.09.032.
[136] J. Page, "Chapter II-1-A - The Role of Solar-Radiation Climatology in the Design of Photovoltaic Systems," in *McEvoy's Handbook of Photovoltaics (Third Edition)*, S. A. Kalogirou Ed.: Academic Press, 2018, pp. 601-670.
[137] M. K. Islam, T. Ahammad, E. H. Pathan, A. Mushfiqul, and M. R. H. Khandokar, "Analysis of maximum possible utilization of solar radiation on a solar photovoltaic cell with a proposed model," *International journal of modeling and optimization*, vol. 1, no. 1, p. 66, 2011.
[138] J. Duffie and W. Beckman, "Solar Energy Thermal Processes.(3rd Edn), Hoboken," ed: NJ: Wiley, 2006.
[139] J. J. Michalsky, "The Astronomical Almanac's algorithm for approximate solar position (1950–2050)," *Solar Energy*, vol. 40, no. 3, pp. 227-235, 1988/01/01/ 1988, doi: https://doi.org/10.1016/0038-092X(88)90045-X.
[140] C. Demain, M. Journée, and C. Bertrand, "Evaluation of different models to estimate the global solar radiation on inclined surfaces," *Renewable Energy*, vol. 50, pp. 710-721, 2013/02/01/ 2013, doi: https://doi.org/10.1016/j.renene.2012.07.031.

[141] I. Sarbu and C. Sebarchievici, "Chapter 2 - Solar Radiation," in *Solar Heating and Cooling Systems*, I. Sarbu and C. Sebarchievici Eds.: Academic Press, 2017, pp. 13-28.
[142] D. R. Myers, "Solar radiation modeling and measurements for renewable energy applications: data and model quality," *Energy*, vol. 30, no. 9, pp. 1517-1531, 2005.
[143] K. Scharmer, *The European solar radiation Atlas: fundamentals and maps*. Presses des MINES, 2000.
[144] P. G. I. S. (PVGIS). "
AVERAGE DAILY IRRADIANCE DATA." PVGIS. https://re.jrc.ec.europa.eu/pvg_tools/en/tools.html (accessed 2020).
[145] S. Salman, X. Ai, and Z. Wu, "Design of a P-&-O algorithm based MPPT charge controller for a stand-alone 200W PV system," *Protection and Control of Modern Power Systems*, vol. 3, no. 1, p. 25, 2018/08/17 2018, doi: 10.1186/s41601-018-0099-8.
[146] K.-D. Jäger, O. Isabella, A. H. Smets, R. A. van Swaaij, and M. Zeman, *Solar energy: fundamentals, technology and systems*. UIT Cambridge, 2016.
[147] R. Kumar and G. K. Dalal, "Design and Simulation of Photovoltaic Water Pumping System," *International Journal of Science and Research*, pp. 2208-2213, 2014.
[148] U. U. Khan, M. Raheem, S. Ata, and Z. H. Khan, "Design and implementation of a low-cost MPPT controller for solar PV system," in *2016 International Conference on Open Source Systems & Technologies (ICOSST)*, 15-17 Dec. 2016 2016, pp. 156-163, doi: 10.1109/ICOSST.2016.7838594.
[149] Z. Xuesong, S. Daichun, M. Youjie, and C. Deshu, "The simulation and design for MPPT of PV system Based on Incremental Conductance Method," in *2010 WASE International Conference on Information Engineering*, 14-15 Aug. 2010 2010, vol. 2, pp. 314-317, doi: 10.1109/ICIE.2010.170.
[150] S. Sumathi, L. A. Kumar, and P. Surekha, "Application of MATLAB/SIMULINK in solar PV systems," in *Solar PV and wind energy conversion systems*: Springer, 2015, pp. 59-143.
[151] S. Selvan, "Modeling and Simulation of Incremental Conductance MPPT Algorithm for Photovoltaic Applications," *International Journal of Scientific Engineering and Technology*, vol. 2, pp. 2277-1581, 08/01 2013.
[152] X. Liu and L. A. C. Lopes, "An improved perturbation and observation maximum power point tracking algorithm for PV arrays," in *2004 IEEE 35th Annual Power Electronics Specialists Conference (IEEE Cat. No.04CH37551)*, 20-25 June 2004 2004, vol. 3, pp. 2005-2010 Vol.3, doi: 10.1109/PESC.2004.1355425.
[153] R. Alik and A. Jusoh, "Modified Perturb and Observe (P&O) with checking algorithm under various solar irradiation," *Solar Energy*, vol. 148, pp. 128-139, 2017/05/15/ 2017, doi: https://doi.org/10.1016/j.solener.2017.03.064.
[154] J. Youngseok, S. Junghun, Y. Gwonjong, and C. Jaeho, "Improved perturbation and observation method (IP&O) of MPPT control for photovoltaic power systems," in *Conference Record of the Thirty-first IEEE Photovoltaic Specialists Conference, 2005.*, 3-7 Jan. 2005 2005, pp. 1788-1791, doi: 10.1109/PVSC.2005.1488498.
[155] S. Ozdemir, N. Altin, and I. Sefa, "Fuzzy logic based MPPT controller for high conversion ratio quadratic boost converter," *International Journal of Hydrogen Energy*, vol. 42, 03/01 2017, doi: 10.1016/j.ijhydene.2017.02.191.
[156] V. Padmanabhan, V. Beena, and M. Jayaraju, "Fuzzy logic based Maximum Power Point Tracker for a Photovoltaic system," in *2012 International Conference on Power, Signals, Controls and Computation*, 3-6 Jan. 2012 2012, pp. 1-6, doi: 10.1109/EPSCICON.2012.6175255.

[157] Y. Chouay and M. Ouassaid, "An Experimental Artificial Neural Network Based MPP Tracking for Solar Photovoltaic Systems," in *International Conference Europe Middle East & North Africa Information Systems and Technologies to Support Learning*, 2019: Springer, pp. 533-542.
[158] M. Sechilariu and F. Locment, "Chapter 3 - Backup Power Resources for Microgrid," in *Urban DC Microgrid*, M. Sechilariu and F. Locment Eds.: Butterworth-Heinemann, 2016, pp. 93-132.
[159] B. R. Limited. "How Do Diesel Generators Work." Bellwood Rewinds Ltd. https://www.bellwoodrewinds.co.uk/how-do-diesel-generators-work/ (accessed 2020).
[160] T. Waris and C. V. Nayar, "Variable speed constant frequency diesel power conversion system using doubly fed induction generator (DFIG)," in *2008 IEEE Power Electronics Specialists Conference*, 15-19 June 2008 2008, pp. 2728-2734, doi: 10.1109/PESC.2008.4592357.
[161] T. Waris and C. V. Nayar, *Variable Speed Constant Frequency Diesel Power Conversion System Using Doubly Fed Induction Generator (DFIG)*. 2008, pp. 2728-2734.
[162] P. Stott, M. Mueller, V. D. Colli, F. Marignetti, and R. Di Stefano, "DC link voltage stabilisation in hybrid renewable diesel systems," in *2007 International Conference on Clean Electrical Power*, 2007: IEEE, pp. 20-25.
[163] R. Cardenas, R. Pena, J. Proboste, G. Asher, and J. Clare, "MRAS observer for sensorless control of standalone doubly fed induction generators," *IEEE Transactions on Energy Conversion*, vol. 20, no. 4, pp. 710-718, 2005, doi: 10.1109/TEC.2005.847965.
[164] J. B. Andriulli *et al.*, "ORNL/TM-1999/213 Advanced Power Generation Systems for the 21st Century: Market Survey and Recommendations for a Design Philosophy," 11/01 1999.
[165] B. A. Kumar, K. A. Kumar, T. Radha, T. R. Chelliah, D. Khare, and U. S. Ramesh, "Control strategy for fuel saving in asynchronous generator driven electric tugboats," in *2016 IEEE Uttar Pradesh Section International Conference on Electrical, Computer and Electronics Engineering (UPCON)*, 9-11 Dec. 2016 2016, pp. 467-472, doi: 10.1109/UPCON.2016.7894699.
[166] S. S. Chandel, M. Nagaraju Naik, and R. Chandel, "Review of solar photovoltaic water pumping system technology for irrigation and community drinking water supplies," *Renewable and Sustainable Energy Reviews*, vol. 49, pp. 1084-1099, 2015/09/01/ 2015, doi: https://doi.org/10.1016/j.rser.2015.04.083.
[167] K. Meah, S. Fletcher, and S. Ula, "Solar photovoltaic water pumping for remote locations," *Renewable and Sustainable Energy Reviews*, vol. 12, no. 2, pp. 472-487, 2008/02/01/ 2008, doi: https://doi.org/10.1016/j.rser.2006.10.008.
[168] D. Kaya, E. A. Yagmur, K. S. Yigit, F. C. Kilic, A. S. Eren, and C. Celik, "Energy efficiency in pumps," *Energy Conversion and Management*, vol. 49, no. 6, pp. 1662-1673, 2008/06/01/ 2008, doi: https://doi.org/10.1016/j.enconman.2007.11.010.
[169] G. B. Gharehpetian and S. M. M. Agah, *Distributed generation systems: design, operation and grid integration*. Butterworth-Heinemann, 2017.
[170] E. Papadopoulou, *Energy management in buildings using photovoltaics*. Springer Science & Business Media, 2012.
[171] R. Khatri, "Design and assessment of solar PV plant for girls hostel (GARGI) of MNIT University, Jaipur city: A case study," *Energy Reports*, vol. 2, pp. 89-98, 2016/11/01/ 2016, doi: https://doi.org/10.1016/j.egyr.2016.05.002.
[172] Z. E. R. A. (ZERA). "Solar PV system sizing." ZERA. https://www.zera.co.zw/solar-pv-system-sizing/ (accessed 2020).

[173] ARTsolar. "ART solar -360 Watt Solar Panel." ARTsolar company. https://artsolar.net/product/360-watt-solar-panel-monocrystalline/ (accessed 2020).
[174] K. Bücher, "Site dependence of the energy collection of PV modules," *Solar Energy Materials and Solar Cells*, vol. 47, no. 1, pp. 85-94, 1997/10/01/ 1997, doi: https://doi.org/10.1016/S0927-0248(97)00028-7.
[175] D. H. Wang, C. V. Nayar, and C. Wang, "Modeling of stand-alone variable speed diesel generator using doubly-fed induction generator," in *The 2nd International Symposium on Power Electronics for Distributed Generation Systems*, 16-18 June 2010 2010, pp. 1-6, doi: 10.1109/PEDG.2010.5545769.
[176] S. Qazi, *Standalone Photovoltaic (PV) Systems for Disaster Relief and Remote Areas*. Elsevier, 2016, p. 1.
[177] F. M. González-Longatt, "Circuit based battery models: A review," in *Congreso Iberoamericano de estudiantes De Ingenieria Electrica. Cibelec*, 2006.
[178] A. A. Aldair, A. A. Obed, and A. F. Halihal, "Design and implementation of ANFIS-reference model controller based MPPT using FPGA for photovoltaic system," *Renewable and Sustainable Energy Reviews*, vol. 82, pp. 2202-2217, 2018/02/01/ 2018, doi: https://doi.org/10.1016/j.rser.2017.08.071.
[179] M. A. Abido, M. S. Khalid, and M. Y. Worku, "An Efficient ANFIS-Based PI Controller for Maximum Power Point Tracking of PV Systems," *Arabian Journal for Science and Engineering*, vol. 40, no. 9, pp. 2641-2651, 2015/09/01 2015, doi: 10.1007/s13369-015-1749-z.
[180] H. Hussein, A. Aloui, and B. Alshammari, "ANFIS-based PI controller for maximum power point tracking in PV systems," *International Journal of ADVANCED AND APPLIED SCIENCES*, vol. 5, 02/01 2018, doi: 10.21833/ijaas.2018.02.015.
[181] M. Y. Worku and M. A. Abido, "Grid Connected PV System Using ANFIS Based MPPT Controller in Real Time," *Renewable energy & power quality journal*, pp. 35-40, 2016.
[182] M. Berrera, A. Dolara, R. Faranda, and S. Leva, "Experimental test of seven widely-adopted MPPT algorithms," in *2009 IEEE Bucharest PowerTech*, 28 June-2 July 2009 2009, pp. 1-8, doi: 10.1109/PTC.2009.5282010.
[183] S. K. Kollimalla and M. K. Mishra, "A Novel Adaptive P&O MPPT Algorithm Considering Sudden Changes in the Irradiance," *IEEE Transactions on Energy Conversion*, vol. 29, no. 3, pp. 602-610, 2014, doi: 10.1109/TEC.2014.2320930.
[184] K. Solar. "Solar pump." Hari Sharan. https://kenbrooksolar.com/price-list/solar-water-pumps-price-1-2-3-5-10-hp (accessed 2020).

APPENDIX A: PERTURBATION AND OBSERVATION MPPT ALGORITHM

```
function D  = P & O(V, I)


Dinit = 0.05;
Dmax = 1;
Dmin = 0;
deltaD = 0.005;


persistent Vold Pold Dold M;

dataType = 'double';

if isempty(Vold)
    Vold=0;
    Pold=0;
    Dold=Dinit;
    M=1;
end
P= V*I;
dV= V - Vold;
dP= P - Pold;

M=abs(dP);

if M < 0.05
    D=Dold;
else
    if dP < 0
        if dV < 0
            D = Dold - deltaD*M;
        else
            D = Dold + deltaD*M;
        end
    else
        if dV < 0
            D = Dold + deltaD*M;
        else
            D = Dold - deltaD*M;
        end
    end

end

if D >= Dmax | D<= Dmin
    D=Dold;
end

Dold=D;
Vold=V;
Pold=P;
```

APPENDIX B: SOLAR IRRADIANCE AND TEMPERATURE DATA

PVGIS-5 geo-temporal irradiation database

Provided inputs

Latitude/Longitude:	-20.983, 32.104
Horizon:	Calculated
Database used	PVGIS-CMSAF
Month:	January

Outline of horizon at chosen location:

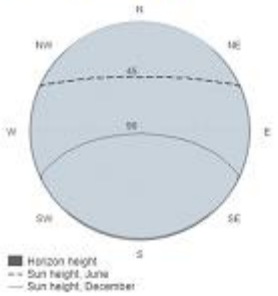

Daily average irradiance on fixed plane with slope 35° and azimuth 0°

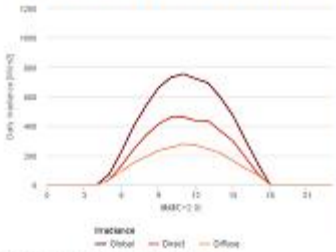

Irradiance on a fixed plane

Time	00:45	01:45	02:45	03:45	04:45	05:45	06:45	07:45	08:45	09:45	10:45	11:45	12:45	13:45	14:45	15:45	16:45	17:45	18:45	19:45	20:45	21:45	22:45	23:45
G	0	0	0	0	0	70	225	400	540	660	730	754	721	660	594	472	307	147	0	0	0	0	0	0
Gb	0	0	0	0	0	34	129	242	338	413	459	461	436	405	366	299	189	77	0	0	0	0	0	0
Gd	0	0	0	0	0	35	92	151	191	234	255	278	276	244	216	164	113	68	0	0	0	0	0	0

G: Global irradiance on a fixed plane [W/m2].
Gb: Direct irradiance on a fixed plane [W/m2].
Gd: Diffuse irradiance on a fixed plane [W/m2].

Daily average temperature

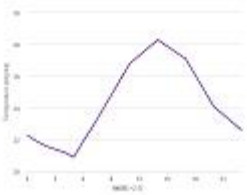

Average daily temperature profile

Time	00:45	01:45	02:45	03:45	04:45	05:45	06:45	07:45	08:45	09:45	10:45	11:45	12:45	13:45	14:45	15:45	16:45	17:45	18:45	19:45	20:45	21:45	22:45	23:45
Td	22.3	21.9	21.6	21.4	21.2	20.9	21.9	22.8	23.8	24.8	25.8	26.8	27.3	27.8	28.3	27.9	27.5	27.1	26.1	25.1	24.1	23.6	23.1	22.8

T: Average daily temperature profile [°C].

Joint Research Centre

Report generated on 2019/07/24

Daily irradiance data

PVGIS-5 geo-temporal irradiation database

Provided inputs

Latitude/Longitude:	-20.983, 32.104
Horizon:	Calculated
Database used	PVGIS-CMSAF
Month:	February

Outline of horizon at chosen location:

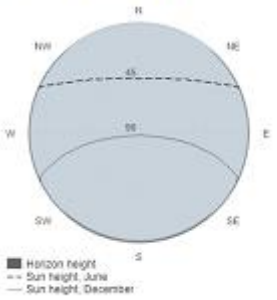

Daily average irradiance on fixed plane with slope 35° and azimuth 0°

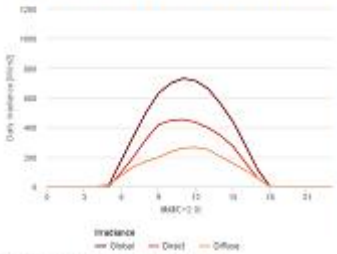

Irradiance on a fixed plane

Time	00h00	01h00	02h00	03h00	04h00	05h00	06h00	07h00	08h00	09h00	10h00	11h00	12h00	13h00	14h00	15h00	16h00	17h00	18h00	19h00	20h00	21h00	22h00	23h00
G	0	0	0	0	0	12	178	344	502	631	698	721	714	661	560	440	281	115	0	0	0	0	0	0
Gb	0	0	0	0	0	1	98	203	321	418	447	454	434	397	345	273	164	57	0	0	0	0	0	0
Gd	0	0	0	0	0	11	77	134	170	198	235	261	265	250	203	158	111	57	0	0	0	0	0	0

G: Global irradiance on a fixed plane [W/m2].
Gb: Direct irradiance on a fixed plane [W/m2].
Gd: Diffuse irradiance on a fixed plane [W/m2].

Daily average temperature

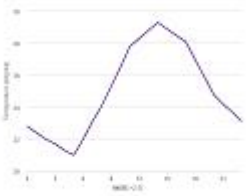

Average daily temperature profile

Time	00h00	01h00	02h00	03h00	04h00	05h00	06h00	07h00	08h00	09h00	10h00	11h00	12h00	13h00	14h00	15h00	16h00	17h00	18h00	19h00	20h00	21h00	22h00	23h00
Td	22.8	22.4	22	21.7	21.3	21	22	23.1	24.1	25.3	26.5	27.6	28.3	28.8	29.3	28.9	28.5	28.1	27	25.9	24.8	24.2	23.7	23.1

T: Average daily temperature profile [°C].

Joint Research Centre

Report generated on 2019/07/24

Daily irradiance data

PVGIS-5 geo-temporal irradiation database

Provided inputs

Latitude/Longitude:	-20.983, 32.104
Horizon:	Calculated
Database used	PVGIS-CMSAF
Month:	March

Outline of horizon at chosen location:

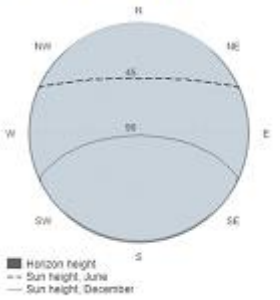

Daily average irradiance on fixed plane with slope 35° and azimuth 0°

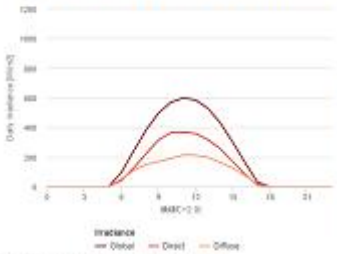

Irradiance on a fixed plane

Time	00x05	01x05	02x05	03x05	04x05	05x05	06x05	07x05	08x05	09x05	10x05	11x05	12x05	13x05	14x05	15x05	16x05	17x05	18x05	19x05	20x05	21x05	22x05	23x05
G	0	0	0	0	0	0	0	96	241	383	497	569	599	585	527	428	299	159	38	0	0	0	0	0
Gb	0	0	0	0	0	0	0	42	126	223	315	384	409	398	358	316	255	167	81	10	0	0	0	0
Gd	0	0	0	0	0	0	0	52	109	150	169	190	214	212	197	162	124	74	17	0	0	0	0	0

G: Global irradiance on a fixed plane [W/m2].
Gb: Direct irradiance on a fixed plane [W/m2].
Gd: Diffuse irradiance on a fixed plane [W/m2].

Daily average temperature

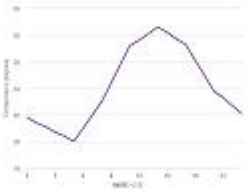

Average daily temperature profile

Time	00x05	01x05	02x05	03x05	04x05	05x05	06x05	07x05	08x05	09x05	10x05	11x05	12x05	13x05	14x05	15x05	16x05	17x05	18x05	19x05	20x05	21x05	22x05	23x05
Td	21.8	21.4	21.1	20.7	20.4	20	21	22	23	24.4	25.8	27.2	27.6	28.1	28.6	28.2	27.7	27.3	26.1	25	23.8	23.3	22.7	22.1

T: Average daily temperature profile [°C].

Joint Research Centre

Report generated on 2019/07/24

Daily irradiance data

PVGIS-5 geo-temporal irradiation database

Provided inputs

Latitude/Longitude:	-20.983, 32.104
Horizon:	Calculated
Database used	PVGIS-CMSAF
Month:	April

Outline of horizon at chosen location:

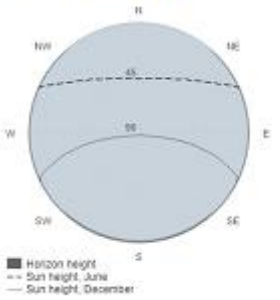

Daily average irradiance on fixed plane with slope 35° and azimuth 0°

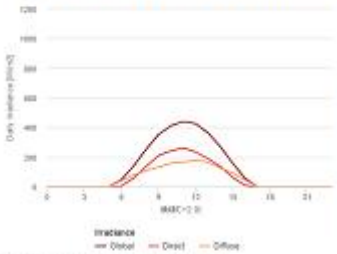

Irradiance on a fixed plane

Time	00x05	01x05	02x05	03x05	04x05	05x05	06x05	07x05	08x05	09x05	10x05	11x05	12x05	13x05	14x05	15x05	16x05	17x05	18x05	19x05	20x05	21x05	22x05	23x05
G	0	0	0	0	0	0	45	140	252	352	411	440	425	362	269	157	54	0	0	0	0	0	0	0
Gb	0	0	0	0	0	0	4	57	136	209	241	262	234	167	135	61	8	0	0	0	0	0	0	0
Gd	0	0	0	0	0	0	40	78	107	132	157	165	178	164	125	91	44	0	0	0	0	0	0	0

G: Global irradiance on a fixed plane [W/m2].
Gb: Direct irradiance on a fixed plane [W/m2].
Gd: Diffuse irradiance on a fixed plane [W/m2].

Daily average temperature

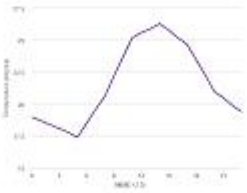

Average daily temperature profile

Time	00x05	01x05	02x05	03x05	04x05	05x05	06x05	07x05	08x05	09x05	10x05	11x05	12x05	13x05	14x05	15x05	16x05	17x05	18x05	19x05	20x05	21x05	22x05	23x05
Td	19	18.7	18.4	18.1	17.8	17.4	18.5	19.6	20.6	22.2	23.7	25.2	25.6	25.9	26.3	25.8	25.2	24.7	23.5	22.3	21	20.5	19.9	19.4

T: Average daily temperature profile [°C].

Joint Research Centre

Report generated on 2019/07/24

Daily irradiance data

PVGIS-5 geo-temporal irradiation database

Provided inputs

Latitude/Longitude:	-20.983, 32.104
Horizon:	Calculated
Database used	PVGIS-CMSAF
Month:	May

Outline of horizon at chosen location:

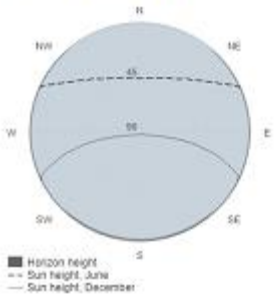

Daily average irradiance on fixed plane with slope 35° and azimuth 0°

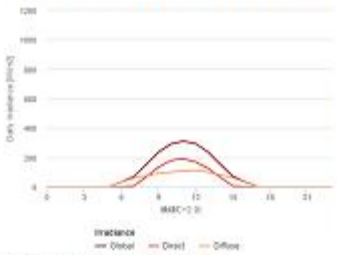

Irradiance on a fixed plane

Time	00x05	01x05	02x05	03x05	04x05	05x05	06x05	07x05	08x05	09x05	10x05	11x05	12x05	13x05	14x05	15x05	16x05	17x05	18x05	19x05	20x05	21x05	22x05	23x05
G	0	0	0	0	0	0	34	69	151	236	291	311	294	236	152	71	33	0	0	0	0	0	0	0
Gb	0	0	0	0	0	0	0	6	67	134	179	191	170	126	64	6	0	0	0	0	0	0	0	0
Gd	0	0	0	0	0	0	33	60	76	91	100	107	112	100	80	62	32	0	0	0	0	0	0	0

G: Global irradiance on a fixed plane [W/m2].
Gb: Direct irradiance on a fixed plane [W/m2].
Gd: Diffuse irradiance on a fixed plane [W/m2].

Daily average temperature

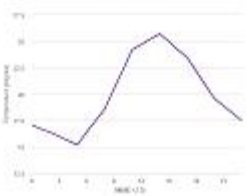

Average daily temperature profile

Time	00x05	01x05	02x05	03x05	04x05	05x05	06x05	07x05	08x05	09x05	10x05	11x05	12x05	13x05	14x05	15x05	16x05	17x05	18x05	19x05	20x05	21x05	22x05	23x05
T2	17.1	16.7	16.4	16	15.6	15.2	16.4	17.5	18.6	20.5	22.3	24.2	24.7	25.2	25.7	25	24.2	23.5	22.2	20.9	19.6	18.9	18.2	17.5

T: Average daily temperature profile [°C].

Joint Research Centre

Report generated on 2019/07/24

Daily irradiance data

PVGIS-5 geo-temporal irradiation database

Provided inputs

Latitude/Longitude:	-20.983, 32.104
Horizon:	Calculated
Database used	PVGIS-CMSAF
Month:	June

Outline of horizon at chosen location:

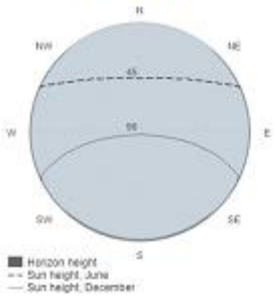

Daily average irradiance on fixed plane with slope 35° and azimuth 0°

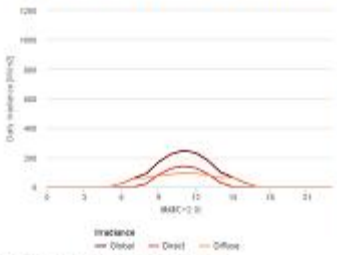

Irradiance on a fixed plane

Time	00x05	01x05	02x05	03x05	04x05	05x05	06x05	07x05	08x05	09x05	10x05	11x05	12x05	13x05	14x05	15x05	16x05	17x05	18x05	19x05	20x05	21x05	22x05	23x05
G	0	0	0	0	0	0	22	58	89	168	222	247	231	179	99	64	26	0	0	0	0	0	0	0
Gb	0	0	0	0	0	0	0	0	21	82	125	141	128	87	29	0	0	0	0	0	0	0	0	0
Gd	0	0	0	0	0	0	21	57	60	76	85	94	91	81	62	63	25	0	0	0	0	0	0	0

G: Global irradiance on a fixed plane [W/m2].
Gb: Direct irradiance on a fixed plane [W/m2].
Gd: Diffuse irradiance on a fixed plane [W/m2].

Daily average temperature

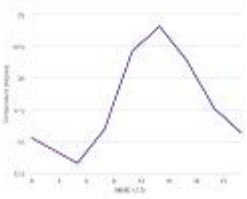

Average daily temperature profile

Time	00x05	01x05	02x05	03x05	04x05	05x05	06x05	07x05	08x05	09x05	10x05	11x05	12x05	13x05	14x05	15x05	16x05	17x05	18x05	19x05	20x05	21x05	22x05	23x05
T2	15.3	14.9	14.5	14.1	13.7	13.3	14.2	15.1	16	18.1	20.1	22.1	22.8	23.4	24.1	23.2	22.3	21.4	20.1	18.9	17.6	17	16.3	15.7

T: Average daily temperature profile [°C].

Joint Research Centre

Report generated on 2019/07/24

Daily irradiance data

PVGIS-5 geo-temporal irradiation database

Provided inputs

Latitude/Longitude:	-20.983, 32.104
Horizon:	Calculated
Database used	PVGIS-CMSAF
Month:	July

Outline of horizon at chosen location:

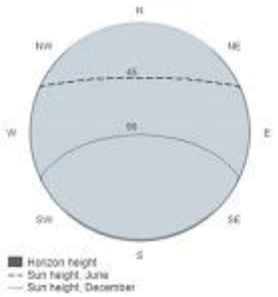

Daily average irradiance on fixed plane with slope 35° and azimuth 0°

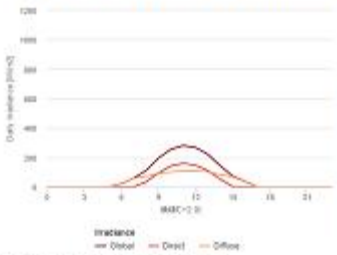

Irradiance on a fixed plane

Time	00x05	01x05	02x05	03x05	04x05	05x05	06x05	07x05	08x05	09x05	10x05	11x05	12x05	13x05	14x05	15x05	16x05	17x05	18x05	19x05	20x05	21x05	22x05	23x05
G	0	0	0	0	0	0	21	60	111	166	255	281	267	226	142	72	36	0	0	0	0	0	0	0
Gb	0	0	0	0	0	0	0	0	34	94	143	161	147	109	51	2	0	0	0	0	0	0	0	0
Gd	0	0	0	0	0	0	20	59	71	92	101	108	108	101	83	68	35	0	0	0	0	0	0	0

G: Global irradiance on a fixed plane [W/m2].
Gb: Direct irradiance on a fixed plane [W/m2].
Gd: Diffuse irradiance on a fixed plane [W/m2].

Daily average temperature

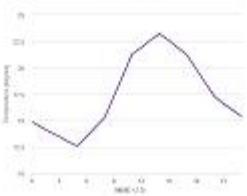

Average daily temperature profile

Time	00x05	01x05	02x05	03x05	04x05	05x05	06x05	07x05	08x05	09x05	10x05	11x05	12x05	13x05	14x05	15x05	16x05	17x05	18x05	19x05	20x05	21x05	22x05	23x05
Td	14.9	14.4	13.9	13.5	13	12.6	13.5	14.4	15.3	17.3	19.3	21.3	21.9	22.6	23.2	22.6	21.9	21.2	19.9	18.6	17.3	16.6	16	15.4

T: Average daily temperature profile [°C].

Joint Research Centre

Report generated on 2019/07/24

Daily irradiance data

PVGIS-5 geo-temporal irradiation database

Provided inputs

Latitude/Longitude:	-20.983, 32.104
Horizon:	Calculated
Database used	PVGIS-CMSAF
Month:	August

Outline of horizon at chosen location:

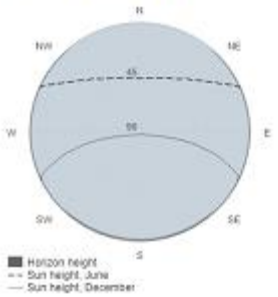

Daily average irradiance on fixed plane with slope 35° and azimuth 0°

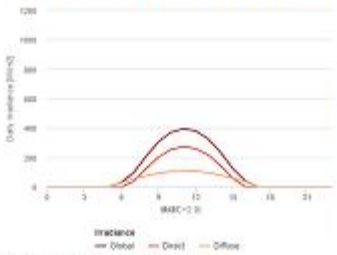

Irradiance on a fixed plane

Time	00x0	01x0	02x0	03x0	04x0	05x0	06x0	07x0	08x0	09x0	10x0	11x0	12x0	13x0	14x0	15x0	16x0	17x0	18x0	19x0	20x0	21x0	22x0	23x0
G	0	0	0	0	0	0	30	97	207	306	371	394	391	326	236	123	43	0	0	0	0	0	0	0
Gb	0	0	0	0	0	0	0	37	124	202	253	275	259	218	145	59	1	0	0	0	0	0	0	0
Gd	0	0	0	0	0	0	30	56	74	93	104	105	108	96	81	58	39	0	0	0	0	0	0	0

G: Global irradiance on a fixed plane [W/m2].
Gb: Direct irradiance on a fixed plane [W/m2].
Gd: Diffuse irradiance on a fixed plane [W/m2].

Daily average temperature

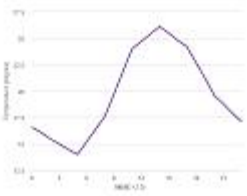

Average daily temperature profile

Time	00x0	01x0	02x0	03x0	04x0	05x0	06x0	07x0	08x0	09x0	10x0	11x0	12x0	13x0	14x0	15x0	16x0	17x0	18x0	19x0	20x0	21x0	22x0	23x0
T#	16.8	16.1	15.5	15	14.5	14	15.2	16.4	17.6	19.7	21.9	24	24.7	25.4	26.1	25.5	24.8	24.2	22.7	21.2	19.6	18.8	17.9	17.1

T: Average daily temperature profile [°C].

Joint Research Centre

Report generated on 2019/07/24

European Commission

Daily irradiance data

PVGIS-5 geo-temporal irradiation database

Provided inputs

Latitude/Longitude:	-20.983, 32.104
Horizon:	Calculated
Database used	PVGIS-CMSAF
Month:	September

Outline of horizon at chosen location:

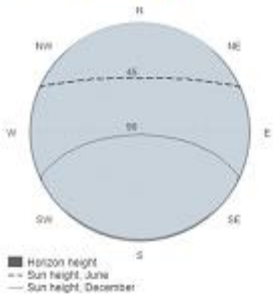

Daily average irradiance on fixed plane with slope 35° and azimuth 0°

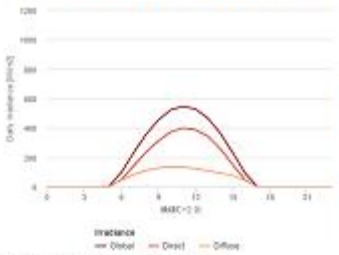

Irradiance on a fixed plane

Time	00h00	01h00	02h00	03h00	04h00	05h00	06h00	07h00	08h00	09h00	10h00	11h00	12h00	13h00	14h00	15h00	16h00	17h00	18h00	19h00	20h00	21h00	22h00	23h00
G	0	0	0	0	0	4	98	233	357	455	524	547	528	465	363	231	93	0	0	0	0	0	0	0
Gb	0	0	0	0	0	0	49	143	236	313	374	400	387	343	257	149	46	0	0	0	0	0	0	0
Gd	0	0	0	0	0	3	46	84	111	129	136	132	125	108	95	75	43	0	0	0	0	0	0	0

G: Global irradiance on a fixed plane [W/m2].
Gb: Direct irradiance on a fixed plane [W/m2].
Gd: Diffuse irradiance on a fixed plane [W/m2].

Daily average temperature

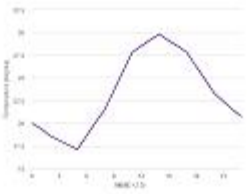

Average daily temperature profile

Time	00h00	01h00	02h00	03h00	04h00	05h00	06h00	07h00	08h00	09h00	10h00	11h00	12h00	13h00	14h00	15h00	16h00	17h00	18h00	19h00	20h00	21h00	22h00	23h00
Td	20	19.4	18.8	18.1	17.6	17.1	18.8	20.1	21.5	23.0	25.7	27.8	28.5	29.2	29.8	29.1	28.5	27.8	26.3	24.8	23.3	22.4	21.5	20.7

T: Average daily temperature profile [°C].

Joint Research Centre

Report generated on 2019/07/24

European Commission

Daily irradiance data

PVGIS-5 geo-temporal irradiation database

Provided inputs

Latitude/Longitude:	-20.983, 32.104
Horizon:	Calculated
Database used	PVGIS-CMSAF
Month:	October

Outline of horizon at chosen location:

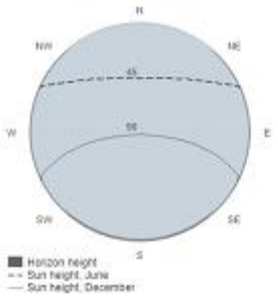

Daily average irradiance on fixed plane with slope 35° and azimuth 0°

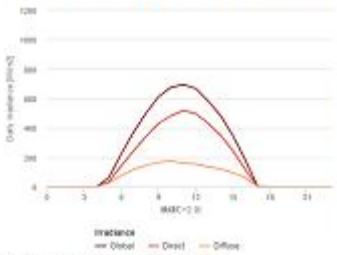

Irradiance on a fixed plane

Time	00x15	01x15	02x15	03x15	04x15	05x15	06x15	07x15	08x15	09x15	10x15	11x15	12x15	13x15	14x15	15x15	16x15	17x15	18x15	19x15	20x15	21x15	22x15	23x15
G	0	0	0	0	0	64	225	374	502	613	676	686	669	584	485	348	184	3	0	0	0	0	0	0
Gb	0	0	0	0	0	36	144	246	343	431	483	519	497	432	352	245	119	0	0	0	0	0	0	0
Gd	0	0	0	0	0	27	76	119	147	167	177	160	156	137	122	96	62	3	0	0	0	0	0	0

G: Global irradiance on a fixed plane [W/m2].
Gb: Direct irradiance on a fixed plane [W/m2].
Gd: Diffuse irradiance on a fixed plane [W/m2].

Daily average temperature

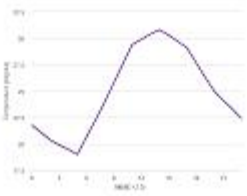

Average daily temperature profile

Time	00x15	01x15	02x15	03x15	04x15	05x15	06x15	07x15	08x15	09x15	10x15	11x15	12x15	13x15	14x15	15x15	16x15	17x15	18x15	19x15	20x15	21x15	22x15	23x15
Td	21.8	21.1	20.4	19.9	19.5	19	20.7	22.3	24	25.8	27.6	29.4	29.9	30.4	30.8	30.3	29.7	29.1	27.7	26.3	25	24.1	23.3	22.4

T: Average daily temperature profile [°C].

Joint Research Centre

Report generated on 2019/07/24

Daily irradiance data

PVGIS-5 geo-temporal irradiation database

Provided inputs

Latitude/Longitude:	-20.983, 32.104
Horizon:	Calculated
Database used	PVGIS-CMSAF
Month:	November

Outline of horizon at chosen location:

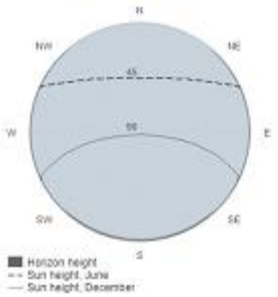

Daily average irradiance on fixed plane with slope 35° and azimuth 0°

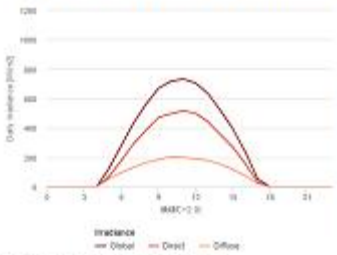

Irradiance on a fixed plane

Time	00x05	01x05	02x05	03x05	04x05	05x05	06x05	07x05	08x05	09x05	10x05	11x05	12x05	13x05	14x05	15x05	16x05	17x05	18x05	19x05	20x05	21x05	22x05	23x05
G	0	0	0	0	0	0	125	281	436	563	670	718	733	705	633	519	394	238	54	0	0	0	0	0
Gb	0	0	0	0	0	0	69	180	294	386	472	497	517	496	442	354	269	159	31	0	0	0	0	0
Gd	0	0	0	0	0	0	55	97	134	165	184	206	200	191	178	154	117	76	22	0	0	0	0	0

G: Global irradiance on a fixed plane [W/m2].
Gb: Direct irradiance on a fixed plane [W/m2].
Gd: Diffuse irradiance on a fixed plane [W/m2].

Daily average temperature

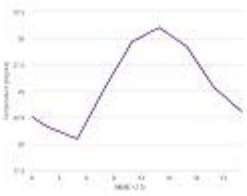

Average daily temperature profile

Time	00x05	01x05	02x05	03x05	04x05	05x05	06x05	07x05	08x05	09x05	10x05	11x05	12x05	13x05	14x05	15x05	16x05	17x05	18x05	19x05	20x05	21x05	22x05	23x05
T2	22.6	22	21.5	21.2	20.8	20.5	22.1	23.7	25.3	26.8	28.2	29.7	30.1	30.6	31	30.4	29.8	29.2	27.9	26.6	25.3	24.6	23.8	23.1

T: Average daily temperature profile [°C].

Joint Research Centre

Report generated on 2019/07/24

Daily irradiance data

PVGIS-5 geo-temporal irradiation database

Provided inputs

Latitude/Longitude:	-20.983, 32.104
Horizon:	Calculated
Database used	PVGIS-CMSAF
Month:	December

Outline of horizon at chosen location:

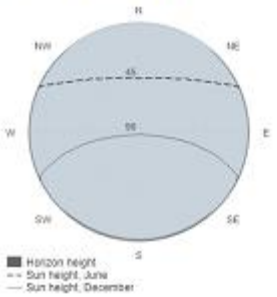

Daily average irradiance on fixed plane with slope 35° and azimuth 0°

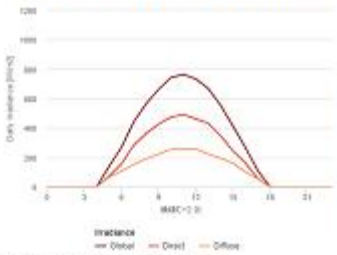

Irradiance on a fixed plane

Time	00x05	01x05	02x05	03x05	04x05	05x05	06x05	07x05	08x05	09x05	10x05	11x05	12x05	13x05	14x05	15x05	16x05	17x05	18x05	19x05	20x05	21x05	22x05	23x05
G	0	0	0	0	0	0	138	267	442	595	682	743	764	734	676	555	414	269	112	0	0	0	0	0
Gb	0	0	0	0	0	0	71	155	282	363	426	474	492	462	433	349	245	164	57	0	0	0	0	0
Gd	0	0	0	0	0	0	65	107	152	191	222	254	257	257	223	195	161	102	54	0	0	0	0	0

G: Global irradiance on a fixed plane [W/m2].
Gb: Direct irradiance on a fixed plane [W/m2].
Gd: Diffuse irradiance on a fixed plane [W/m2].

Daily average temperature

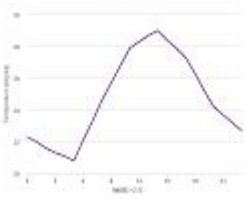

Average daily temperature profile

Time	00x05	01x05	02x05	03x05	04x05	05x05	06x05	07x05	08x05	09x05	10x05	11x05	12x05	13x05	14x05	15x05	16x05	17x05	18x05	19x05	20x05	21x05	22x05	23x05
T2	22.3	22	21.6	21.3	21.1	20.8	22.1	23.3	24.6	25.7	26.8	27.9	28.3	28.7	29	28.4	27.9	27.3	26.3	25.2	24.2	23.7	23.2	22.7

T: Average daily temperature profile [°C].

Joint Research Centre

Report generated on 2019/07/24

Daily irradiance data

PVGIS-5 geo-temporal irradiation database

Provided inputs

Latitude/Longitude:	-20.983, 32.104
Horizon:	Calculated
Database used	PVGIS-CMSAF
Month:	December

Outline of horizon at chosen location:

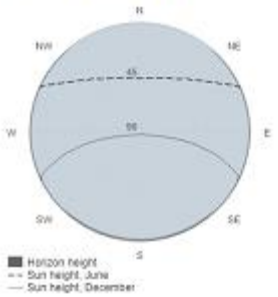

Daily average irradiance on fixed plane with slope 35° and azimuth 0°

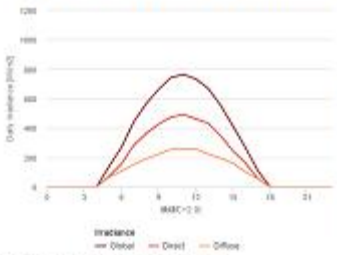

Irradiance on a fixed plane

Time	00x05	01x05	02x05	03x05	04x05	05x05	06x05	07x05	08x05	09x05	10x05	11x05	12x05	13x05	14x05	15x05	16x05	17x05	18x05	19x05	20x05	21x05	22x05	23x05
G	0	0	0	0	0	0	138	267	442	595	682	743	764	734	676	555	414	269	112	0	0	0	0	0
Gb	0	0	0	0	0	0	71	155	282	363	426	474	492	462	433	349	245	164	57	0	0	0	0	0
Gd	0	0	0	0	0	0	65	107	152	191	222	254	257	257	223	195	161	102	54	0	0	0	0	0

G: Global irradiance on a fixed plane [W/m2].
Gb: Direct irradiance on a fixed plane [W/m2].
Gd: Diffuse irradiance on a fixed plane [W/m2].

Daily average temperature

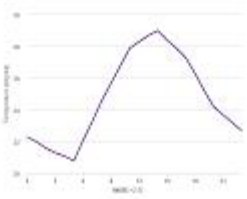

Average daily temperature profile

Time	00x05	01x05	02x05	03x05	04x05	05x05	06x05	07x05	08x05	09x05	10x05	11x05	12x05	13x05	14x05	15x05	16x05	17x05	18x05	19x05	20x05	21x05	22x05	23x05
T2	22.3	22	21.6	21.3	21.1	20.8	22.1	23.3	24.6	25.7	26.8	27.9	28.3	28.7	29	28.4	27.9	27.3	26.3	25.2	24.2	23.7	23.2	22.7

T: Average daily temperature profile [°C].

Joint Research Centre

Report generated on 2019/07/24